Hydraulic transport in inclined large diameter pipelines

M.A. De Vreede

Delft University of Technology
Section of Dredging Engineering
Master thesis 10 April 2018

TU Delft

Hydraulic transport in inclined large diameter pipelines

by

M.A. De Vreede

to obtain the degree of Master of Science in Offshore and Dredging engineering
at the Delft University of Technology,
Faculty of Mechanical, Materials and Marine Engineering
Department of Marine and Transport Technology
To be presented and defended on Tuesday April 24, 2018.

Student number:	1526111	
Project duration:	May 2017 – April 2018	
Thesis committee:	Dr. ir. A. M. Talmon,	TU Delft, daily supervisor and chairman of graduation committee
	Prof. dr. ir. C. van Rhee,	TU Delft, supervisor
	Dr. F. Wang,	NERCD, daily supervisor
	Dr. ir. H.J. de Koning Gans,	TU Delft

TU Delft

中交疏浚技术装备国家工程研究中心有限公司
CCCC NATIONAL ENGINEERING RESEARCH CENTER OF DREDGING TECHNOLOGY AND EQUIPMENT CO.,LTD

Preface

This thesis report is the result of several months of research within the setting of a joint research project between Delft University of technology and the national engineering research center of dredging technology and equipment. This collaboration raised the opportunity to do several months of laboratory experiments at the NERCD test site in Shanghai, China. The rest of the thesis work was completed in the Netherlands under the supervision of Professor Cees van Rhee and Doctor Arno Talmon. The author participated in the 5th international dredging technology development conference of China, where the preliminary findings were presented. The conference took place in November 2017 in Beijing and was organised by the EADA and the CHIDA. A paper containing the preliminary results of the inclined experiments was published in the proceedings of the conference.

I want to express my gratitude towards mr Zhang Qingbo and prof. Cees van Rhee for making this joint research programme possible. Furthermore, I want to thank my entire graduation committee consisting of professor Cees van Rhee, doctor Arno Talmon and doctor Wang. Especially doctor Arno Talmon, fulfilling the roles of daily supervisor and chairman of the graduation committee, proved to be invaluable with regard to the progress of the project and he remained an inexhaustible source of knowledge and guidance throughout the duration. The daily supervision of doctor Wang was a great asset in China with regard to the experiments themselves. The input of Mr Hong Guojun, the manager of the NERCD and mr Shu Wei, manager of the test site, were greatly appreciated. Their efforts were key in pushing the experiments forward. Mr Xiuhan Chen and miss Lu Zhang were very important in the initiation process of the project as well as the completion of the experiments. They were of great help with regard to the communication between different parties and helping this project becoming a success. The author wants to mention Jelte de Ridder who has been there every step of the way during the research and was a great project partner for the experimental research campaign. A word of thanks to everybody at the university and the NERCD who contributed to this project, for the help in making all of this possible.

Last but not least a special thanks to friends and family who supported the entire graduation process and my studies.

M.A. De Vreede
Delft, 10 April 2018

Abstract

Little is documented in literature regarding hydraulic processes in inclined and large diameter pipelines. The bulk of the previous research dates back 20 to 50 years and was done for small diameter pipelines of up to 150 mm.

This research focuses on gathering data and testing the existing models and ideas with regard to large diameter inclined pipelines and the hydraulic transport within them. The overall goals of the project are to gather knowledge on the less documented and studied principles of pipeline flows and validate ideas and semi-empirical models from previous researches.

Extensive laboratory experiments were conducted as part of a joint research programme between Delft University of Technology and the National Engineering Research Center for dredging equipment and technology in Shanghai. The experiments were executed with a flow loop with a pipe diameter of 300 mm. It contains a measurement section of over 110 meters, part of which is inclinable. Pipe inclination angles of 17.9, 28.9 and 44 degrees were tested with slurry concentrations up to 15 % at flow velocities between 2 and 7 m/s. The flow velocities, delivered concentrations, total pressures, differential pressures and pump data were recorded. Conducting these experiments on this scale under controlled laboratory conditions is a unique research.

Three semi-empirical models by Worster and Denny, Gibert and Wilson for inclined slurry transport are validated. A comparison is made between ideas from literature regarding deposition limit velocities, delivered concentrations, pipe inclination angles, stratified flow regimes, particle suspension and different flow directions.

The observations from previous researches with small pipe diameters are generally in line with the results of the experiments conducted for this thesis. The semi-empirical models prove to deliver accurate predictions of the total pressure gradients in heterogeneous flow regimes. With regard to stratified flows, it is proposed to modify the semi-empirical models by adding a factor to the suspension and solids effect terms. The factor is a function of deposition limit velocity, flow velocity, inclination angle and flow direction.

Summary

Introduction

The objective of this thesis is to gather knowledge on the less documented and studied principles of inclined pipeline flows. This goal is accomplished by comparing the results of experiments conducted with a flow loop with 300 mm pipe diameter to previously done researches and conceived ideas with regard to inclined slurry transport.

State of art

The three most interesting semi-empirical models for inclined heterogeneous flow (Worster and Denny, Gibert, Wilson) all contain the Darcy Weisbach friction losses for horizontal water flow, the solids effect and particle suspension. The different models have different exponents added to the cosine of the solids effect term. For Worster and Denny it is 1, Gibert 1.5 and Wilson $1 + M$. The semi-empirical models do not account for differences in internal flow structure that occur in ascending and descending flow directions.

Shook and Roco, Matousek and Doron created two and three layer models based on force balances of stratified flows rather than (semi-)empirical observations. The models identify different layers for different flow regimes. Inputs for the layered models are the cross sectional area and friction factors on the interfaces of the different layers. These inputs are hard to acquire.

The experimental researches regarding inclined pipe flows are mostly limited to small diameter pipelines with maximum of 150 mm. A large range of different particle sizes is tested. De Hoog et al., Wilson and Tse, Hashimoto et al., Matousek and Vlasak, Doron, Spelay, Eltoukhy, Diniz and Coiado found that the deposition limit velocity (DLV) in ascending flows is higher than for horizontal flow. In descending flow directions it is lower. The highest deposition limit velocity is found at 30 degrees pipe inclination in the ascending flow direction. At mixture flow velocities over the DLV, the bed moves, delivered concentration increases and the in-situ concentration decreases.

Eltoukhy, Diniz and Coiado, Matousek and Wilson concluded that the hydraulic gradients in ascending inclined pipe flow are always higher than the horizontal pressure gradients and in inclined descending lower. Furthermore, the delivered concentration was found proportional with the pressure gradients in ascending slurry flows and inverse proportional with descending flows. Higher inclination angles corresponded with higher pressure gradients in the ascending flow and with lower pressure gradients in the descending flow directions. Generally, higher flow velocities cause higher pressure gradients.

With regard to the frictional pressure drop, Matousek and Vlasak concluded that the effect of pipe inclination is negligible at concentrations below 8 % or high flow velocities for finer particles. When coarser particles are tested, the frictional pressure drop increases with increasing pipe inclinations, and the maximum is reached at pipe inclination angles between 20 and 40 degrees.

Spelay et al. found that below 20 degrees pipe inclination, the turbulent suspension mechanisms play an important role on the deposition limit velocity. For finer particles, pipe inclination has nearly no effect on DLV. For coarser solids, the DLV increases significantly with increasing pipe inclinations and decreasing flow velocities.

As found by Vlasak, the concentration in a slurry flow with large particles is linearly distributed with a value of 0 in the upper portion of the pipe and the maximum near the bottom. Pipe inclinations below ± 30 degrees, have little influence on the concentration distribution. At higher flow velocities, the concentration near the pipe bottom decreased a with a greater effect at higher pipe inclinations angles. A larger zero concentration

area is observed in the descending section than in the ascending section and at higher pipe inclinations. The effect of the inclination angle on the pressure gradient of the mixture is mostly due to the static pressure gradients of the mixture.

Test setup

To gain insight in the characteristics of inclined slurry transport, a flow loop is used with a pipe diameter of 300 mm. The flow loop contains inclinable, horizontal and perspex measurement sections that cover a combined distance of over 110 meters. The inclinable section can reach pipe inclination angles of up to 45 degrees. The measurement section includes 34 total pressure sensors and 32 differential pressure meters, a flow meter, concentration meter, thermometers and a u-loop. The pump has capacity of 1600 m^3/h, its RPM, power and the pressures over it are recorded. The two slurry tanks have a capacity of 100 m^3 each and the setup can be cooled with a special cooling section. The used sand is considered broad graded and coarse and has a d_{50} of 0.77 mm.

Inclination angles of, 0, 17.9, 18.9 and 44 degrees are tested with six different delivered solids concentrations between 0 and 15%. Each test cycle is executed three times at several different flow rates. A water run is conducted to gain reference measurements. When the water cycle is done, the flow rate is increased to 1600 m^3/h, sediment is added and the flow rate is incrementally decreased in steps between 50 and 100 m^3/h.

Results

The reference measurements prove that the pressure sensors and flow meter function correctly. The delivered concentrations are best determined using the u-loop or the results from the ultrasonic density meter divided by 1.9. The accuracy of the results varies for different tests, configurations and concentrations.

The higher inclination angles show a higher spread in total pressure gradients with different spreading in ascending, descending and horizontal sections. Whereas the horizontal pressure gradients of the water flow experiments in the same flow loop configuration display a constant trend. When slurries are tested, the results of the ascending section appear more constant improving with increasing delivered concentration. A small portion of the measurements can be viewed as less accurate than the other test results due to physical phenomena, availability or malfunctioning of sensors or the general build-up of the flow loop. Most of the results however, fall within a reasonable accuracy range when compared to the trends of the results.

The pressure gradients for the horizontal section show a peak for the flow velocities where the stationary bed was observed in the perspex section. Similar to the horizontal section, an elevation in total pressure gradients is observed in the ascending section. This elevation is presumably associated with the stationary bed and is observed at higher flow rates than the stationary bed in the horizontal section. At higher inclination angles the peak for the ascending stationary bed smooths out, during the 44 degrees experiments it is hardly visible.

The delivered concentrations, as determined using both the u-loop and the ultrasonic density meter, decrease at lower flow velocities as a result of the solids that are left in the stationary beds in the horizontal and ascending sections. In the descending section, a peak in total pressure gradient is observed at low flow velocities, high concentrations and increasingly high pipe inclination angles. It is probably due to the effect of thickening of the suspension.

Generally, it was observed that higher pipe inclination angles or higher delivered concentration cause higher total pressure gradients in the ascending section and lower total pressure gradients in the descending sections. They are the result of a combination of (hydro)static and frictional gradients. In the ascending flow directions, the delivered concentration profiles are proportional with the total pressure profiles. In the descending section they are inversely proportional. The total pressure gradients in the ascending flow direction are observed to always be higher than the horizontal gradients and in descending flow direction they are always lower.

Evaluation of results

The calculated estimation of the total pressure gradients using the semi-empirical models is generally close to the measured total pressure gradients. However, the measured total pressure gradients are still marginally underestimated in the ascending and overestimated in the descending section by the calculated total pressure gradients especially in for stratified flow regimes. The semi-empirical model by Worster and Denny is closest to the measured results in the ascending flow direction and Wilson in the descending. The differences between the models are marginal (non existent for low concentrations) and are caused by the exponent attached to the cosine of the solids effect term. A result is that the increase of inclination angles decreases the differences between the different models since the impact of the solids effect on the total pressure gradient reduces. An increase in the measured solids effect in the horizontal section increases the differences between the models.

In line with the conclusions from literature, the flow velocity at which stationary deposits are formed in ascending sections, increases with increasing pipe inclination until a maximum is reached around 30 degrees pipe inclination. For increasing pipe inclinations, the step change associated with the stationary bed shifts towards higher flow velocities and gradually smooths out until it is no longer visible at 44 degrees pipe inclination.

Regardless of concentration or flow velocity the total pressure gradients measured in ascending flow directions are always higher than the horizontal hydraulic gradients and descending always lower. Furthermore higher inclination angles cause higher total pressure gradients in ascending flow directions and lower total pressure gradients in descending flow directions. An increase in total pressure gradients is witnessed at low flow velocities in both the descending flow directions as a result of stratified flows. The mechanical friction of the solids with the pipe wall causes higher pressure losses. The internal structure properties that were observed in other researches can unfortunately not be validated. The delivered concentration was indeed found proportional with the total pressure gradients in ascending slurry flows and inverse proportional in descending flows.

Identifying different layers when calculating the pressure losses in a stratified flow, can be a solution to the over- and underestimations of the total pressure gradients by the semi-empirical models. However, these models need input values such as the velocities of the different layers or their cross sectional areas, which are hard to estimate.

For this research 300 mm pipe diameter is used, which is twice the largest pipe diameter of previous experimental researches. The results are quite similar with regard to DLV and stratification. Different effectivenesses of turbulent suspension in relation to the pipe diameter play an important role in the frictional mechanisms inside the pipeline. More effective turbulent suspension due to the d/D of 0.0025 causes different frictional pressure losses than the d/D of over 0.1 that is used in other researches.

The inclined pipeline section at 44 degrees pipe inclination is the shortest length that was tested. As it is still has a length 17.5 m, and a L/D of over 58, it can hardly be considered a short pipeline. However, it can be argued that the increased variations in the total pressure gradients of the descending section are caused by the (shorter) length of the pipeline section.
Modification

Conclusions and recommendations

Semi-empirical models

The calculated estimation of the total pressure gradients using the semi-empirical models is generally quite accurate but does not account for differences internal flow structure and stratification effects. As a result, the measured total pressure gradients are marginally underestimated in the ascending and overestimated in the descending section during stratified flow regimes. The differences between the models are marginal (non existent for low concentrations) and Worster and Denny most closely predicts the total pressure gradients in the ascending section and Wilson in the Descending. The increase of inclination angles decreases the differences between the different models caused by the impact of the cosine in the solids effect term. An increase in the measured solids effect in the horizontal section increases the differences between the models. Identifying

different layers when calculating pressure losses in a stratified flow, can be a solution to the over- and under-estimations of the total pressure gradients by the semi-empirical models. However, the input values these models require such as the friction factors on the interfaces of the different layers or their cross sectional areas are difficult estimate.

Observations in literature

In line with the observarions by de Hoog et al., Wilson and Tse, Hashimoto et al., Matousek and Vlasak, Doron, Spelay, Eltoukhy, Diniz and Coiado. The deposition limit velocity in ascending flows is higher than horizontal flow. In descending flow directions it is probably lower. The highest deposition limit velocity is found around 30 degrees pipe inclination in the ascending flow direction. Regardless of concentration or flow velocity the total pressure gradients in ascending flow directions are higher than the horizontal pressure gradients and descending always lower. The delivered concentration is proportional with the pressure gradients in ascending slurry flows and inverse proportional with descending flows. Higher inclination angles corresponded with higher total pressure gradients in the ascending flow and with lower total pressure gradients in the descending flow directions. Higher flow velocities cause higher total pressure gradients. The effect of the pipe inclination angles on the pressure gradient of the mixture is mostly due to the static pressure gradients of the mixture. Total pressure gradients increase for decreasing flow velocities in both the flow directions as a result of stratified flows. The mechanical friction of the solids with the pipe wall causes higher pressure losses.

Main research question

"Are the existing mathematical, physical and semi-empirical models and ideas with regard to slurry transport in inclined pipelines applicable to large diameter inclined pipes?"

For this research a pipe diameter of 300 mm is used, which is twice the largest pipe diameter of previous experimental researches. The results are quite similar with regard to DLV and stratification effects.

The semi-empirical models are quite accurate with regard to inclined pipe flows for heterogeneous flow regimes. The models do not take different flow regimes into account and have to be modified in order to account for flow stratification. A distinction is made between ascending and descending flow directions. The solids effect is shifted according to the Wilson and Tse graph. In the ascending flow direction this shift and the elimination of the cosine, gives more accurate total gradient predictions. In descending flow direction, a ratio between suspended particles and particles in the stratified bed becomes key in the accuracy of the prediction. A modification on the suspension and solids effect terms in the semi-empirical models is required which is a function of the deposition limit velocity, flow velocity, pipe inclination angle and flow direction. In general, the conclusions from previous researches with regard to (smaller diameter) inclined slurry transport are applicable to the larger pipe diameters tested for this thesis research.

Recommendations

- Add electro-resistive tomography instruments or radio metric density meters to the flow loop.
- Solve issue with regard to concentration determination.
- Add perspex segments to the inclined sections of the flow loop.
- Increase pipe diameters of the flow loop.
- Test more pipe inclination angles.
- Increase pump capacity to test higher flow velocities.
- Test larger particle sizes and sands with narrower particle size distributions.
- Increase delivered concentrations.
- Validate the two and three layer models.
- Combine experimental results with computational fluid.
- Create modification on semi-empirical models to account for inclined stratified flows.

Contents

Nomenclature

List of symbols with description and units in order of appearance.

Symbol	Description	Unit
D	pipe diameter	$[m]$
L	length pipeline section	$[m]$
V	flow velocity	$[m/s]$
τ_0	shear stress at pipe wall	$[Pa]$
P_1	local pressure 1	$[Pa]$
P_2	local pressure 2	$[Pa]$
ΔP	pressure drop	$[Pa]$
i_l	hydraulic gradient liquid	[-]
i_m	hydraulic gradient mixture	[-]
ρ_l	liquid density	$[kg/m^3]$
ρ_m	mixture density	$[kg/m^3]$
ρ_s	solids density	$[kg/m^3]$
g	gravitational constant	$[m/s^2]$
H	head	$[m]$
ω	inclination angle	$[^o]$
H_{pipe}	height difference between pressure taps	$[m]$
λ_f	Darcy Weisbach friction coefficient	[-]
V_f	mean slurry flow velocity water	$[m/s]$
Re	Reynolds number	[-]
k	pipe wall roughness	$[m]$
μ_f	dynamic viscosity	$[Pa.s]$
ν_f	kinematic viscosity	$[m^2/s]$
ΔP_ω	total pressure drop over inclined section	$[Pa]$
U	slurry flow velocity	$[m/s]$
C_{vd}	delivered volumetric concentration	[-]
S_s	relative solids density	[-]
K	empirical constant Gibert	[-]
d	solid particle diameter	$[m]$
v_t	terminal settling velocity solids particles	$[m/s]$
M	particle size distribution factor Wilson	[-]
d_{50}	50 % passing particle diameter	$[m]$
d_{85}	85 % passing particle diameter	$[m]$
μ_{sf}	coefficient for mechanical friction	[-]
V_{50}	flow velocity at which half the solids are suspended	$[m/s]$
V_m	mean mixture flow velocity	$[m/s]$
ρ_1	density of the suspension in the upper layer	$[kg/m^3]$
A_1	cross section area of the upper layer	$[m^2]$
τ_1	shear stress at the flow boundary as defined by O_1	$[Pa]$
O_1	perimeter of pipe in the upper layer	$[m]$
τ_{12}	Shear stress at the interface between the upper and lower layer	$[Pa]$
O_{12}	perimeter of the stratified flow interface	$[m]$
A_2	cross sectional area of the lower layer	$[m^2]$
τ_{2f}	shear caused by the liquid flow as defined by O_2	$[Pa]$

O_2	perimeter of the lower layer	
F_W	force exerted by the submerged weight of the granular bed	$[N]$
F_N	intergranular force on the pipe wall	$[N]$
A	cross sectional area pipe	$[m^2]$
β	pipe inclination angle Doron	$[^o]$
S_h	perimeter heterogeneous layer shear stress	$[m]$
S_{sb}	perimeter stationary bed layer shear stress	$[m]$
S_{mb}	perimeter moving bed layer shear stress	$[m]$
S_{hmb}	perimeter interfacial layer between heterogeneous layer and moving bed	$[m]$
S_{mbsb}	perimeter interfacial layer between moving bed layer and stationary bed layer	$[m]$
τ_h	heterogeneous layer shear stress	$[Pa]$
τ_{mb}	moving bed layer shear stress	$[Pa]$
τ_{sb}	stationary bed layer shear stress	$[Pa]$
τ_{hmb}	interfacial layer shear stress between heterogeneous layer and moving bed	$[Pa]$
τ_{mbsb}	interfacial layer shear stress between moving bed and stationary bed	$[Pa]$
F_{hG}	weight heterogeous layer	$[N]$
F_{mbG}	weight moving bed layer	$[N]$
F_{sbG}	weight stationary layer	$[N]$
F_{mbsb}	Coulombic friction force between moving bed and stationary bed	$[N]$
F_{mb}	Coulombic friction force between moving bed and pipe wall	$[N]$
F_{sb}	Coulombic friction force between stationary bed and pipe wall	$[N]$
A_h	cross sectional area heterogeneous layer	$[m^2]$
A_{mb}	cross sectional area moving bed layer	$[m^2]$
A_{sb}	cross sectional area stationary bed layer	$[m^2]$
z	height difference between pressure taps on u-loop	$[m]$
C_{vi}	in situ concentration	
S_{mi}	relative in situ mixture density	[-]
v_t'	hindered settling velocity	$[m/s]$
Q_l	liquids flow rate	$[m^3/h]$
Q_s	solids production	$[m^3/h]$
U_l	flow velocity liquid	$[m/s]$
U_s	velocity solids	$[m/s]$
C_1	delivered solids concentration 1	[-]
C_2	in situ solids concentration 2	[-]

List of Figures

List of Tables

1 Introduction

1.1. Background

Hydraulic transport using horizontal or vertical, small diameter, pipelines has been widely studied and documented. Hydraulic processes in inclined and large diameter pipelines are much less documented in literature and the bulk dates back 20 to 50 years. A large portion of the previous research with regard to pipelines at a certain tilt was done for small diameter pipelines up to 150 mm. This research focuses on gathering data and testing the existing models and ideas with regard to large diameter inclined pipelines and the hydraulic transport within them. The overall goals of the project are to gather knowledge on the less documented and studied principles of pipeline flows and put the more documented ideas to the test.

The topic, research and experiments are the result of a joint research programme between Delft university of technology in Delft and the National engineering research center for dredging technology and equipment in Shanghai. The test setup and experiments are a unique opportunity to gain an insight in the processes taking place in a large diameter inclined pipeline. Moreover, the study is noteworthy since the experiments are conducted under controlled laboratory circumstances.

The focus in this study is especially on the pressure gradients, volumetric concentrations, inclination angles, transport velocities, deposition limit velocity and friction losses. The results of the experiments are used to validate the existing semi-empirical models for hydraulic transport in inclined pipelines and gain an insight on the processes within them. Furthermore, the results of the experiments are compared to the conclusions of previous experiments that were conducted with smaller pipe diameters. The study can prove to be useful for the dredging- and mining industries with regard to the frictional losses, efficiency of transport or the wear in pipelines. Inclined pipelines are widely used within these industries at for instance road crossings, mine shafts or the riser of a trailer suction hopper dredger.

1.2. Objective

The goal of this project is to gather knowledge on the less documented and studied principles of pipeline flows. This knowledge is to be validated using the models and literature that is already available. The models and other literature were based on hydraulic transport in smaller diameter pipeline sections and one of the objectives of this study is to find out whether the conclusions from those researches are applicable on pipelines with a larger diameter. The aforementioned research parameters are used to gain an insight in the processes taking place within the inclined pipeline sections. Doing these tests in a controlled laboratory environment shows great promise for the measurements but also for future laboratory work regarding inclined slurry transport. Pressure gradients, concentration, inclination angles and flow velocity profiles are investigated in order to validate existing models and ideas.

The flow loop that is used in these experiments was outfitted with a large number of pressure sensors and differential pressure sensors at constant intervals. This provides the opportunity to gain an insight in the pressure gradient profile over longer distances as a result of, for instance, flanges or bends. In the inclined

sections of the setup, the ascending and descending hydraulic flow phenomena are studied in detail. The scope of this thesis focuses mainly on the inclined pipeline sections and the total pressure gradients at different flow velocities with different concentrations.

1.3. Research questions

In order to achieve the research objectives, one main research question is formulated:
"Are the existing mathematical, physical and semi-empirical models and ideas with regard to slurry transport in inclined pipelines applicable to large diameter inclined pipes?"

The answer to the main research question is found using the six sub research questions:

- "What are the existing models and ideas with regard to hydraulic transport in inclined pipelines?"
- "Which test setup and experiment protocol are required to gain an insight in flow characteristics in an inclined large diameter pipeline?"
- "To what extent do the acquired results from the laboratory experiments agree with the estimated values from the semi-empirical models?"
- "Do the acquired results from the laboratory experiments agree with the observations and insights from past experiments?"
- "Are the semi-empirical models applicable on short inclined pipeline sections?"
- "Are the results of experiments with small pipe diameters similar to the measurement results with larger pipe diameters?"

1.4. Methodology

The sub-questions are organized following the structure of the thesis and the methodology of the research. This study starts with the state of the art where the literature and existing ideas regarding inclined pipelines are discussed. Next is the experimental phase of the research, the layout of the test setup is discussed as well as the protocol and data acquisition methods. After the experiments, the semi-empirical models are compared and validated using the acquired data. Furthermore, the similarities between the measured results and conclusions from literature are analysed and compared. From this evaluation, the applicability of the ideas and models from literature on larger diameter pipelines or short pipeline sections is found.

2

State of the art

The literature that was investigated for this thesis research is discussed in this chapter and split up over the sections definitions, semi-empirical models, physical models, inclined coarse particle transport and settling slurries. Several models and ideas for hydraulic transport in inclined, horizontal and vertical pipelines are considered. The models discussed in this section are: the Darcy and Weisbach model for water flow in horizontal pipelines, the Equivalent liquid model. The four semi-empirical models for inclined heterogeneous transport by Worster & Denny [1955], Gibert [1960], Graf [1984] and Wilson [2006] are discussed. The two, two layer models by Shook and Roco [1991], Matousek [1997] and the three layer model by Doron [1997] are looked into. Furthermore, some of the results of experimental researches with regard to inclined pipe flow by Hashimoto [1980], Clift [1981], Graf [1984], Wilson and Tse [1984], Matousek [1997], Diniz and Coiado [1999], Eltoukhy [2013], Vlasak [2014], Matousek and Vlasak [2015], Spelay [2016] and de Hoog [2017] are discussed. In those experimental studies, the focus is mainly on deposition limit velocities, inclination angles, flow velocities, concentrations, particle sizes and pressure losses. The conclusion to this chapter provides an answer to the research question "What are the existing models and ideas with regard to hydraulic transport in inclined pipelines?".

2.1. Definitions

In this section, the basics and definitions behind frictional head loss in inclined and horizontal flow directions are described. The sections regard the pressure losses and - gradients, manometric gradients, liquid flow, Darcy Weisbach, the equivalent liquid model, the relation between production and concentration and the solids effect.

2.1.1. Frictional head loss

Figure 2.1, from the Matousek lecture notes [Matousek, 2004], displays a horizontal pipeline section with diameter D and length L.

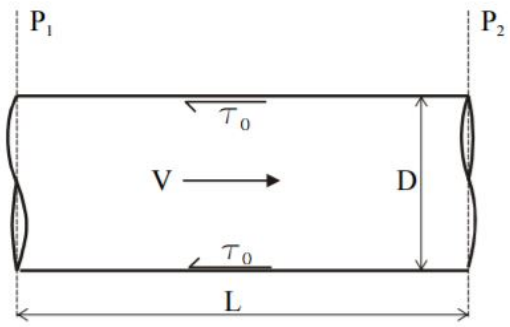

Figure 2.1: Flow in a horizontal pipeline section

Hydraulic transport in the pipeline section takes place at flow velocity V in the direction of the arrow. The τ_0 represent the local shear stress at the pipe wall causing a pressure drop between upstream and downstream. Two pressures P_1 and P_2 are recorded, the pressure drop or differential pressure ΔP is defined by: $\Delta P = P_1 - P_2$ [Pa]. By dividing the pressure drop by the length of the pipeline section, the pressure gradient is determined: $\Delta P/L$ [Pa/m].

The dimensionless hydraulic gradient or frictional head loss of a mixture i_m is found when the measured pressure drop is divided by $\rho_l g L$. With the density of the carrier liquid ρ_l and gravitational constant g. Equation 2.1 shows the definition of the dimensionless hydraulic gradient for horizontal mixture flows.

$$i_m = \frac{\Delta P}{\rho_l g L} \tag{2.1}$$

The mechanical energy per unit mass is defined as head in equation 2.2 where H is head.

$$H = \frac{\Delta P}{\rho_l g} \tag{2.2}$$

In horizontal water flow, the hydrostatic pressure component is not taken into account and only frictional losses are considered. When a pipe is tilted or inclined, a hydrostatic component starts influencing the local pressures P_1 and P_2. Figure 2.2 [Matousek, 2004] displays a downwards inclined pipeline section with a two layer pattern length L and inclination angle ω.

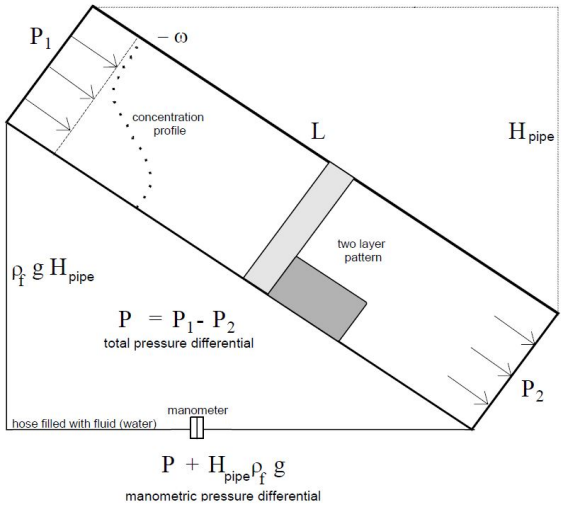

Figure 2.2: Flow in inclined pipeline section

The total pressure gradient over the pipeline section in figure 2.2 is $(P_1 - P_2)/L$. It is built up from two components; a static and a frictional pressure gradient. The static pressure gradient is a result of the static force the that is exerted at the pressure taps by the mixture. It is given by equation 2.3.

$$\frac{P_{hydrostat}}{L} = \frac{\rho_m g H_{pipe}}{L} = \frac{\rho_m g L sin(\omega)}{L} = \rho_m g sin(\omega) \tag{2.3}$$

The frictional pressure gradient $\Delta P_{fric}/L$ is the result of equation 2.4 where the static pressure gradient of the mixture is subtracted from the the total pressure gradient.

$$\frac{\Delta P_{fric}}{L} = \frac{P_1 - P_2}{L} - \frac{\rho_m g H_{pipe}}{L} \tag{2.4}$$

In equation 2.4, ρ_m is the mixture density and H_{pipe} the height difference between the two pressure taps. H_{pipe} equals $Lsin(\omega)$, the height H_{pipe} varies with the inclination angle ω. When the pressure difference is measured with differential pressure sensors, the hydrostatic pressure in the impulse tubes automatically compensates for the hydrostatic water pressures in the pipe so the water pressure difference is not included in its results.

When manometric pressure differentials are recorded, the influence of the hydrostatic pressure is included in the results. The manometric pressure differential corresponds with the difference between the local pressures P_1 and P_2 with the hydrostatic pressure difference included.

2.1.2. Liquid flow

The Darcy Weisbach method for frictional losses in water flow [Matousek, 2004] in horizontal pipeline sections is described in this section. The method presumes a turbulent flow regime for a horizontal pipelines. The pressure gradient for Darcy Weisbach friction losses $(-dp/dx)$ is determined using equation 2.5.

$$-\frac{dP}{dx} = \frac{\Delta P}{L} = \frac{P_1 - P_2}{L} = \frac{\lambda_f}{D}\frac{1}{2}\rho_l V_l^2 \tag{2.5}$$

The hydraulic gradient for horizontal liquid flows that follows from the Darcy Weisbach equations is expressed in equation 2.6 by i_l.

$$i_l = \frac{\Delta P_l}{\rho_l g L} = \frac{\lambda_f V_f^2}{2gD} \tag{2.6}$$

The Darcy Weisbach friction factor (λ_f) is found using the Churchill approximation [Churchill, 1977]. With equations 2.7, 2.8, 2.9 and 2.10 the friction factor can be found. In the equations, L is the length of the pipeline section over which the pressure change is checked. The D is the pipe diameter, ρ_l is the water density and V_f is the mean slurry flow velocity in the pipe. Where Re is the Reynolds number, k is the pipe wall roughness, μ_f is the dynamic viscosity and ν_f is the kinematic viscosity.

$$\lambda_f = 8\left[\left(\frac{8}{Re}\right)^{12} + (X+Y)^{-1.5}\right]^{\frac{1}{12}} \tag{2.7}$$

$$X = \left(-2.457 ln\left[\left(\frac{7}{Re}\right)^{0.9} + \frac{0.27k}{D}\right]\right)^{16} \tag{2.8}$$

$$Y = \left(\frac{37530}{Re}\right)^{16} \tag{2.9}$$

$$Re = \frac{V_f D \rho_f}{\mu_f} = \frac{V_f D}{\nu_f} \tag{2.10}$$

The pressure gradient of the liquid flow in an inclined section with length L and inclination angle ω, is found by combining equations 2.5 with equation 2.3. Equation 2.11 is the result of this combination with ΔP_ω representing the total pressure drop over the inclined pipe section.

$$\frac{\Delta P_\omega}{L} = \frac{\lambda_f}{D}\frac{1}{2}\rho_l V_l^2 + \rho_l g sin(\omega) \tag{2.11}$$

The pressure gradients in kPa/m for liquid flow in inclined pipe sections, as they were found with equation 2.11 were plotted in figure 2.3 as a function of the flow velocity U in meters per second.

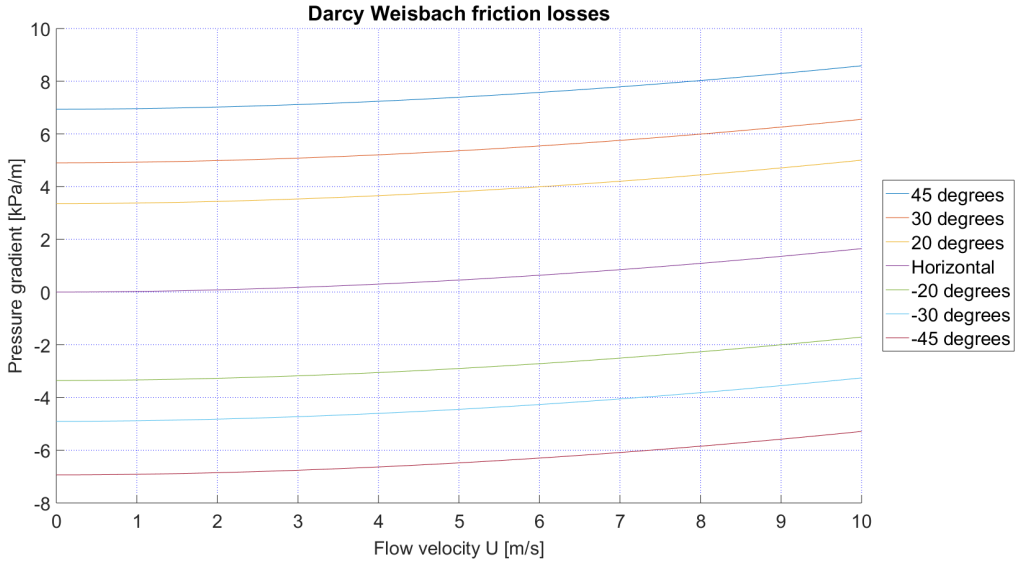

Figure 2.3: Pressure gradient for Darcy Weisbach liquid flow in horizontal and inclined pipeline sections

2.1.3. Production and concentration

To determine the production of solids Q_s when the flow velocity of the water U_l is the equal to the velocity of the solids U_s equation 2.12 is used where C_1 is solids concentration, A is pipe cross sectional area and Q_l is the flow rate of water.

$$Q_s = C_1 Q_l = C_1 U_l A \tag{2.12}$$

When the flow velocity of water is higher than the velocity of the solids, the production of solids is determined using equation 2.13. In this case, C_2 is the solids concentration.

$$Q_s = C_2 U_s A \tag{2.13}$$

For equal production, the ratio between the two concentrations is found in equation 2.14.

$$U_s C_2 = U_l C_1 \tag{2.14}$$

This equation illustrates that when the flow velocity of the solids in the pipe is lower than flow rate of the carrier liquid, the concentration of solids that is measured in the pipe (C_2, in situ concentration) is higher than the solids concentration that is measured at the end of the pipeline (C_1, delivered concentration).

2.1.4. Equivalent liquid model

The Equivalent liquid model (ELM) [Matousek, 2002] can basically be viewed as a modification on the Darcy-Weisbach model for liquid flows. In the equivalent liquid model, the frictional head loss for mixture flows is determined. According to the Equivalent liquid model, the density of the mixture influences the wall shear stress. The ELM states that the frictional head loss of the mixture is given by: $i_m = i_l \frac{\rho_m}{\rho_l}$. This means that equation 2.1 can be modified to account for slurries instead of liquids. This results in equation 2.15, the hydraulic gradient for mixture flows (i_m) with mixture density ρ_m. In this model it is assumed that there are no other losses due to, for instance, particle collisions, sliding or stationary beds. Moreover, the solid particles in the slurry have to be fine enough not to influence the flow patterns and sub-layers.

$$i_m = \frac{\Delta p_m}{\rho_l g \Delta L} = \frac{\lambda_f V_f^2}{2gD} \frac{\rho_m}{\rho_l} = i_l \frac{\rho_m}{\rho_l} \tag{2.15}$$

The results of equation 2.15 are dimensionless hydraulic gradients. To translate these into pressure gradients, the i_m is multiplied by $\rho_l g$ as seen in equation 2.16

$$i_m \rho_l g = i_l \frac{\rho_m}{\rho_l} \rho_l g = i_l \rho_m g \tag{2.16}$$

From equation 2.16 it is clearly visible that the ELM is based on a ratio between the hydraulic gradients of the mixture and the liquid.

2.1.5. Solids effect

The solids effect is defined as hydraulic loss due to frictional resistance by the presence of solids (i.e. a stratified bed). Mathematically it is defined as the difference between the hydraulic gradients of the mixture and the transport liquid: $i_m - i_l$ for horizontal pipes and $i_{m,\omega} - i_l$ for inclined pipes. In the semi-empirical models that are discussed in the next section (except Graf), the solids effect is multiplied with the cosine of the inclination angle. As a result, the solids effect for horizontal pipe flows is higher than in inclined pipe flows. The effect is associated with the presence or absence of a stratified bed, since it decreases with increasing velocity and decreasing concentrations [Wilson et al., 2006]. The Worster & Denny, Wilson and Gibert models all use the same solids effect component in their model in terms of its structure. The cosine, however, has a different exponent added in the latter two models. In the model by Wilson it was introduced to account for differences in particle size distributions.

2.2. Semi-empirical models

The semi-empirical models by Worster and Denny [1955], Gibert [1960], Wilson [2006] and Graf [1984] are discussed in this section. First the three semi-empircal models by Worster and Denny, Gibert and Wilson are considered. Then a description of how the hydraulic gradients they include are translated into pressure gradients and finally the model by Graf.

2.2.1. Inclined Worster and Denny

A model for heterogeneous hydraulic transport in inclined pipelines is first mentioned in literature by Worster and Denny in their paper "hydraulic transport of solid material in pipes (1955)" [Worster and Denny, 1955]. Worster and Denny conducted experiments in horizontal pipelines of 2, 4 and 6 inch pipe diameters. The focus in their experiments was on hydraulic gradients, settling velocities, concentrations, particle diameter and - degradation. To account for pipe inclination angles, they combined the models for the hydraulic gradients in a horizontal pipe (equation 2.17) with the gradients in a vertical pipe (equation 2.18). By multiplying the solids effect of the horizontal equation with $cos(\omega)$ and the submerged density in the vertical section with $sin(\omega)$ and adding them together equation 2.19 is found. This model accounts for the manometric gradients in inclined pipelines at up- or downward sloping angles.

$$i_{m,hor} = i_l + (i_m - i_l) \tag{2.17}$$

$$i_{m,ver} = i_l + C_{vd}(S_s - 1) \tag{2.18}$$

$$i_{m,\omega} = i_l + (i_m - i_l)cos(\omega) + C_{vd}(S_s - 1)sin(\omega) \tag{2.19}$$

Equation 2.19 is built up of three components. The first is the hydraulic gradient for the horizontal liquid flow (i_l) from the Darcy Weisbach method. The second term is the solids effect of the slurry flow in a horizontal pipeline multiplied with the cosine of the inclination angle (ω). The term $c_{vd}(S_s - 1)sin\omega$ is the suspension term in the model and it accounts for the effect of the suspended particles in the slurry with delivered concentration C_{vd} and relative solids density S_s. Figure 2.4 displays how the model is constructed from vertical and horizontal hydraulic gradients.

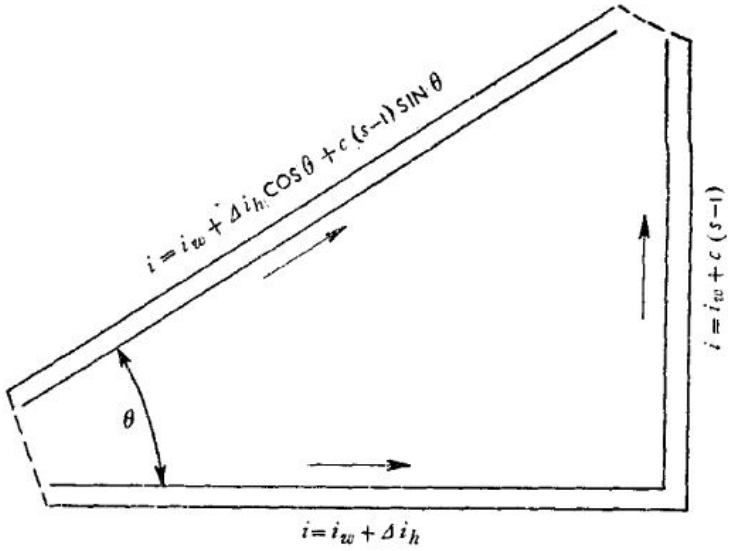

Figure 2.4: The basis for Worster and Denny model where the manometric gradient in inclined pipelines is a combination of the vertical and horizontal gradients

Worster and Denny tested and confirmed their model using a 1.5 inch (3.81 cm) diameter pipe system at several different pipe inclination angles. They stated in their paper that the results found in the 1.5 inch setup had not yet been tested for larger pipeline diameters.

2.2.2. Inclined Gibert

The model Gibert [Gibert, 1960] created is a modified version of the semi-empirical Durand and Condolios [Durand and Condolios, 1952] [Durand, 1953] correlation for horizontal pipe flows. He adapted their model and included pipe inclination angles. Gibert's modification is given by equation 2.20. In equation 2.20, K is an empirical constant, V_m is the flow velocity of the mixture, D is the pipe diameter, d is the solid particle diameter and v_t is the terminal settling velocity solid particles.

$$\frac{i_{m,\omega} - i_l}{i_l C_{vd}} = K\left(\frac{V_m^2}{gD}\frac{\sqrt{gd}}{v_t cos(\omega)}\right)^{-1.5} \tag{2.20}$$

When this is rewritten to find the manometric gradient for inclined slurry flows, equation 2.21 is found.

$$i_{m,\omega} = i_l C_{vd} K\left(\frac{V_m^2}{gD}\frac{\sqrt{gd}}{v_t cos(\omega)}\right)^{-1.5} + i_l \tag{2.21}$$

When equation 2.21 is modified into the same shape as the equation 2.19 [Matousek, 2004], equation 2.22 is the result.

$$i_{m,\omega} = i_l + (i_m - i_l)cos(\omega)^{1.5} + C_{vd}(S_s - 1)sin(\omega) \tag{2.22}$$

The semi-empirical model was based on findings with an inclinable flow loop with 150 mm pipe diameter. Gibert tested several different inclination angles, concentrations and flow velocities.

2.2.3. Inclined Wilson

Wilson came up with an heterogeneous inclined hydraulic transport model in 1997 [Wilson et al., 2006]. He modified the Worster and Denny model to make it take the effect of different particle size and particle size distributions into account. The M factor in equation 2.26 is introduced for this purpose. Factor M is an approximation that was introduced as a result of the Wilson-GIW correlation [Wilson et al., 2006] which was based on the log-log linear relation between the relative solids effect $\left(\frac{i_m - i_f}{C_{vd}(S_s-1)}\right)$ and the mean slurry velocity

after Clift et al. [Matousek, 2004]. The M factor varies from 0.25 for a broad particle size distribution to 1.7 for uniformly graded sand. The M factor is found by solving equation 2.23 where d_{50} is the 50 % passing particle diameter and d_{85} is the 85 % passing particle diameter.

$$M \approx \left[ln\left(\frac{d_{85}}{d_{50}}\right)\right]^{-1} \tag{2.23}$$

The semi-empirical equation 2.24 provides a prediction for the manometric mixture gradients during hydraulic transport in an inclined pipeline. The equation can be cast into the same form as the Worster & Denny and Gibert models. By doing this, the different models can be compared to each other and the data.

$$i_{m,\omega} = i_l + \frac{\mu_{sf}}{2}\left(\frac{v_m}{v_{50}}\right)^{-M}(S_s-1)C_{vd}(cos(\omega))^(1+M) + C_{vd}(S_s-1)sin(\omega) \tag{2.24}$$

Similar to the other two models, i_f is the hydraulic gradient for water flow. The second term of equation 2.24 consists of two main parts, the Wilson-GIW correlation for horizontal flows which is an empirical correlation that approximates the theoretical solids effect. It consists of the μ_{sf} coefficient of mechanical friction between solids and pipe wall; V_m mean mixture velocity;S_s relative solids density and C_{vd} delivered volumetric concentration. The last term in the equation is the suspension term. The V_{50}, the velocity at which half the solids are suspended, is given by equation 2.25.

$$V_{50} \approx 3.93(d_{50})^{0.35}\left(\frac{S_s-1}{1.65}\right)^{0.45} \tag{2.25}$$

When the solids effect term is modified into $(i_m - i_l)cos(\omega)^{(1+M)}$, equation 2.26 is left.

$$i_{m,\omega} = i_l + (i_m - i_l)cos(\omega)^{(1+M)} + C_{vd}(S_s-1)sin(\omega) \tag{2.26}$$

The experiments that were conducted to find the data at the bases of this semi-empirical model is found in sections 2.4.2 and 2.3.1.

2.2.4. Pressure gradients

The semi-empirical models that were discussed in sections 2.2.1, 2.2.2 and 2.2.3 represent manometric pressure gradients. To account for the geodetic height difference, a dimensionless term $sin(\omega)$ has to be added as a fourth term. To convert the dimensionless gradient into the total pressure gradients, they have to be multiplied by $\rho_l g$. Equations 2.27 to 2.29 show the results for the Worster Denny model (2.27), the Gibert model (2.28) and the Wilson model (2.29). In the equations, the $\Delta P_\omega / L$ represents the total pressure gradient in Pa/m, $\Delta P_{l,hor}/L$ the Darcy Weisbach pressure gradient for water and $\Delta P_{m,hor}/L$ the pressure gradient for horizontal mixture flow.
Worster and Denny total pressure gradient:

$$\begin{aligned}\frac{\Delta P_\omega}{L} &= i_l\rho_l g + (i_m - i_l)cos(\omega)\rho_l g + C_{vd}(S_s-1)sin(\omega)\rho_l g + sin(\omega)\rho_l g = \\ \frac{\Delta P_{l,hor}}{L} &+ \left(\frac{\Delta P_{m,hor}}{L} - \frac{\Delta P_{l,hor}}{L}\right)cos(\omega) + C_{vd}(S_s-1)sin(\omega)\rho_l g + sin(\omega)\rho_l g\end{aligned} \tag{2.27}$$

Gibert total pressure gradient:

$$\begin{aligned}\frac{\Delta P_\omega}{L} &= i_l\rho_l g + (i_m - i_l)cos(\omega)^{1.5}\rho_l g + C_{vd}(S_s-1)sin(\omega)\rho_l g + sin(\omega)\rho_l g = \\ \frac{\Delta P_{l,hor}}{L} &+ \left(\frac{\Delta P_{m,hor}}{L} - \frac{\Delta P_{l,hor}}{L}\right)cos(\omega)^{1.5} + C_{vd}(S_s-1)sin(\omega)\rho_l g + sin(\omega)\rho_l g\end{aligned} \tag{2.28}$$

Wilson total pressure gradient:

$$\begin{aligned}\frac{\Delta P_\omega}{L} &= i_l\rho_l g + (i_m - i_l)cos(\omega)^{(1+M)}\rho_l g + C_{vd}(S_s-1)sin(\omega)\rho_l g + sin(\omega)\rho_l g = \\ \frac{\Delta P_{l,hor}}{L} &+ \left(\frac{\Delta P_{m,hor}}{L} - \frac{\Delta P_{l,hor}}{L}\right)cos(\omega)^{(1+M)} + C_{vd}(S_s-1)sin(\omega)\rho_l g + sin(\omega)\rho_l g\end{aligned} \tag{2.29}$$

2.2.5. Inclined Graf

Graf et al. proposed a model for inclined hydraulic transport [Graf, 1984]. The model is a modified version of Einstein's model for horizontal pipeline transport [Einstein and Graf, 1966] . It is displayed in equation 2.30 and represents the head loss of mixture flow in inclined pipelines. The equation is basically the same as the model Einstein came up with, except a sine was added to the second term on the right hand side of the equation.

$$\left(\frac{\Delta H}{\Delta L}\right)_m = \left(\frac{\Delta H}{\Delta L}\right)_l [1 + C(S_s - 1)] + C(S_s - 1) sin(\omega) \tag{2.30}$$

The liquid head loss is represented by $\left(\frac{\Delta H}{\Delta L}\right)_l$, C is the volumetric slids concentration of pseudo-homogeneous flow (i.e. delivered concentration). Graf et al. conducted experiments in a flow loop with a 76 mm pipe diameter and 2.85 mm sand. They tested different pipe inclinations and measured the head loss. At horizontal flow direction results were similar to the model predictions without the sine term added. Note that the results were only similar when pseudo-homogeneous flows were tested. For inclined pipe flows, they concluded that the model underestimated the head losses.

2.3. Physical models

Matousek and Doron had a different approach towards modelling a slurry flow. They came up with two and three layer models to account for flow stratification in a mixture flow using the force balances. This section describes the structure of the models. It starts with an explanation regarding stratified flows and is followed by the description of the two and three layer models.

2.3.1. Stratified flows

The models that were discussed in the previous sections assume an uniform concentration distribution in the pipeline cross section. Therefore these models are inadequate when unevenly distributed concentration profiles and/or lower flow velocities and/or coarser particles are modelled. The turbulence of the carrier liquid causes particles to be suspended. When the particle size is too large, or the turbulence too little to suspend the particles, the particles sink to the bottom of the pipe and form a bed. When a bed is formed, the flow is considered stratified. Matousek stated [Matousek, 1997] that the semi-empirical models for inclined pipe flow can only be valid when the flow is not stratified. During his research in Delft with a 150 mm inclinable flow loop he also observed "different degrees of flow stratification in the ascending pipe and the descending pipe for the same slurry flow conditions (flow velocity, delivered concentration, inclination angle)" in pipeline sections with inclination angles below 45 degrees. In the ascending section, it was found that the weight of the submerged bed acting against the flow direction, formed a thick shear layer. In the descending section, the reverse effect is accomplished, the velocity of the sliding bed is enough to keep the shear layer from forming. In other words: due to the submerged weight of the solid particles in the sliding bed, the sliding bed in an ascending section becomes stationary at higher flow rates than in a horizontal section. In the descending section, the opposite was observed, the same factors that slow the sliding bed in the ascending flow direction cause the bed to keep sliding in the descending flow direction. When finer particles are tested, the turbulence of the flow can keep the solids suspended at lower velocities and the aforementioned effect diminishes.

The static head or hydrostatic pressure of a slurry flow in an inclined pipeline is subject to change in case of varying concentration profiles. Matousek identifies two slurry states: a slurry state with suspended particles and a slurry state with particles in the bed. The suspended particles transfer their submerged weight to the carrier liquid contributing to the mixture density. The particles in the bed transfer their submerged weight to the pipe wall, the contact load. The result is that only the particles that are suspended in the slurry flow contribute to the static pressure differential of the mixture.

Matousek concluded that, to account for the contact loads, the suspended particles and the different mechanisms occurring in the ascending and descending sections, a two layer model had to be applied. In figures 2.2 and 2.5 schematic overviews of such approaches are displayed with two different layers, one for the solids in the bed and one for the suspension.

2.3.2. Inclined 2 layer model Matousek

With the conclusions regarding stratified flows in mind, Matousek created a two layer model [Matousek, 1997] that was based on the two layer model by Shook and Roco [Shook and Roco, 1991]. The models are built on the idea that a stratified flow in an inclined pipe line section consists of two layers as illustrated in figures 2.2 and 2.5. To account for both stratified and non-stratified flows, the model is built up from the force balances of two layers, the upper and lower layer. When the flow is stratified, the thickness of both the upper and lower layer are taken into account. For a non-stratified flow, the thickness of the lower layer equals zero, therefore the lower layer does not play a role in the calculation. In figure 2.5, a schematic representation of the two layer model by Matousek is displayed.

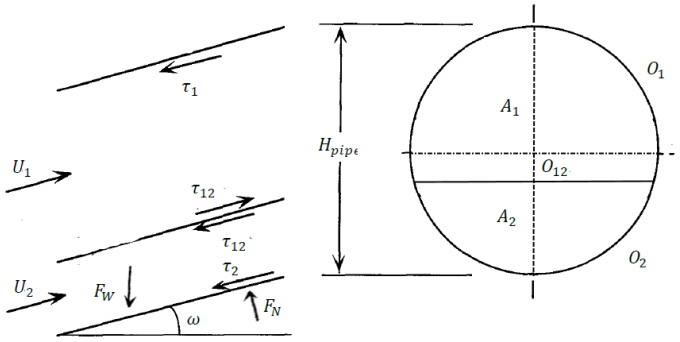

Figure 2.5: Schematic pipe section with two layers identified with model components labelled

Equation 2.31 contains the force balance of the upper layer where ΔP is the total pressure drop, ρ_1 is the density of the suspension in the upper layer, A_1 the cross section area of the upper layer, τ_1 the shear stress at the flow boundary as defined by O_1, the perimeter of pipe in the upper layer. Shear stress at the interface between the upper and lower layers is defined by τ_{12} and O_{12} is the perimeter of the stratified flow interface.

$$(\Delta P + H_{pipe}\rho_1 g)A_1 = \tau_1 O_1 L + \tau_{12} O_{12} L \tag{2.31}$$

The force balance in the lower layer is defined by equation 2.32. The cross sectional area of the lower layer is represented by A_2, τ_{2f} is the shear caused by the liquid flow as defined by O_2, the perimeter of the lower layer. The force exerted by the submerged weight of the granular bed is represented by F_W and the normal intergranular force on the pipe wall by F_N. The μ_s is the mechanical friction coefficient of solids against the pipe wall.

$$(\Delta P + H_{pipe}\rho_1 g)A_2 - F_W sin(\omega) = \tau_2 O_2 L + \mu_s F_N cos(\omega) - \tau_{12} O_{12} L \tag{2.32}$$

The combination of the upper and lower layers gives the force balance in the whole pipe section with cross sectional area A. Equation 2.33 displays this force balance.

$$(\Delta P + H_{pipe}\rho_1 g)A - F_W sin(\omega) = \tau_1 O_1 L + \tau_2 O_2 L + \mu_s F_N cos(\omega) \tag{2.33}$$

The terms on the right hand side of equation 2.33 represent the total pressure difference, the static pressure difference caused by the suspension in the upper layer and the weight of the lower layer. The terms on the right hand side represent the shear losses caused by the wall friction of the upper- and lower layers and the loss caused by the intergranular normal force on the pipe wall. The terms representing the losses caused by friction at the interface between the upper and lower layers, work in opposite direction so their effect is eliminated when equation 2.31 and 2.32 are added together.

The model takes into account that the ascending and descending flow directions have different effects on a stratified slurry flow. These inclination effects were not represented in the models for heterogeneous hydraulic transport in sections 2.2.1 to 2.2.3. Matousek states that the basis of this model for inclined slurry transport are in the physical picture of a friction process. Therefore the model distinguishes between frictional and static pressure differentials.

2.3.3. Inclined 3 layer model Doron

Doron and Barnea came up with a three layer model for horizontal flow [Doron et al., 1993]. It is modified to account for pipe inclination angles [Doron et al., 1997]. They identified three layers; a stationary bed layer at the bottom, a sliding bed layer on top of the stationary bed and a heterogeneous mixture flow layer in the upper part of the pipe cross section. Figure 2.6 illustrates the structure of the flow in a schematic pipe section with pipe inclination angle β.

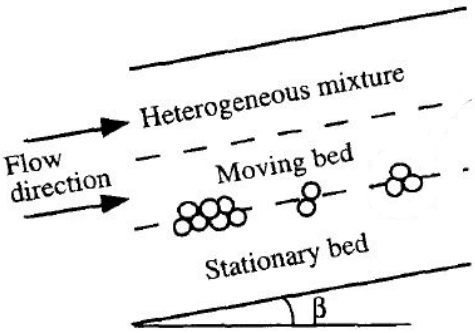

Figure 2.6: Schematic pipe section with three layers identified [Doron et al., 1997]

Similar to the two layer model by Matousek, the three layer model is based on the physical picture of a slurry flow in a pipeline section. Three equations for the different layers added together give the theoretical three layer model. Figure 2.7 illustrates the terms used in the equations of the model.

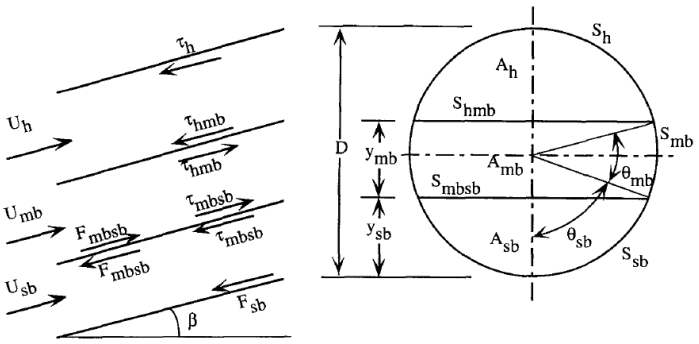

Figure 2.7: Schematic pipe cross section three layer model [Doron et al., 1997] with model components labelled

The losses in the heterogeneous mixture term, are built up from the upper layer shear losses, the interfacial shear losses and the gravitational force as seen in equation 2.34. S_h and S_{hmb} represent the perimeter where upper layer shear stress τ_h and the interfacial layer shear stress τ_{hmb} act on. The weight of the layer is represented by F_{hG}. The pressure drop is $\frac{dP}{dx}$ and A_h is the cross sectional area of the pipe occupied by the top layer.

$$A_h \frac{dP}{dx} = -\tau_h S_h - \tau_{hmb} S_{hmb} - F_{hG} \tag{2.34}$$

The moving bed with cross sectional area A_{mb} is described by the six terms on the right hand side of equation 2.35. It contains three interfaces and therefore three interface friction forces; the same one as in equation 2.34, the interface friction force between the stationary and moving beds $\tau_{mbsb} S_{mbsb}$ and the friction force between the moving bed and the pipe wall $\tau_{mb} S_{mb}$. The gravitational force on the moving bed is represented by F_{mbG}, F_{mbsb} the Coulombic friction force between the moving and stationary beds and F_{mb} the Coulombic friction force at the contact surface with the pipe wall. The Coulombic friction forces are the normal force components in the force balance.

$$A_{mb}\frac{dP}{dx} = -F_{mbsb} - \tau_{mbsb}S_{mbsb} - F_{mb} - \tau_{mb}S_{mb} + \tau_{hmb}S_{hmb} - F_{mbG} \tag{2.35}$$

The stationary bed would be represented by subscript *sb* but was not found in the publication. As was the prediction of the total pressure losses. Doron and Barnea substantiated their model with laboratory experiments. They used an inclinable flow loop with 50 mm pipe diameter. The flow loop that was used for the validation of their model was limited to pipe inclination angles of 7 degrees ascending and descending pipe tilt. During the experiments, a stationary bed was observed at low slurry flow velocities. The results of the experiments more or less agreed with the model. The model did, however, suffer from over-predictions of the limit deposit velocity.

2.4. Inclined coarse particle transport transport

In this section, an overview of the produced literature with regard to some of the experiments with inclined pipelines is found. The researches discussed in this section are produced by Hashimoto et al. [1980], Wilson and Tse [1984], Vlasak [2014] and de Hoog [2017]. The focus is especially on experimental research and focuses mostly on settling- and deposition limit velocity of slurries with coarse particles.

2.4.1. Hashimoto

Hashimoto et al. conducted experiments with an inclined pipeline [Hashimoto et al., 1980]. The tests were mainly focused on stationary deposits in the pipe. Coarse material was tested with d/D ratio over 0.1. The tested pipe inclinations were up to 45 degrees and the results of the experiments are plotted in figure 2.8. They concluded that, to avoid stationary deposits in the ascending flow direction in inclined pipes, higher flow velocities are required.

2.4.2. Wilson and Tse

Wilson and Tse conducted experiments with inclined pipelines at a maximum pipe inclination angle of 40 degrees [Wilson and Tse, 1984]. Four particle sizes between 1 and 6 mm were tested. They observed that the velocity at the limit of deposit has a maximum at ascending flow direction of 30 degrees pipe inclination. The velocity was found to be 50% higher than in horizontal flow. In figure 2.8 the graph displays the Durand number expressed by $\Delta_D = V_{sm}\sqrt{2g(S_s-1)D}$ with deposition limit velocity V_{sm} as a function of pipe inclination angles.

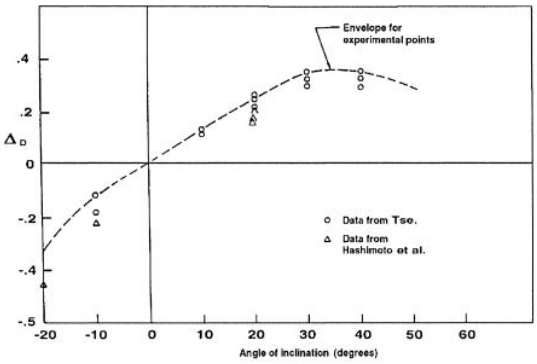

Figure 2.8: Deposition limit velocities Wilson and Tse [Wilson and Tse, 1984]

The graph shows that the deposition limit velocity increases with increasing pipe inclinations to reach a maximum velocity at an angle of about 30 degrees and then decline again. From a force-balance model Wilson and Tse concluded that the resisting forces in an inclined pipe section are exceed those that move the slurry and therefore it gets stationary. They figured that the pipe inclination introduces an axial component that

acts on the submerged particle weight and increases the motion resisting forces.

2.4.3. Vlasak

Experiments conducted by Pavel Vlasak [Vlasak et al., 2014] with regard to inclined coarse particle transport, were done with a 100 mm diameter inclinable pipeline. The transport material consisted of basalt pebbles that had a d_{50} of 11.5 mm and a narrow particle size distribution. He found that the slurry flow in the ascending section of the pipeline became stratified at higher flow velocities than deposition limit velocity, which was defined as the highest flow velocity at which slurry flow gets stratified in horizontal slurry flows. Particle saltation was found to be the dominant transport mode at higher mixture flow velocities. The concentration was linearly distributed with a value of zero in the upper portion of the pipe and the maximum near the bottom. Pipe inclination below ± 30 degrees, had little influence on the concentration distribution. At higher pipe inclinations, the region with zero concentration in the upper part of the pipe cross section grew larger in the descending flow direction at decreasing mixture flow velocity and delivered concentrations. At higher flow velocities, the concentration near the pipe bottom decreased a marginally with a greater effect at larger pipe inclinations angles. A larger zero concentration area was observed in the descending section than in the ascending section. The maximum concentrations were measured at 0.15D to 0.3D from the bends in the ascending flow direction and in the middle of the pipe when descending flow directions were tested.

2.4.4. De Hoog et al.

In 2017 de Hoog et al. published a paper with their results regarding experiments with inclined coarse slurry transport [de Hoog et al., 2017]. They conducted experiments with a pipe diameter of 100 mm and three different d_{50}s of 4.6, 6.3 and 12 mm. They tested inclination angles up to 52 degrees. The focus of the experiments was on the pressure losses, flow velocity, delivered concentrations, deposition limit velocities (DLV) and flow velocity profiles. The DLV is defined as the bare minimum flow velocity to avoid stationary deposits.

With the experiment results, an insight was gained into the DLV at different inclination angles. The highest deposit limit velocity was observed at 30 degrees pipe inclination in the ascending flow direction. The effect of the inclination angle on the total pressure gradient of the mixture was found to be mostly due to the static pressure gradients of the mixture.

During their experiments, the slurry runs were started at low flow velocities and then increased which meant that a stationary bed was already present. The solid particles in the slurry are mainly transported by saltation over the top of the bed. In the experiment results, it was found that a peak in the hydraulic gradients appeared at the deposition limit velocities. At higher mixture flow velocities than the DLV, the bed starts to move. For lower mixture flow velocities it remains stationary. At low flow velocities, a higher in situ concentration is observed and a higher hydraulic mixture gradients than at higher flow velocities. When the flow velocity is increased and the bed is no longer stationary, the delivered concentrations increase but the in situ concentration decreases.

Edwin de Hoog supplemented Wilson and Tse's $\Delta_D - \omega$ figure with extra values regarding the deposition limit velocities for different pipe inclination angles. The result is seen in figure 2.9, which shows the maximum deposition limit velocities are reached at 30 degrees ascending pipe inclination.

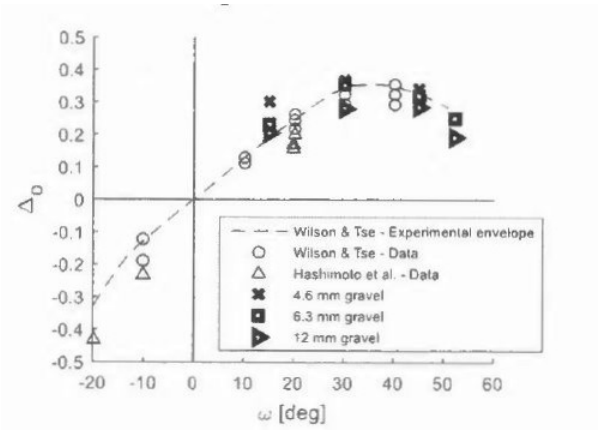

Figure 2.9: Deposition limit velocities De Hoog et al. additional data of Wilson and Tse and Hashimoto et al. is included

2.5. Settling slurries in inclined hydraulic transport

The studies discussed in this section are especially focussed on settling slurries. Comparable to the previous section, the deposition limit is discussed. Contrary to the previous section, the emphasis is on different particle diameters and distributions. In this section the experiments by Diniz and Coiado [1999], Eltoukhy [2013], Matousek and Vlasak [2015] and Spelay [2016] are discussed.

2.5.1. Diniz and Coiado

Diniz and Coiado [Diniz and Coiado, 1999] conducted experiments with a 7.5 cm diameter inclinable pipe flow loop. They used uniform sand with a d_{50} of 0.2 mm and tested solids concentrations up to 15 % at pipe inclination angles of 5 to 45 degrees. Their aim was to gain an insight in the head losses in upward and downward flow directions at several pipe inclinations. The concentrations, tilt angles and flow velocities were varied. The results were used to verify the semi-empirical model of Worster and Denny [Worster and Denny, 1955] and the physical model proposed by Graf [Graf, 1984]. The verification was conducted by quantifying the differences of the results and model predictions.

They observed that regardless of the inclination angles or concentrations, the head losses in descending flow directions are always lower than horizontal flow direction which are always lower than ascending flow directions. At ascending flow directions, the presence of solids in the flow causes higher head losses which increased with increasing concentrations or increasing inclination angles. In horizontal flow direction, the increase in solids concentration caused higher head losses. At descending pipe inclinations, the head loss decreased as the concentrations were increased. At flow velocities above 3.0 m/s in ascending flow directions, Graf's predictions came very close to the experiment results. The semi-empirical model by Worster and Denny proved valid for inclination angles below 30 degrees (ascending) and flow velocities over 3.0 m/s. At descending flows the models were far from the measured values.

Diniz and Coiado came up with three empirical equations for the head loss as a function of flow velocities which were basically fitting functions to the data. When flow velocities below 3 m/s were tested, they were far from the results of the experiments.

2.5.2. Eltoukhy

In 2013 Eltoukhy produced a paper regarding findings of his experiments with a 75 mm pipe diameter flow loop setup [Eltoukhy, 2013]. He conducted several test runs and focused on variations in concentration, flow velocity and inclination angles using solids with a d_{50} of 0.20 mm. He tested inclination angles of 0, 5, 10, 25, 35, 45 and 90 degrees in both ascending and descending flow directions. Delivered solids concentrations of 0, 5, 10 and 15 % were tested at flow velocities between 3 and 5 m/s. Based on the analysis of the recorded data he concluded that the pressure gradients are always higher in ascending flow directions than in horizontal

flow direction and in descending always lower than in horizontal, regardless of pipe inclination angle, concentration or flow velocity. In ascending flow directions, the pressure gradients were found to be proportional with the solids concentration of the same angle. In descending direction they were found to be inversely proportional with the solids concentration. According to his findings, higher ascending pipe inclination angles correspond to higher hydraulic gradients where higher descending pipe inclination angles correspond with lower hydraulic gradients. Generally, it was found that the result of higher mix flow velocities, are higher hydraulic gradients for equal concentrations and pipe inclination angles.

2.5.3. Matousek and Vlasak

Matousek and Vlasak produced a paper regarding their findings of experiments with a flow loop with 100 mm pipe diameter [Matousek and Vlasak, 2015]. The intention was to gain more insight in multiple layer slurry flows. The focus in these experiments was on inclined pipe flows with fine to coarse material, concentration distribution and resistance. The aim was to recognize flow patterns and dominating particle dispersion mechanisms in order to formulate a complete picture of the behaviour of settling slurries. Particle support mechanisms and friction mechanisms are studied. They many different testing materials including glass beads, fine to coarse sand, gravel and basalt pebbles were tested at different concentrations.

They found that the frictional pressure drop in ascending inclined flow directions increases with increasing pipe inclination angles. The maximum value of the pressure drop is reached between 20 and 40 degrees pipe inclination. At higher inclination angles, the frictional pressure drop gradually declines, depending on concentration and flow velocity. The difference between frictional pressure drop in ascending and descending flow directions was observed to increase with increasing flow velocity. In the descending flow direction the frictional pressure drop was observed to decrease with increasing pipe inclination angles. It was found that at delivered concentrations below 8 %, the effect of pipe inclination on the pressure drop can effectively be neglected. At higher concentrations, the influence was found insignificant especially at high flow velocities.

2.5.4. Spelay

A 100 mm test flow loop was also used by Spelay et al. to investigate inclined settling slurries [Spelay et al., 2016]. Their focus was on deposition limit velocity for fine, intermetiate and coarse at different particle sizes up to 8 mm at different concentrations. Their focus within the research was in the ascending and flow directions with pipe inclinations up to 20 degrees. They observed that for coarse particles with d_{50} between 2 and 8 mm, the deposition limit increased significantly with increasing pipe inclinations. For finer particles it was found that pipe inclination only marginally impacted the flow velocity at which a bed of stationary deposit was formed in the pipeline (DLV). Therefore they concluded that the DLV in relation to the pipe inclination was correlated with the efficiency of turbulent suspension of the particles. When the suspension mechanisms are less effective at lower flow velocities, the solids particles start to transmit their submerged weight to the pipe wall. In that case, the effect pipe inclination starts playing a more important role with regard to the DLV.

2.5.5. Vertical transport

To determine the delivered concentrations with a u-loop, the physical equations for slurry transport in a vertical pipe are rearranged. Clift and Clift described their findings for vertical transport and the determination of the concentration in a publication [Clift and Clift, 1981]. Wilson recapped the theory in his book [Wilson et al., 2006] and shows the basic equation for rising vertical flow with equation 2.36. Where $(P_1 - P_2)$ is the total pressure difference between two points on the riser at height difference z meters. The water density is ρ_l, relative solids density S_s, in situ solids concentration C_{vi}, gravitational constant g, pipe diameter D and mean mixture flow velocity V_m. The mixture density ρ_m is equal to $\rho_l(1 + (S_s - 1)C_{vd})$ with $C_v d$ the delivered volumetric concentration.

$$\frac{P_1 - P_2}{z} = \rho_l g(1 + (S_s - 1)C_{vi}) + \frac{\rho_m f V_m^2}{2gD} \tag{2.36}$$

Equation 2.36 was derived from the force balance in equation 2.37. In this case, S_{mi} is the relative in situ solids density and the wall shear stress τ_0 is written as $\rho_l f V_m^2/8$.

$$\frac{p_1 - p_2}{z} = \rho_l g S_{mi} + (4\tau_0/D) \tag{2.37}$$

$$\frac{p_3 - p_4}{z} = -\rho_l g S_{mi} + (4\tau_0/D) \tag{2.38}$$

Adding together the force balances of the riser and the downcomer of the u-loop, provides the possibility to determine the in situ concentration. When they are added, the wall shear stresses cancel out as a result of their opposing directions in the ascending and descending legs of the u-loop. Equation 2.37 and 2.38 display the force balances in the up- and downcomers. The first term on the right hand side of the equations is the same, except for their opposing signs. The upward and downward mean flow velocities are also the same, the Clifts conclude, that the shear stress terms can therefore be eliminated by combining the two equations into the equation for the C_{vi}, the in situ solids concentration. Equation 2.39 displays how the in situ concentration is determined by combining the force balance equations 2.37 for the riser and 2.38 for the downcomer.

$$C_{vi} = \frac{1}{S_s - 1}\left(\frac{(p_1 - p_2) + (p_4 - p_3)}{2\rho_l g z} - 1\right) \tag{2.39}$$

The delivered solids concentration C_{vd} is determined from the in situ concentration C_{vi} using equation 2.40 for the riser and equation 2.41 for the down comer. The hindered settling velocity divided by flow velocity, the v_t'/V_m ratio, can be neglected since it is usually less than 0.1. Therefore, the delivered solids concentration is assumed equal to the in situ solids concentration in the u-loop.

$$C_{vi} = \frac{C_{vd}}{1 - (v_t'/V_m)} \tag{2.40}$$

$$C_{vi} = \frac{C_{vd}}{1 + (v_t'/V_m)} \tag{2.41}$$

Equation 2.40 illustrates the relation between the in situ concentration and the delivered concentration in a riser. The equation illustrates that when the flow velocity decreases, the in situ concentration decreases as well for the same delivered concentration. This effect is due to the thickening of the profile mixture. In other words, the sand in the mixture is moving slower than the water due to the gravity acting on the sand particles. At low flow velocities, this causes a concentration meter in a vertical riser to show a value that is high er than the delivered solids concentration. In the downcomer, this principle works inverted as illustrated with equation 2.41, thinning the mixture density. The theory of thickening or thinning mixtures is substantiated by equations 2.12 to 2.14. It is based on the idea that if the production Q remains equal, the in-situ concentration has to change.

2.6. Conclusions state of the art

The theoretical background of this research consists of several components regarding horizontal, vertical and inclined water- and mixture flows. The Darcy Weisbach equation for liquid flow in horizontal pipelines theoretically quantifies the pressure losses due to friction in horizontal pipelines. The Equivalent liquid model is a modification to Darcy Weisbach, where the Darcy Weisbach results are multiplied with the ratio of mixture density to water density. The equivalent liquid model assumes a homogeneously distributed.

"What are the existing models and ideas with regard to hydraulic transport in inclined pipelines?".

The three most interesting semi-empirical models for inclined heterogeneous flow (Worster and Denny, Gibert, Wilson) all contain terms for Darcy Weisbach friction loss in horizontal water flow, the solids effect and particle suspension. The solids effect is multiplied with the cosine of the pipe inclination angle, the different models have different exponents added to the cosine term. Worster and Denny has 1, Gibert 1.5 and Wilson

$1 + M$. To translate the models from manometric gradients into total pressure gradients, a hydrostatic component ($sin(\omega)$) is added and the equations are multiplied by $rho_l g$.

Shook and Roco, Matousek and Doron created two and three layer models based on force balances of stratified flows rather than (semi-)empirical observations. The multiple layer models identify the different layers with different slurry states, suspended and stratified for the two layer models. In the three layer model, the stratified layer is split into stationary- and moving bed layers. An input value of the layered models is the cross sectional area of the different layers. To account for flow regimes without stratification or a fully stratified flow, the cross sectional areas can be set at zero so they are not included in the results.

The experimental researches regarding inclined pipe flows are mostly limited to small diameter pipelines with maximum of 150 mm with a large range of different particle sizes. In the publications of De Hoog et al., Wilson and Tse, Hashimoto et al., Matousek and Vlasak, Doron, Spelay, Eltoukhy, Diniz and Coiado it is agreed that the slurry flow in ascending flow directions becomes stationary at flow velocities higher than the deposition limit velocity for horizontal flow. The highest velocity at which stationary deposits were observed at 30 degrees pipe inclination in the ascending flow direction. Only the particles that are suspended in the slurry flow contribute to the static pressure differential of the mixture. The solid particles in the slurry are mainly transported by saltation over the top of the bed. At mixture flow velocities above the DLV, the bed moves, delivered concentration increases and the in-situ concentration decreases. For mixture flow velocities below the DLV, the bed remains stationary or grows, the in-situ concentration increases and the delivered concentration decreases. Furthermore it was concluded that hydraulic gradients in inclined-up pipe flow are always higher than the horizontal hydraulic gradients and in inclined descending pipe flow always lower than horizontal, regardless of concentration or flow velocity. The concentration in the pipe was found to be proportional with the hydraulic gradients in inclined-up slurry flows and inverse proportional with inclined down flows. Higher inclination angles cause higher hydraulic gradients in inclined-up flow and lower hydraulic gradients in inclined-down flow directions. In general it was found that higher flow velocities cause higher hydraulic gradients.

Vlasak observed that the concentration in a slurry flow with large particles is linearly distributed with a value of 0 in the upper portion of the pipe and the maximum near the bottom. Pipe inclinations below ± 30 degrees, had little influence on the concentration distribution. At higher flow velocities, the concentration near the pipe bottom decreased a little bit with a greater effect at larger pipe inclinations angles. The effect of the inclination angle on the pressure gradient of the mixture is mostly due to the static pressure gradients of the mixture.

The internal structure of inclined pipe flows was observed to be different for ascending and descending flow directions. De Hoog observed a lower bed in the descending section than in the ascending section at equal flow velocities and concentrations. Generally, it was concluded that suspended mixture flows have little effect from pipeline inclinations. In stratified flows, however, a significant difference between ascending and descending flow directions was observed.

With regard to the frictional pressure drop, Matousek and Vlasak concluded that the effect of pipe inclination is negligible at concentrations (below 8 %) or high flow velocities for finer particles. When coarser particles were tested, the frictional pressure drop increased with increasing pipe inclinations, and the maximum was reached at angles between 20 and 40 degrees pipe inclination angles.

Spelay et al. found that below 20 degrees pipe inclination, the turbulent suspension mechanisms play an important role on the deposition limit velocity. For finer particles, pipe inclination has nearly no effect on DLV. For coarser solids, the DLV increases significantly with increasing pipe inclinations and decreasing flow velocities.

3

Test setup

The test setup, test protocol and data processing are discussed in this chapter. It is divided into three sections in that elaborate on the approach with regard to the experiments. The conclusion of the chapter is the answer to the research question "Which test setup and experiment protocol are required to gain an insight in flow characteristics in inclined large diameter pipelines?". The chapter is split into the sections setup, test protocol and post-processing. The configuration of the flow loop is discussed in detail in section 3.1. Next the experiment protocol is discussed and the last section considers the methods that are used to post-process the acquired data.

3.1. Outline setup

In this section the test setup and its components are discussed. The technical drawings of the flow loop are found in appendix B and a schematic overview drawing of the setup is displayed in figure 3.1. In figure 3.1 the slurry would "start" at the slurry tanks (1) (not displayed). Upstream from the the slurry tanks, the water reservoir is located. The slurry tanks and water reservoir are connected via a set of pipes and valves. The pump is located at 2, downstream from the reservoirs in the figure. Directly after the pump a section that serves as a U-loop (3) is found. The U-loop is outfitted with 2 differential pressure meters (one on each leg) and an ultrasonic density meter. After the u-loop, the pipe is led through a water basin (4) that can serve as cooling section. From the cooling system, the pipe is led upwards where the electromagnetic flow meter (5) is attached to the vertical ascending leg of the vehicle crossing. Directly downstream from the vehicle crossing, the inclinable segment (6) starts with the ascending section, then a 180 degree turn and the descending section. Several differential pressure meters and total pressure sensors are attached to it. The horizontal section (7) begins right after the inclinable segment downstream from the descending section. This horizontal section includes differential pressure meters and total pressure sensors. The horizontal pipe has a perspex observation section built in to monitor sliding or stationary beds. After the horizontal measurement section, the second 180 degree turn (8) is located which leads the flow led back to the slurry tanks. The ascending and descending legs of the inclinable section have a combined maximum length of approximately 50 meters depending on the inclination angle. At inclination angles over 18 degrees, the inclinable section is shortened to fit under the roof of the laboratory. The horizontal measurement section excluding the inclinable section is a little under 60 meters long. With the exception of the connections at the slurry reservoir, the pipe diameter of the whole setup is 300 mm.

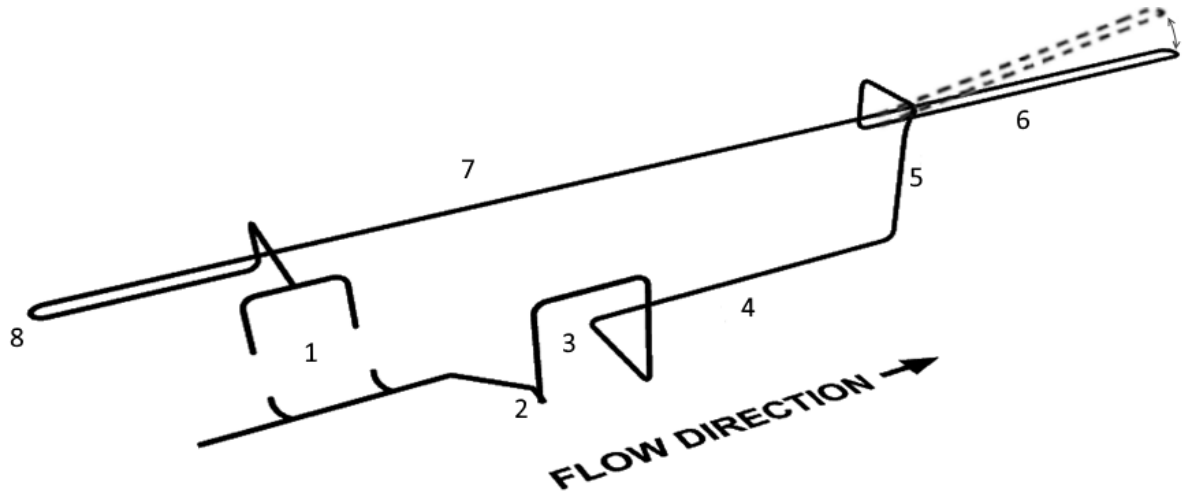

Figure 3.1: Schematic display of test setup

3.1.1. Slurry- and water reservoir

Figure 3.1 shows two entrances and exits to the slurry tanks at location 1. During the experiments, these two tanks are used to store sand and run the slurry through. Appendix B shows that there are four slurry tanks attached to the system, only two of them are used. These slurry tanks can be monitored and their valves can be opreated from the control room. The tanks can hold up to 100 cubic meter of slurry or any other liquid or solid each. The bottom of the tanks is conically shaped and the opening at the bottom of the slurry tank is 40 cm in diameter. The water reservoir can contain 166.5 m^3 and is situated upstream from the slurry tanks. The exit pipe of the flow at the slurry tanks is kept submerged under the water level to keep air bubbles from entering the system.

3.1.2. Valves

Valves are situated at several locations. Some of them are remotely controlled and can be adjusted to open or close gradually. This type of valves is located below the slurry tanks and after the water reservoir. These are all remotely controlled from the control room. Two manually operated valves are located at the end of the flow loop just before the slurry tanks. These are used to select in which tank the mixture ends up. A second function of these valves is to choke the system. The valves can be closed partially and to increase the pressure in the flow loop and decrease the flow velocity in the system. This is done when the pressure at the top of the inclinable section becomes to low and the venting valve starts sucking air into the system. A total of 4 air venting valves is installed in the setup. Three of them are mechanically automated and vent the air whenever it is necessary. They are located on the two road crossings and on the highest point of the inclinable section. One air venting valve is manually operated and situated upstream from the second 180 degree bend.

3.1.3. Pump

The pump that is used in this flow loop configuration is a wear-resistant centrifugal dredge pump, type ASP1050-300-7000030W. The pump has a designed discharge rate of 1600 m^3/h at 740 revolutions per minute. The designed input power and head are 151.6 KW and 25.35 m. It is powered by an electric engine. The pump characteristics and performance are displayed in figure 3.1.3. Depending on the length and height of the set-up, the maximum flow velocity differs for different experiments. When water was tested in horizontal flow loop setup, flow rates below 1000 m^3/h or over 1600 m^3/h were inaccessible. These flow rates correspond with flow velocities between 5 and 6.5 m/s. Over the maximum, the pump engine would break and below the minimum, the system would start sucking in air through the vents. To counteract the air that was sucked into the system, the chocking method was devised to reach lower flow velocities. This made it possible to reach flow rates as low as 700 m^3/h or around 3 m/s.

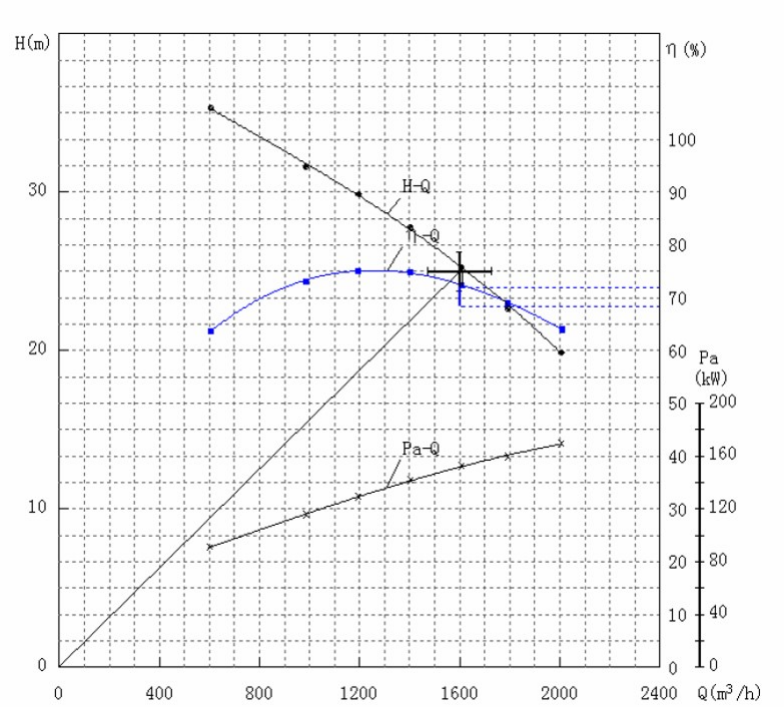

Figure 3.2: pumpcharacteristics as a function of flow rate. Efficiency (η-Q), pressure (head, H-Q), Power (Pa-Q)

3.1.4. U-loop

The theories behind the u-loop have been thoroughly described by Clift and Clift [Clift and Clift, 1981]. The actual patent on this device was owned by Hagler [Clift and Clift, 1981]. The u-loop is indicated with 3 in figure 3.1. The loop is a device that is used (often in the field) to determine the C_{vd}, the delivered volumetric solids fraction and the mixture density with equation 3.1 and the method described in section 2.5.5. Figure 3.1.4 displays the schematic layout of the u-loop.

$$C_{vd} = \frac{\rho_m - \rho_f}{\rho_s - \rho_f} \tag{3.1}$$

The differential pressure sensors are connected to pressure taps 1, 2, 3 and 4 in figure 3.1.4. One differential pressure meter measures the pressure difference between pressure taps 1 and 2. The other sensor is connected to taps 3 and 4. The pump is indicated with number 5 and the ultrasonic density meter is located at 6. The flow direction in the u-loop is indicated with the black arrows. The location of the differential pressure taps was chosen so that it is five pipe diameters (1.5 meters) from the next bend to account for effects on the flow by the bend. They are located as far from the previous bend as possible, while maintaining a distance of two meters between the two pressure taps. Keeping distance from the previous bends (or the pump) ensures a mixture that is more homogeneously distributed. The delivered concentration can be used to find the density of the mixture. Equation 3.1 displays the method used to find this mixture density.

In practice, the u-loop is used to find the delivered concentration and the density of the mixture. In the water flow tests, the u-loop is used to verify the correct working of the ultrasonic density meter. Appendix C and section 2.5.5 contain more information with regard to the determination of the delivered concentrations.

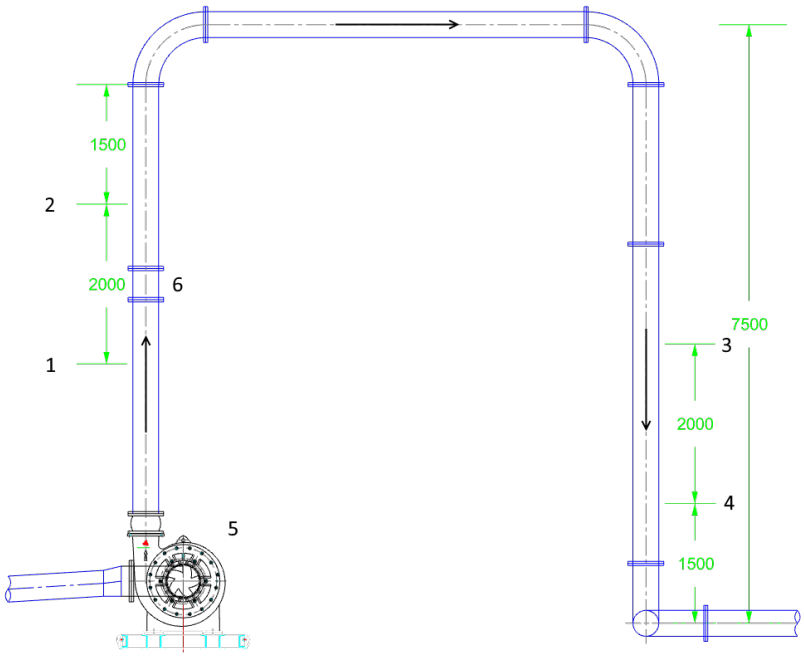

Figure 3.3: Schematic drawing of the u-loop section of the test setup

3.1.5. Cooling section

In order to keep the temperature in the flow loop constant, the pipeline is led through a cooling section (4). It is located downstream from the u-loop and upstream of the the first vehicle crossing lane. Whenever cooling of the slurry or pipeline is needed, the reservoir is filled with water to submerge the pipe. This keeps the temperature in the system constant so that no large fluctuations occur in the viscosity or density of the slurry.

3.1.6. Horizontal section

The horizontal section of the setup is indicated with numbers 6 and 7 in figure 3.1. It is the primary measurement section of the test setup and runs along the full length of the laboratory. Section 6 of the horizontal measurement section is inclinable (see section 3.1.7). When the setup is inclined, the horizontal section contains 16 pressure taps indicated with numbers 19 up to and including 34 in figure 3.1.9, the pressure taps are 3 meters apart. For this thesis, the focus is mainly on hydraulic transport in inclined pipelines. The horizontal section is primarily used for reference purposes and creating a "stable" flow in the flow loop. 15 differential pressure meters and 16 total pressure sensors are installed at the pressure taps in the horizontal section (in inclined configuration). Downstream from the inclinable section, upstream from pressure tap 18 in figure 3.1.9, a gap of 10 meters with no pressure taps is located. Neither total pressures nor differential pressures are recorded in and over that part of the setup. The horizontal section contains a perspex segment (section 3.1.8) which is found between pressure taps 23 and 24 in figure 3.1.9. Temperature sensors are installed in the flow loop between pressure tap 18 and 19, and in the vehicle crossing upstream from the slurry tanks.

3.1.7. Inclinable section

The inclinable section is indicated with 6 in figure 3.1. It is connected with flexible piping to lift it to different pipe inclination angles. The inclinable section contains pressure taps 1 up to and including 18 (figure 3.1.9). Similar to the horizontal section, it contains differential pressure meters and total pressure sensors. The sensors are connected to pressure taps every 3 metres. The 180 degree bend includes an air vent to remove air from the flow loop during operation. The inclination angle can be adjusted over the course of approximately one day. No modifications to the pipe length are required for pipe inclination angles up to 18 degrees. For larger pipe inclination angles, the pipe is shortened to fit under the roof of the laboratory. To shorten the pipe, several sections of pipe (including pressure sensors) are removed from the flow loop on either side of

the inclinable section. In figure 3.4 the 0, 20, 30 and 45 degrees pipe inclination angles are displayed. The setup is supported by scaffolding, appendix B contains detailed drawings of the scaffolding placement for different pipe inclination angles.

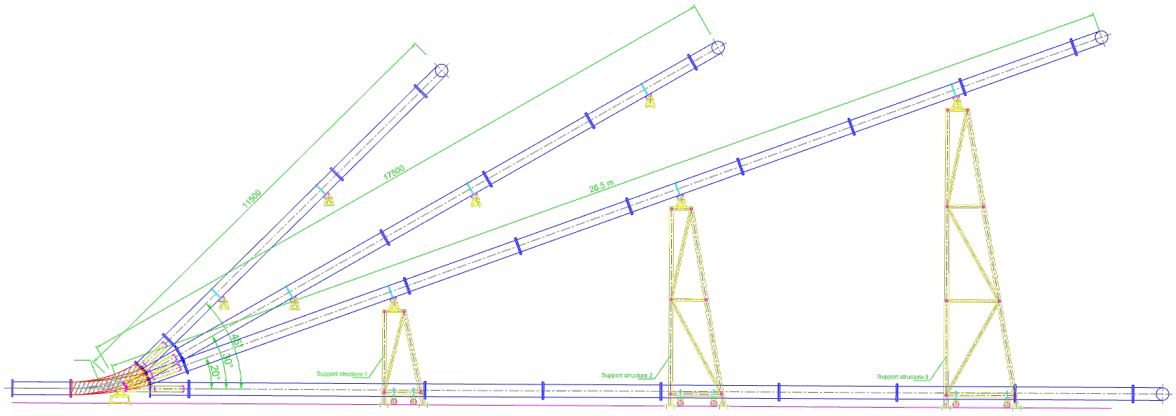

Figure 3.4: Schematic drawing of the inclinable section at inclination angles of 0, 20, 30 and 45 degrees

The first inclination angle that was tested for this thesis research was 17.9 degrees. The setup lay-out is basically the same as the 20 degrees pipe inclination angle in figure 3.4. The photo on the front page of this thesis report displays the 17.9 degrees pipe inclination angle configuration. Before the lifting operation takes place the system is drained from water and sand to allow the inclinable section to be lifted by the cranes and not risk buckling, bending or breaking of the flow loop.

3.1.8. Perspex section

The flow loop includes a perspex section to monitor the slurry- and water flows. The perspex section is used to check for air in the system, monitor the flow and the height of a sliding or stationary bed. The perspex section is located between pressure tap 24 and 25 (figure 3.1.9). To monitor and record the flow in the perspex section during testing, a camera on a tripod and light were installed next to it. On the perspex section, a graduated partitioning was added to determine the exact height of a visible stratified bed. The section can withstand a maximum water pressure of approximately 200 kPa. The pressure in the flow loop is kept below 160 kPa for safety purposes. A mirror was placed under the section at a slight angle to improve the overview over the section. A photograph of the perspex section is displayed in figure 3.5.

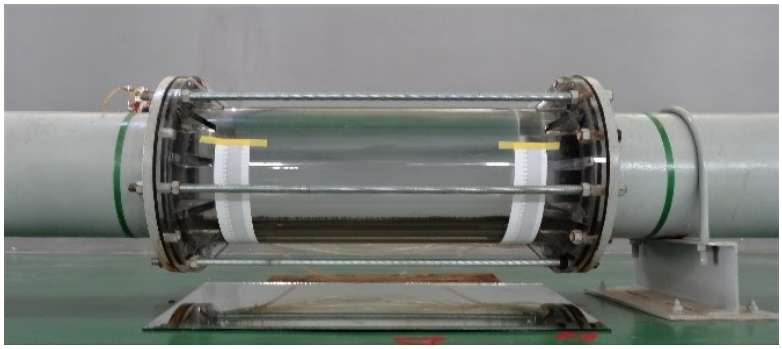

Figure 3.5: The perspex segment installed in the horizontal section of the flow loop

3.1.9. Sensors

Seven different sensor types are incorporated in the test setup. It includes 32 differential pressure sensors and 34 total pressure sensors in the horizontal and inclinable sections. These sensors are attached to the same pressure taps causing redundancy of the sensors enabling verification of their results. Up- and downstream from the pump, the pressure is recorded by two total pressure sensors. The pump RPM and engine power is collected in the control room. In the U-loop (section 3.1.4), two sets of differential pressure sensors, and an ultrasonic density meter are installed. The electromagnetic flow meter is installed near the vehicle crossing lane downstream from the cooling section. The setup includes two temperature sensors, one halfway the loop and one near the end close to the slurry reservoirs. All data is recorded with the central computer system which is also used to monitor the sensor output. The sensor ranges from table 3.3 are set into the central computer. The sensors are connected to receivers which process the signals before they are recorded by the computer.

Differential pressure sensors

The differential pressure sensors (dp sensors) in the horizontal and inclinable sections are Rosemount 3051 differential pressure transmitters with a range of 0 to 10 kPa. Rubber impulse tubes are used to connect the pressure taps to the sensors. The layout of the pressure taps is found in igure 3.1.9. The pressure tap with the total pressure sensor installed and connected to the impulse tubes for the dp sensors is illustrated in figure 3.1.9. The 'a' in the figure points at the total pressure sensor, 'b' is the impulse tube for the differential pressure meters and 'c' is used to vent the differential pressure system. Three valves are attached to the set, to close off the entire pressure tap, to vent the differential pressure system and to close the impulse tube. The dp-sensors measure the pressure difference between two successive pressure taps.

The dp-system is vented by pumping water from a separate water reservoir into the flow loop through the differential pressure sensors and impulse tubes. Any air bubbles in the impulse tubes or sensors are flushed into the flow loop and transported to venting valves. This procedure is conducted before the liquid flow tests take place. An additional benefit of using this method is that any sand caught in the impulse tubes from previous experiments is flushed from the system.

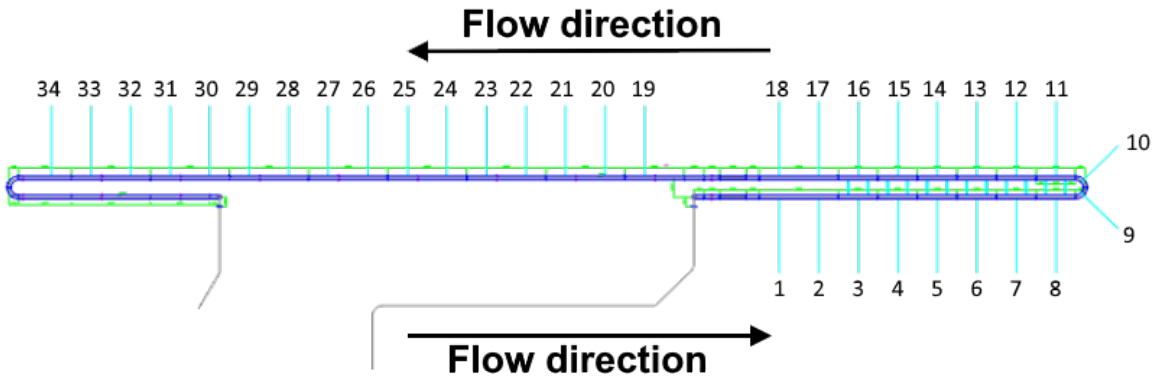

Figure 3.6: Distribution of the pressure taps over measurement section

Total pressure sensors

The total pressure sensors are connected to the same pressure taps as the differential pressure sensors (figure 3.1.9). They are indicated with 'a' in figure 3.1.9. These sensors measure the total pressure inside the pipe at each pressure tap. The total pressure sensors are piezoresistive MPM4730 pressure transmitters with a range of 0 to 200 kPa and an accuracy of 0.1 %.

Figure 3.7: Pressure sensor set with total pressure sensor (a), differential pressure sensor impulse tube (b), venting tube (c)

Eletromagnetic flowmeter
The Electromagnetic flow meter (EMF) applies a magnetic field to a flow in the pipe. It creates a potential difference that is proportional to the flow velocity. This makes it possible to measure the average flow flux of a mixture in the pipeline. The EMF is located at position 5 in figure 3.1, it was originally located in the riser of the U-loop (3.1.9, 2). Due to severe vibrations (amplified by the weight of the EMF) it was moved to the current position. The move significantly improved the EMF results in terms of stability and accuracy. The vibrations in the riser of the u-loop were reduced to nearly nothing. The EMF is an LDG-S electromagnetic flow meter by SURE instruments, with a range of 0 to 2000 m^3/h and accuracy of 0.5 %.

Ultrasonic density meter
To gain insight into the concentration, a Tengine TPD ultrasonic density meter was installed in the system at the u-loop (figure 3.1.9, 1). In figure 3.1.4 its location is indicated with '6'. The concentration is calculated by this stand-alone device. The delivered concentration is found using equation 3.2.

$$C_{vd} = \frac{\rho_m - \rho_l}{\rho_s - \rho_l} \tag{3.2}$$

The range of the concentration meter is 0 to 40 % volumetric concentration with a resolution of 0.1 percent and an accuracy of ± 2.5 %. During the data analysis phase of this research, it was found that the sensor had not been calibrated accurately. This caused it to display a measured concentration that was a factor 1.8 to 2.0 too high. The determination of the value is found in appendix C.

Differential pressure sensors U-loop
The U-loop contains two differential pressure sensor sets (figure 3.1.9, 5). They measure the total pressure difference in the ascending and descending legs of the u-loop. The results are used to determine the concentration in the system. For this application Rosemount 3051SAL differential pressure transmitters were installed. The sensors sets are based on a closed system that uses diaphragms and oil in the impulse tubes. Using a closed sysem eliminates the possibility of sand getting trapped in the impulse tubes or sensors. The pressure contains a membrane that transfers the local pressure through the impulse tubes to the differential pressure sensor. The pressure taps are on the u-loop are two meters apart. A schematic drawing of the u-loop, including locations of the pressure taps is displayed in figure 3.1.4. The range of the sets is -32 to 32 kPa.

Total pressure meters pump
Before and after the pump, two piezoresistive MPM4730 pressure transmitters are installed (figure 3.1.9, 3). The sensor upstream from the pump has a range of ± 0.1 mPa and downstream has a range of 0 to 0.3 mPa.

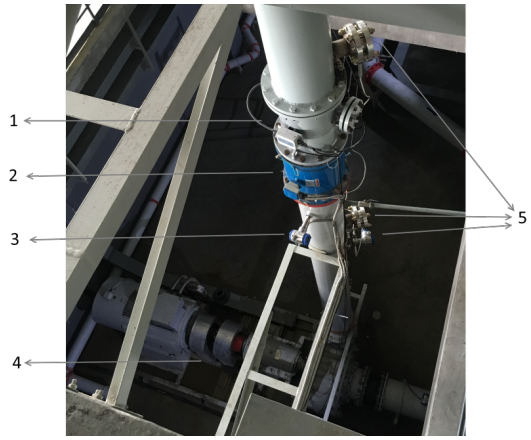

Figure 3.8: Ascending leg of the u-loop with ultrasonic density meter (1), EMF (2), total pressure sensor (3), pump (4), differential pressure meter (5)

Temperature sensors

An change in slurry temperature alters the viscosity of the carrier fluid which has to be accounted for in the post processing phase. Therefore it is monitored by two temperature sensors in the flow loop. The sensors have a range of 0 to 100 ^{o}C and an accuracy of 0.2%. The temperature can increase as a result of the surrounding temperature in the laboratory or friction of the slurry with the pipe walls. When a temperature increase is too high, the cooling basin is filled with water.

Connectivity and data acquisition

All the sensors were connected to the data receivers at the data acquisition desk located near '7' in figure 3.1. From the receivers the data ends up in the central computer. The data acquisition is done through a portable CTDAQS-5000 data collecting system with a total of 96 different channels. It consists of 3 NI MCC high performance multi data collecting USB-2537 cards. Each card can collect data from 32 different channels. The system has an A/D resolution of 16 bits and a sampling rate of 1 MS/s. It is connected to a computer via usb and the computer processes the data and logs it onto different files. The data can be viewed real time on different waveform displays. The channels that are used and the sensors they are connected to are found in table 3.1. When setup is shortened in order to fit under the roof when the pipe inclination angle is increased, several dp- and pressure sensors are taken out of the system. To keep the channel list the same for the post-processing phase, the channel list remains the same. The excluded sensors can be identified due to their extremely high or low pressure or differential pressure.

Sensors and channels

Sensor description	Number	Channel
Total pressure sensors	1 to 34	0 to 33
Electromagnetic flow meter	35	34
Ultrasonic density-meter	36	35
Temperature sensors	37, 38	36,37
Dp sensors u-loop	39, 40	38,39
Pressure sensor before pump	41	40
Pressure sensor after pump	42	41
Pump power	43	42
RPM pump	44	43
Differential pressure sensors	45 to 77	0 to 31

Table 3.1: Channel list

3.1.10. Sand

This section is used to discuss the sand that was used during the experiments. It came from an airport construction project site near Xiamen, where it is used as to build an artificial island. In figure 3.1.10, the particle size distribution is displayed. The particle size generally lies between 0.15 and 2.5 mm. The d_{50} is averaged over three measurement sets at 0.76 mm. The material is classified as a broad graded coarse sand. Table 3.1.10 shows the d_{10}, d_{50} and the d_{60} of the sand during the three sieving experiments in figure 3.1.10.

Particle size distribution			
	1	2	3
d_{60}	0.9	0.87	0.87
d_{50}	0.8	0.75	0.75
d_{10}	0.45	0.25	0.48

Table 3.2: Particle size distribution

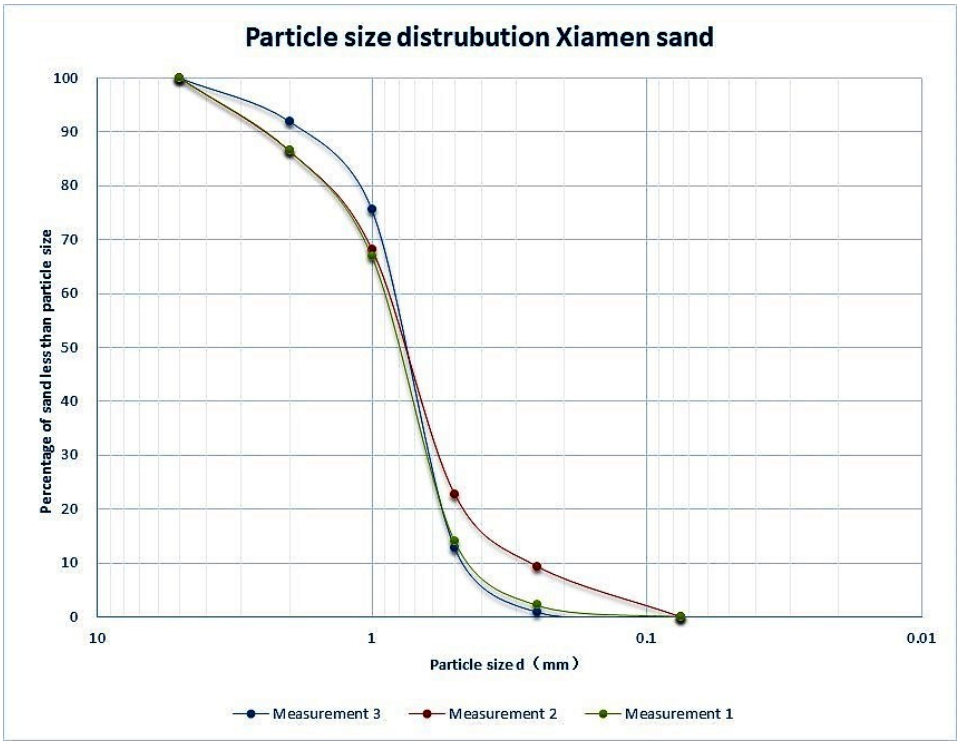

Figure 3.9: Particle size distribution Xiamen sand

Particle degradation is the process of the sand particles breaking up in smaller particles when they are used during experiments. It is caused by the particles colliding with the pipe walls and each other. This might cause the particle size to vary from the beginning to the end of an experiment causing varying sand properties and making the experiments harder to replicate. Sand properties such as settling velocity might vary over time due to varying particle sizes. However, the experiments were generally quite short and new sand was added several times between the experiments. Therefore, particle degradation was ignored.

3.1.11. Measurements

The pressure differences between two consecutive pressure taps, the flow rate and the concentration are the most important information to record during the experiments. They are needed to gain insight in the behaviour of the slurry flow. The pressure difference is determined in two different ways, with the total pressure

sensors and the differential pressure meters. Due to this redundancy, the pressure differentials can be validated against each other. The same applies to the determination of the concentration in the system which is done with the ultrasonic density meter, the u-loop and by taking slurry samples.

The slurry temperature was recorded in two locations to check for temperature changes over the length of the pipeline as well as the change over time. This is to account for the change of viscosity over time since the viscosity depends (among other factors) on the temperature. Furthermore, the test setup is outfitted with a cooling section that is used when temperature data shows too much fluctuations.

The pump data (pressures over the pump, RPM and power) is recorded and monitored for several reasons. During the experiments, the pump RPM is adjusted to change the flow rate. The pump power and pressures are paid close attention to since they are subject to a maxima and minima to avoid damage to the pump. Moreover, a sudden increase in pump pressure or sudden drop in RPM can be indications of a blocked pipe.

3.2. Experiment protocol

Six different concentrations are tested at several different flow velocities for every inclination angle. All tests have the same structure and are conducted three times to be able to check for deviating results. Table A in appendix A shows the planning of the tests. Every test cycle consists of a test run with water before the actual concentration is tested (liquid flow test). During this test, the sensors are calibrated at the start and checked for deviations. The water test is compared to the water test that is done before the previous experiment sequence. It was decided to skip the liquid flow test at the end of every day for two reasons. Firstly, before starting a concentration test, the liquid flow is tested. This means that the liquid flow test of the experiment can be compared to the liquid flow test of the previous experiment to validate the sensors. Secondly, when the tests are done the system is cleaned with water. This process causes air to get into the system meaning the impulse tubes of the differential pressure meters have to be flushed again.

The tests are conducted starting at a high flow velocity and gradually decreasing the flow rate until a stationary bed is observed in the perspex section. This sequence was chosen so that the bed does not have any influence on the flow velocity. If a bed would have formed and the velocity is increased instead of decreased, it would take some time for the bed to start sliding. In other words, it is easier to slow a moving object down by decreasing the momentum that is inserted than to start moving it by increasing the momentum in the system.

The tests at all flow velocities are done for at least 3 minutes to gain a reliable data sample from the sensors. The data from the flow meter and the pressure sensors shows an excitation effect when the flow velocity is either in- or decreased. It takes some time for these effects to dampen out, especially for higher concentrations. So for the 10% and 12.5%, a data sample of 4 minutes was created for each flow velocity. For this reason the flow rate as well as the concentration and the pressure data are carefully monitored. The measurement timing starts when all signals show a signal that does not deviate a lot from the average. The results are data samples of 3 to 5 minutes. The graph in figure 3.10 displays the flow rate of a full test sequence with one water run at different flow velocities and three runs with 2.5% delivered concentration in the system.

The flow rate is decreased or increased by adjusting either the RPM of the pump or closing the chocking valve near the slurry tanks. During the chocking process the pressure sensor with the lowest measured pressure is monitored constantly. The system starts to suck in air when the pressure is below 14 kPa causing the measured data to be useless. In order to keep the pressure in the system high enough a valve at the end of the flow loop can be closed a little bit. This causes both the pressure in the system to increase as well as the flow velocity to decrease. The RPM is decreased to reach the next flow velocity instead of chocking since the pressure in the system has to stay below 150 kPa, to keep prevent accidents. These steps are repeated until the lowest desired flow velocity is reached.

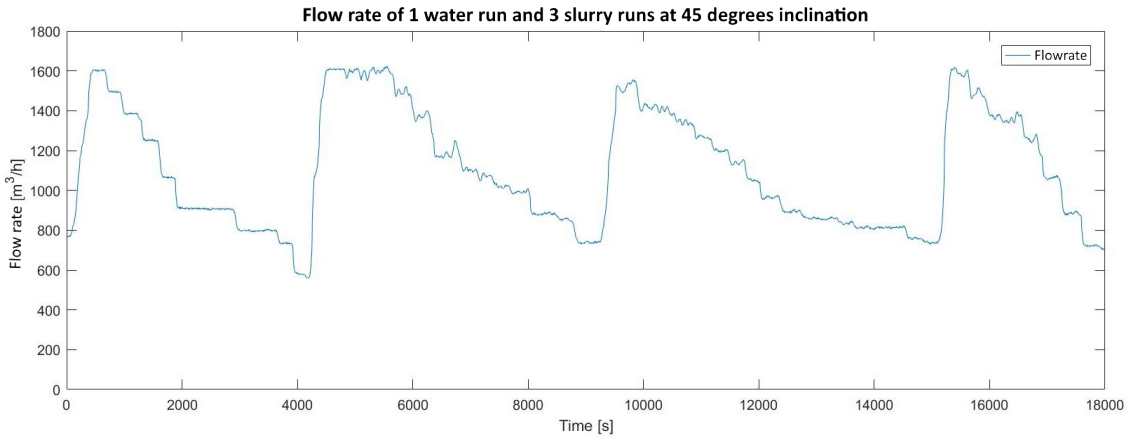

Figure 3.10: Flow rate for 1 water run and 3 slurry runs.

During the experiments, the sensors are monitored at the monitoring station next to the flow loop. The pump RPM is changed from the control room above the test setup. Communication between the control room and the monitoring station is done via radios.

The sensor range is set in the data acquisition computer, where it is translated from an electric signal into usable data with the right units. The function $y = Ax + B$ is used for translation, the values for A and B are found in table 3.3.

Sensors and ranges

Sensor description	A	B	Units
Absolute pressure sensors	62.5	-50	kPa
Electromagnetic flow meter	625	-500	m^3/h
Ultrasonic density-meter	12.5	-10	%
Temperature sensors	31.25	-25	^oC
Dp sensors u-loop	3.125	-2.5	kPa
Pressure sensor before pump	0.65	-1.56	mPa
Pressure sensor after pump	9.4	-7.52	mPa
Pump power	31.25	-25	kW
RPM pump	232.187	-185.85	-
Differential pressure sensors	3.125	-2.5	kPa

Table 3.3: Sensor ranges ($y = Ax + B$)

3.2.1. Test matrix

In table A on page 75 of the appendices, the planning of the experiments is outlined. The first experiments are conducted in the horizontal configuration of the setup. The next experiments take place with the setup under an inclination angle of 17.9, 28.9 and 44 degrees. Inclining the setup is done in one or two days. All experiments take approximately a day to finish without any setbacks or delays, the experiments can be done in approximately six weeks.

3.2.2. Starting up

To start the system up, everything is powered on. The flow loop is filled with water and the pump is started at a flow rate of around 1400 m^3/h. The computer system is started and the channel receivers are switched on. The data acquisition software is started and a new file is created. The ranges of the sensors are entered in the data acquisition software. The input is found in table 3.3.

3.2.3. Venting and calibrating

The flow rate is increased to 1600 m^3/h, the corresponding RPM for water is around 375 RPM. This velocity and RPM correspond with the maximum pump capacity. The perspex section is checked for the presence of air in the flow loop. In case of air is present, it is evacuated from the system by varying the flow rate and opening the air vents. During the entire procedure, the sensors are monitored to ensure values in the correct ranges. In case of a strange value, it is checked, solved or recalibrated.

The differential pressure meters are vented by powering on a small water pump and flushing clean water through the impulse tubes and dp-sensors via the pressure taps into the flow loop. The venting valves at the pressure taps are opened until all the air and sand is out of the impulse tubes. Once the air and sand is out, the venting valves at the pressure taps are closed, followed by the closing of the venting valves at the dp-sensors and the water pump is powered off.

3.2.4. Liquid flow

After venting the differential pressure sensors, water is already run through the flow loop at the highest possible flow rate (1600 m^3/h). A new experiment started so a new datafile is created. The flow rate is lowered incrementally in steps of 50 to 100 m^3/h until 800 m^3/h is reached. Every flow rate is measured steadily for three to four minutes. The flow rate is lowered in accordance with the choking procedure described in section 3.1.2 or by decreasing the pump RPM. The flow rates, RPM's, times, particulars and the valve choking are noted in the experiment logbook. This data can easily be compared to the data that was recorded the day before or in previous experiments so an irregularities are quickly spotted.

3.2.5. Sediment adding

After the liquid flow test, the flow rate is carefully increased to 1600 m^3/h. The pressure should not exceed the 200 kPa the perspex section can withstand. To stay on the safe side it is kept below the 160 kPa and the choking valve is fully opened at the highest flow rate. Sediment is added with a clamshell bucket (if necessary) to increase the delivered solids concentration in the flow loop when the flow rate is 1600 m^3/h. The concentration is monitored during the process until the right concentration is reached on the ultrasonic density meter read-out. Note that there is a small wave visible in the flow rate when the sediment is added. The variations in the flow rate in figure 3.10 at the high flow rate between 4000 and 8000 seconds indicate when a bucket of sand is added.

3.2.6. Experiment cycles

Once the sediment is added the actual test cycles can start, each experiment consists of three full cycles. Every experiment cycle is started at the highest flow rate and is then incrementally decreased with between 50 and 100 m^3/h. When a stratified bed observed, the increment can even be below 50. The flow is decreased until the stationary bed is observed in the perspex section. During the stratified bed phase, videos are taken of the perspex section where the flow regimes are visible. For every flow rate at low concentrations, 4 minutes of data are recorded and at the higher concentrations (10 and 12.5%), 5 minutes is recorded. When a test cycle is complete, the flow rate is increased to 1600 m^3/h. The procedure repeated until three cycles are completed. During the inclined experiments, air is sucked into the system through the air vent located at the highest position, at low flow velocities and pressures. To counteract this problem, the pressure sensors on the inclined section are carefully monitored until the highest located pressure sensor indicates that the total pressure in the pipe is around 15 kPa. The valve at the end of the flow loop is closed slightly to increase the pressure in the system without altering the differential pressures.

3.2.7. Cleaning the system

After the test cycles are done, the system is cleaned and emptied to prevent blockages. To clean the system, the valve under the slurry tank is closed and the valve of the water reservoir is opened. Clean water pushes the sediment into the reservoir. Different slurry tanks, where the slurry ends up, are selected by opening or closing on of the valves at the end of the flow loop.

3.3. Data processing

After the experiments are done using the flow loop described in section 3.1 and the testing protocol described in the previous section, the data is processed and the results are checked, validated, compared and analysed. The processing of the raw data collections in the computer files is described in this section.

The sensors and data collection produce raw datasets for 76 sensors with an interval of 0.05 seconds. The post-processing of the data is done using a re-sampling filter with a cut-off function to get rid of outliers in the datasets and create a more steady signal with a lower frequency. The flow fluxes and pressure signals of an experiment are compared to each other. This is process is needed to find the time intervals at which they are both constant. The flow fluxes and pressures have to coincide with the time intervals at which the flow flux was changed. These time intervals are recorded to create an averaged value of the sensor data and find a single value for each sensor at each flow rate.

3.3.1. Concentration

The results of the ultrasonic density meter are checked using the u-loop. The working of the u-loop is explained in section 3.1.4. Unfortunately, the differential pressure sensors in the U-loop were subject to error and the data is recalibrated after its collection. The recalculation process of the concentration data is described in appendix C. After the recalculation of the differential pressure sensors, the results of the ultrasonic density meter are validated. In appendix C it is found that the concentration data from the ultrasonic density meter has to be divided by 1.8 to 2.0 in order to find the correct concentrations. The tested concentration range lies between 0 and 15% instead of the 0 to 25% that was originally planned.

3.3.2. Pressures

The pressure sensors are validated with three different methods. First of all, the frictional pressure losses of the liquid flow for horizontal pipelines is calculated using Darcy Weisbach. The results of the calculation and the liquid flow experiment are compared to each other. This method is executed when the flow loop is fully horizontal. Secondly, the results of the absolute pressure sensors and the differential pressure sensors are compared to each other. If a sensor gives the wrong value it is double checked, fixed or left out of the results. This check can be done in both horizontal as well as inclined configurations of the setup. The third method is only valid for inclined liquid flow tests in the inclined section. The total pressure gradients for inclined water flow are calculated. The hydrostatic part is subtracted from the experiment results and these are then compared to each other and to the horizontal pressure gradients for liquid flow. Taking into account that there can be a minor measurement error, the results should be roughly the same.

3.3.3. Result analysis

The results of the experiments are first analysed by checking the total pressure profiles and total pressure gradients over the length of the pipeline section. When the slurry flows up, the pressure decreases due to the friction against the pipe walls and the gravity pulling the slurry backwards. When going down, the pressure increases due to the gravity pulling the slurry forwards. The slurry is expected to be affected by the bends as well, with pressure in- and decreasing again. The effects of the bends are expected to be especially visible in the differential pressure figures where they will show peaks, after bends or disturbances, but should dampen out over the length of the pipeline section. The results are then translated from differential pressures into total pressure gradients. And they are used to compare the ascending, descending and horizontal effects. They are expected to reveal physical phenomena regarding the bed and suspension fractions.

3.3.4. Semi-empirical model validation

One of the goals of this research is to validate several semi-empirical models and ideas that focus on inclined pipe flows (the models and ideas can be found in section 2). In chapter 5 the link between the literature and the measurement results is investigated and analysed. The models are validated by comparing the expected

total pressure gradients using the horizontal pressure gradients for mixture flows and calculated water flow losses. The solids effect terms are built up from the pressure gradients for mixture flow from the horizontal experiments. This is done to eliminate any mistake with regard to the concentration or flow velocity measurements. The comparison is made for the horizontal, inclined up and inclined down data separately.

3.4. Conclusion test setup

The pressures differences, flow rates and concentrations are the required to validate the semi-empirical models and other ideas with regard to inclined hydraulic transport. For this validation, experimental data from a flow loop is required with the following specifications and testing procedures.

"Which test set-up and experiment protocol are required to gain an insight in flow characteristics in an inclined large diameter pipeline?"

The measurement section of the setup in horizontal configuration is over 110 meters long, overall it covers a distance of over 170 meters. The setup includes an inclinable section with an ascending and a descending side that can reach pipe inclination angles of up to 45 degrees. The setup includes 34 pressure taps to which 34 total pressure sensors are connected and 32 differential pressure meters. The flow loop includes a flow meter, concentration meter, thermometers and a u-loop for general data collection. The pump has the capacity of 1600 m^3/h and its RPM, power and the pressures over it are recorded. The two slurry tanks have a capacity of 100 m^3 each and the setup can be cooled using a special cooling section. The used sand is considered broad graded and coarse and has a d_{50} of 0.77 mm.

Four inclination angles are tested, 0, 17.9, 18.9 and 44 degrees, 6 different delivered solids concentrations between 0 and 15% are tested, each 3 times at several different flow rates. Before each concentration is tested, a water run is conducted to check the equipment. When the first water cycle is done, the flow rate is increased to 1600 m^3/h. Then sediment is added to increase the concentration and the flow velocity is incrementally decreased in steps of 100 m^3/h. At every flow velocity, the measurements start when the electromagnetic flow meter presents a steady signal. This happens after a few minutes so the data that is used is recorded 3 minutes after the flow rate is increased. The first three test cycles are conducted without an inclination to the system. When they are finished, the inclinable pipe section is inclined to test the other angles. order to account for the time consumed, the test sequences are divided up per day, each day a different concentration is run through the system.

The raw data is processed by filtering out the outliers to create a steadier signal. The absolute pressures and flow rate developments are compared to find time intervals with steady signals. The results are averaged per flow rate to create a single pressure, differential pressure flow rate and concentration per time interval.

4

Results

This chapter focuses on the test results of the laboratory experiments. The inclinable pipe section of the flow loop was set at inclination angles of 17.9, 28.9 and 44 degrees. The chapter is split into four primary sections. The first section contains reference measurements that validate the correct working of the sensors. In the next section the accuracy of the acquired results is discussed. The typical results section contains some representative test results. The total pressure profiles and pressure gradients over the pipe length for different concentrations and equal flow velocity are discussed. The next section contains all the pressure gradients regarding ascending, descending and horizontal hydraulic transport using $\frac{\Delta P}{L} - V$ diagrams. The results are briefly discussed and some preliminary conclusions are drawn, the in depth analysis is found in chapter 5. Note that the concentrations, as they are displayed in the figures, are not the actual delivered solids concentrations. They are displayed as '0p', '2.5p', '5p', '7.5p', '10p' and '12.5p', these are the desired delivered volumetric concentrations in percentages. The actual delivered concentrations however, are different. The reasoning is found in section 4.1 and appendix C, table C.1 in the appendix contains the corresponding averaged delivered concentrations. This notation was chosen to keep the layouts of the figures uniform.

4.1. Reference measurements

The functioning of the flow loop and its sensors is tested by conducting water flow experiments. The aim of this section is to illustrate the results of the verification measurements that were conducted. The concentrations and pressure gradients were recorded using two different methods. This redundancy of instruments allows for their verification. The calculated differential pressures are translated into pressure gradients to compare the acquired data with the Darcy Weisbach water flow model for inclined as well as horizontal liquid flows. Similar results in the $\frac{\Delta P}{L} - V$ diagrams serve as a verification for the pressure gradients and the measured flow velocity.

4.1.1. Verification concentration measurement

The experiments consisted of running several different solids concentrations through the flow loop. The delivered concentration is determined using an ultrasonic density meter and the u-loop. The delivered concentrations and mixture densities are used as input for model validation and further analysis of the data. Several mixture samples were taken during the experiments with 17.9 degrees pipe inclination to verify the functioning of the ultrasonic density meter. Some of the results are displayed in table 4.1. The table shows, that the results of the ultrasonic density meter differ from the results of the slurry samples.

Delivered concentration sampling

	Sample weight [g]	Sample volume [cm^3]	Mixture density [kg/m^3]	Sample concentration	Concentration Ultrasonic
5p	2730	2200	1050	0.030	0.01
	3030	2400	1087	0.053	0.011
	2617	2160	1017	0.010	0.01
7.5p	1783	1220	1117	0.071	0.15
	2482	1840	1120	0.073	0.15
	2111	1500	1127	0.077	0.15
10p	2267	1620	1140	0.085	0.19
	2845	2100	1154	0.094	0.2
	1830	1240	1137	0.083	0.2
12.5p	3005	2140	1207	0.126	0.25
	2954	2100	1206	0.126	0.25
	2943	2060	1224	0.137	0.26

Table 4.1: Delivered concentration sampling

The delivered concentration data from the ultrasonic density meter is verified or corrected using the u-loop. Both the instruments however, produced incorrect data in comparison to the sample data as illustrated for the ultrasonic density meter in table 4.1. Using the water data as a reference, the procedure to determine the concentration with the u-loop was corrected. The method that was used to revise the data is found in appendix C and the theory behind the correction is found in section 2.5.5. This section briefly discusses the results of the revised data and illustrates how the delivered concentration is determined.

Figure 4.1 contains the concentration ratio of the delivered concentrations according to the ultrasonic density meter and the revised procedure from the u-loop. The figure contains all ratios for the experiments at pipe inclination of 44 degrees except for the water data. Similar results were found for the recalculation of the concentrations of the experiments with 28.9 degrees pipe inclination. During the experiments at 17.9 degrees pipe inclination, no u-loop data was available. It is assumed that the same deviation of the ultrasonic density meter is applies as for the other inclined experiments.

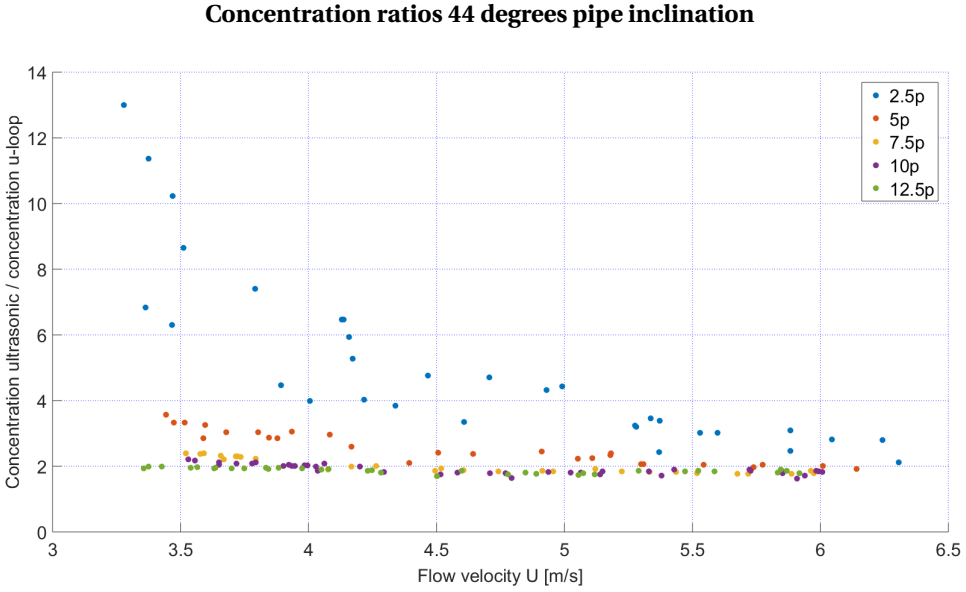

Figure 4.1: Ratio ultrasonic concentration measurement and concentration according to u-loop as a function of flow velocity at 44 degrees inclination

The ratios show a greater spread at low flow velocities and low concentrations. At higher flow velocities, the ratios converge to a value between 1.8 and 2.0 for all the different delivered concentrations.
The increasing spread is caused by a few factors. The u-loop concentration determination method automatically corrects for the subsiding of the particles in the slurry. The data from both the riser and the down going legs are used to find the delivered concentrations. This combination eliminates the effect of subsiding solid particles, particles travel slower in the riser and faster in the down going leg. Due to the combination of the two u-loop legs, the resultant velocity of the solids equals the flow velocity of the carrier liquid. In figure 4.1 this effect is visible when the lower velocities are considered since the subsiding of the particles is more severe there and the ultrasonic density meter does not take the effect of subsiding slurry flows into account.

At low concentrations the scatter is relatively higher compared to the high concentration due to the method in which it is calculated. As the corrected and measured delivered concentrations decrease, a small deviation in one of them is amplified by the ratio. A small deviation at higher concentrations has less or little effect on the ratio.

The recalculated delivered concentrations from the u-loop data are used in the results and analysis of the 28.9 and 44 degree experiments. The ratio of the delivered concentrations according to the ultrasonic density meter and the u-loop are used as a correction factor for the delivered concentrations at 17.9 degrees of pipe inclination. The delivered concentrations during these experiments were found by dividing the results from the ultrasonic density meter by 1.9, the averaged correction factor.

4.1.2. Verification pressure measurement

The measurement section of the flow loop is equipped with total pressure sensors as well as differential pressure meters. As a result, there are two methods to determine the pressure difference between two pressure taps. The differential pressure meters produce head data and the difference between two consecutive total pressure sensors is a total pressure differential. A comparison of the results of the water flow experiments can verify the correct operation of both sensor sets.

When the setup is inclined, the results of the total pressure sensors is compared to the differential pressure data, compensated for the hydrostatic pressures. In the inclined segments of the pipe, the hydrostatic pressures are subtracted from or added to the pressure differentials calculated from the total pressure sensors.

The total pressure differences differ from the results of the differential pressure sensors. The pressure differential sensors automatically compensate for hydrostatic pressure difference due to the water column in the impulse tubes. Subtracting the hydrostatic pressures $\rho_l g sin(\omega)$ from the total pressure differentials in the ascending section, allows for comparison of the methods. In the descending section, the hydrostatic pressure is added to the total pressure differences.

The total pressure gradient is found by dividing the total pressure differences by the distance over which it is measured. Figure 4.2 contains the pressure gradients for water during the experiments at 17.9 degrees pipe inclination experiments and flow velocities of around 5.6 m/s. The total pressure differentials are displayed as 'TOT' and the results of the differential pressures sensors as 'DIFF'.

In general, the direct measured differential pressures and the pressure differences calculated from the total pressure data follow each others trend. There are some peaks and dips visible in the results. Some of them might be a result of the misalignment of the pressure taps. They are visible between 0 and 10, 27 and 45 and 60 and 70 meters from the first sensor. A few other diverging results are ascribed to for instance air bubbles in the impulse tubes or the effect of bends or flanges upstream. This is found for instance between 10 and 20 meters or between 70 and 80. The two large peaks, situated between 20 and 30 meters are caused by the 180 degree bend. These results are not used in the data analysis since it is not part of the research scope of this thesis to investigate bends or waves. In the graph, at 53 meters, the pressure difference is measured over a longer section. Only the total pressure sensors were available for this section of the setup. This value can therefore not be validated by redundant instrumentation and is left out of the dataset used in the analysis section.

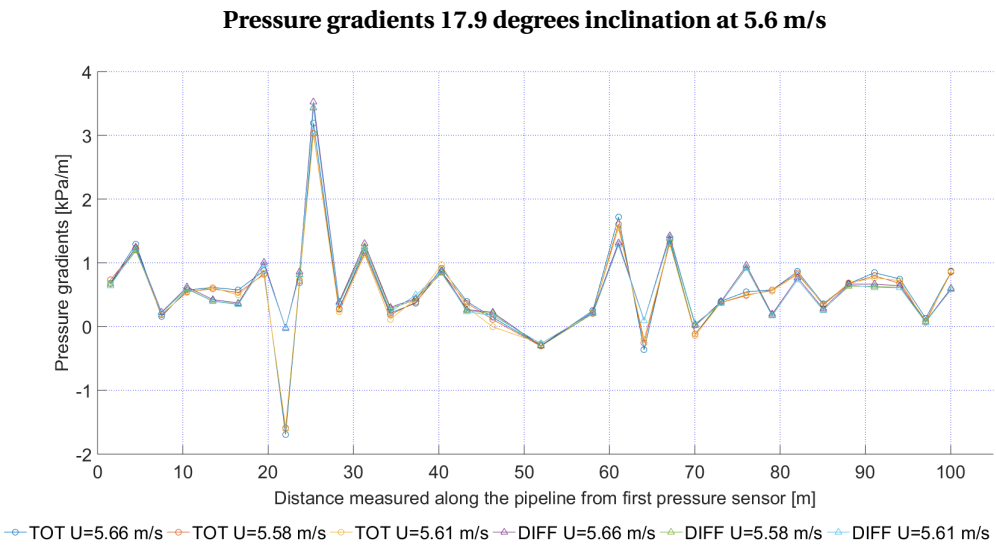

Figure 4.2: Pressure gradients of experiments with 17.9 degrees pipe inlination.

For both the horizontal as well as the inclined experiments, the differential pressure sensors and the total pressure sensors validate each other for the greater part. In section 4.4, the total pressures and their differences are used to find the pressure gradients. The range of the differential pressure sensors can be a reason not to use its results, although a range of 0 to 10 kPa should be enough to cover the head losses during the experiments. The differential pressure sensors are assumed less reliable in their results due to air bubbles that were observed in the pressure hoses. These bubbles can cause measurement errors during the experiments. The total pressure sensors recorded the pressures at the pressure taps eliminating potential errors caused by air bubbles and providing a more constant and correct image of the pressures.

4.1.3. Verification on Darcy Weisbach liquid flow

For each experiment, before sand was added to the system, several reference measurements were conducted with water. These reference measurements were executed to validate the test setup and the sensors. The results of the horizontal section are compared to Darcy Weisbach liquid flow (section 2.1.2). A pipe wall roughness of 0.000005 m was found to give a good correspondence with the measurements. This means that the pipe is assumed virtually hydraulically smooth. One of the outcomes of this comparison is displayed in figure 4.3. It contains the Darcy Weisbach pressure gradient curve for friction losses and the total pressure gradients of the water experiments in the horizontal section of the flow loop. For these results, the data between pressure taps 18 to 26 was used for the horizontal section, 4 to 7 for ascending section and 14 to 17 for the descending section.

The results of the comparison are quite similar to each other. The visible difference from the theoretical curve can be explained by a small amount of solids that is still present in the water. It causes the pressure gradients to diverge from the Darcy Weisbach line. Since the pressure differences were verified in the previous section and since the horizontal pressure gradients coincide with Darcy Weisbach liquid flow in figure 4.3, the measured flow velocity is presumed to be correct.

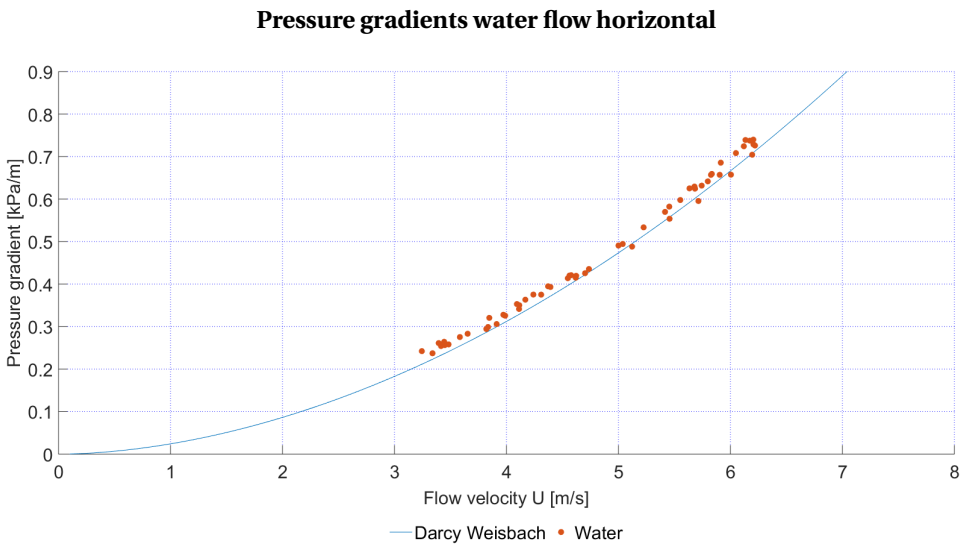

Figure 4.3: Pressure gradients Darcy Weisbach and horizontal section 28.9 degrees experiments

The liquid flow losses can additionally be checked against Darcy Weisbach for the inclined sections. The pressure gradients for inclined data are determined similarly to the gradients of the horizontal liquid flow. They have to be compensated to account for the hydrostatic component in the inclined pipeline section, before comparing them to the horizontal water flow. The theories are found in section 2.1.2. In the $\frac{\Delta P}{L} - V$ diagram in figure 4.4, the hydrostatically compensated data from the inclined section for water flows in the ascending- and descending sections is plotted. Additionally the Darcy Weisbach liquid flow curve and the liquid flow data from figure 4.3 are displayed.

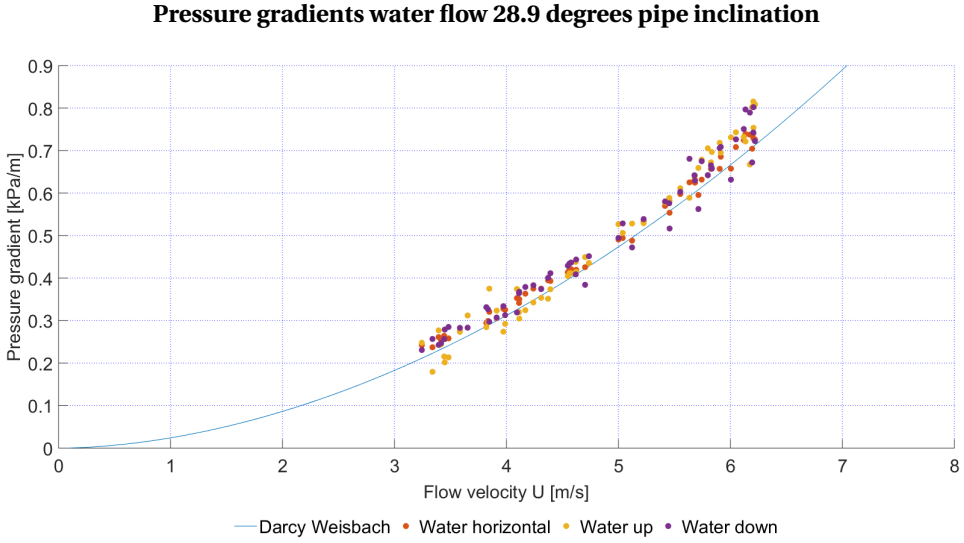

Figure 4.4: Pressure gradients Darcy Weisbach and water 28.9 degrees experiments

There is also some scatter in the data compared to the Darcy Weisbach line, although it resembles the scatter in figure 4.3. Similar to the horizontal comparison, the deviation from the Darcy Weisbach curve is likely caused by a small amount of solids still present in the liquid.

4.2. Accuracy of results

The accuracy of the results depends on several factors. This section discusses factors that influence the accuracy and can potentially cause measurement errors. The accuracy of the sensors themselves is mentioned in section 3.1.9 and generally lies between 0 and ± 0.2 %. This section elaborates on other potential errors that might influence the accuracy of the experiment results. Some factors that are discussed are: the general layout of the flow loop, the measurements, subsiding of the slurries or other physical phenomena.

The pressure taps to which the total- and differential pressure sensors are connected can cause a deviation in the results. If the pressure tap is imperfectly aligned with the previous one or its bore hole is slightly different, it can cause a deviation in the results. The results from the total pressure sensors are used to determine the pressure differentials and with those pressure differentials, the pressure gradients are calculated. A small error can have an amplifying effect on the next calculations.

The (differential) pressure sensors themselves can also cause some problems. If a pressure sensor is not working properly or air is in the impulse tubes of the differential pressure meters, the results are considered as outliers.

The flow meter was at first installed directly downstream from the pump in the riser of the u-loop. Due to its weight, the vibrations of the pump and the length of the riser, severe vibrations were generated. These caused large deviations in the flow rate data as well as the concentration data. The visible vibrations were severely reduced (to zero) in both risers after the flow meter was installed in a different riser pump.

The delivered concentrations of the samples, ultrasonic density meter and u-loop were not in line with each other. To find the delivered concentration, the recalculation method found in appendix C is used. Besides a calibration errors, the results of the ultrasonic density meter are subject to the subsiding of the solids particles in the riser. In extreme, at very low flow rates, the settling velocities of the solids can be higher than the flow velocity. The result is that solids now move past the density meter slower than the carrier liquid. This causes the ultrasonic density meter to show an in-situ concentration instead of the delivered concentration.

Another cause for less accurate results is the number of sensors in the inclined section. The roof limits inclined section to tilt angles below 18 degrees. Inclination angles over 18 degrees can only be reached after shortening the pipe. With less sections of pipe in the inclinable legs of the flow loop, less pressure taps are available. With less sensors available, a minor deviation has a larger impact on the result making it less accurate.

The presence of solids in the system during water tests is not beneficial to the correctness of the results. As mentioned before, some of the values of the total pressure gradients are too high as a result of the presence of solids in the water during the water runs.

The configuration of the flow loop itself can be a cause for inaccuracies in the data. The bends cause more turbulent flows as visible, for instance, in figure 4.8 during the first few meters in the ascending section (0 to 20 meter) and the horizontal section (50 to 100 meters). The differential pressure data contains several peaks and dips due to the effect of the bend upstream. The effect dampens out over the length of the section. Other components in the set-up that may cause deviations of the results are for instance flanges, rubber or perspex sections. Also differences in wall frictions can have a different effects on the pressure gradients.

The accuracy of the results varies for different tests, configurations and concentrations. For example, results of the water flow experiments in the descending section at 44 degrees pipe inclination (figure 4.22) show a big spread in the higher flow velocities. Whereas the horizontal pressure gradients of the water flow experiments in the same flow loop configuration display a constant trend in figure 4.20. When slurries are tested, the results also appear more constant in the ascending section of the experiments at 28.9 degrees pipe inclination than at 44 degrees. Judging from the results, a small portion of the measurements can be viewed as less accurate than the other test results due to physical phenomena, availability or malfunctioning of sensors

or the general layout of the flow loop. Most of the results however, fall within a reasonable accuracy range when compared to the trends of the results.

4.3. Typical results

This section contains an overview of some of the typical results of the experiments. The flow loop contains a total of 76 sensors. At every pipe inclination, six different delivered concentrations were ran through the system at almost 30 flow velocities. That means that a total of over 500 flow rates are recorded, with 76 sensors, the total of averaged measurements exceeds 40,000 values. The total pressure and pressure gradient profiles illustrated in this section, therefore merely contain measurements at the highest common flow velocities for the different pipe inclinations. In this section, some of the total pressure profiles are shown first and the total pressure gradients as a function of distance are displayed. The typical results are briefly discussed in this section.

4.3.1. Total pressure profiles

Figures 4.5, 4.6 and 4.7 contain the total pressure profiles of the three pipe inclination angles; 17.9, 28.9 and 44 degrees at 6 different concentrations and at nearly equal flow velocities. They provide an insight in the total pressure profile over the length of the pipeline. Figure 4.5 displays the total pressure profiles of the experiments with the pipe at 17.9 degrees inclination and flow velocities around 5.5 m/s. Figure 4.6 contains the total pressure profiles of the experiments at 28.9 degrees pipe inclination with flow velocities of approximately 5.7 m/s. Figure 4.7 illustrates the experiments with the pipe inclined at 44 degrees and averaged flow velocities of 5.9 m/s. The flow velocities are among the highest that were tested and he choking valve at the end of the flow loop was not used during these flow velocities. Since they are not affected by chocking, the total pressure profiles for different concentrations can be compared to each other.

Throughout this report, the desired delivered concentrations are referred to as '0p', '2.5p', '5p', '7.5p', '10p' and '12.5p' to keep the layout of the figures uniform. These concentrations correspond to the desired delivered concentrations, as described in section 4.1, the actual delivered concentrations differ from these values for different inclination angles. The total pressure profiles displayed in this section correspond to a small portion of the data. The trends they display, however, are the same for other flow velocities.

All total pressure profiles show the same shape of the total pressure development over the length of the measurement section. The first part is the ascending section, and in all three figures, the total pressure decreases as a result of it. In figure 4.5 the first 8 markers of each line are associated with the ascending section. In figure 4.6 they are the first 5 markers and figure 4.7 the first 3 markers.

The pressure increase in the graph right after the bend, starting at the 11th marker in figure 4.5, is caused by the descending section of the flow loop. After the descending section at marker 18 in figure 4.5, a gap of about 10 meters with no marker is visible. There is no total pressure sensor in that section, neither is there a differential pressure recorded over this section. The horizontal section starts at the gap and ends at the end of the line. The different concentrations in the figures show a clear converging trend towards the end of the flow loop in the horizontal section.

All graphs display fluctuations around the general constant trend in the horizontal section (e.g. figure 4.5 between 60 and 73 m). These variations are probably caused by local imperfections at the pressure taps or the influence of an upstream flange. The 180-degree bend is clearly visible in the data in all three figures and so is the sequence from inclined-up to inclined-down to horizontal. The two markers between the ascending and descending sections correspond with the pressure sensors on the bend.

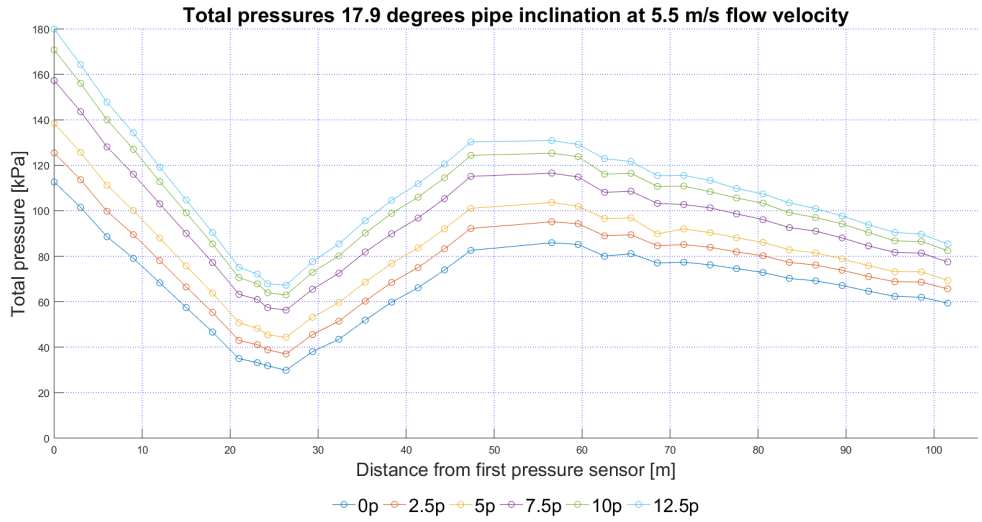

Figure 4.5: Total pressure profiles 17.9^o pipe inclination as a function of pipeline length at 5.5 m/s flow velocity

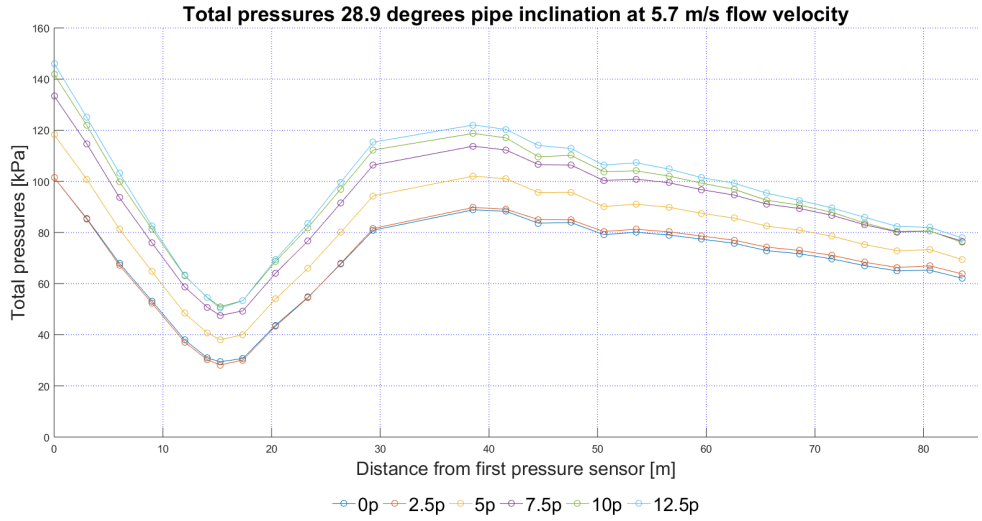

Figure 4.6: Total pressure profiles 28.9^o pipe inclination as a function of pipeline length at 5.7 m/s flow velocity

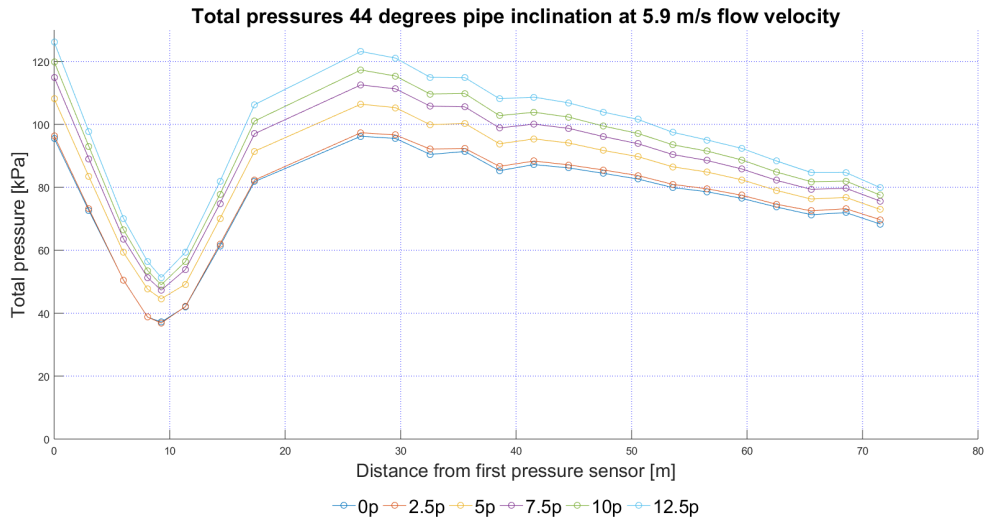

Figure 4.7: Total pressure profiles 44^o pipe inclination as a function of pipeline length at 5.9 m/s flow velocity

Although the lines have similar shapes, a clear relation is visible between the concentration and the starting points, or the overall sequences of the total pressure profiles. The higher concentrations correspond with the higher total pressure markers. The starting points of the lines become lower with increasing pipe inclination angles. At 17.9 degrees pipe inclination, the highest concentration starts at approximately 180 kPa, 145 kPa for 28.9 degrees and 125 kPa at 44 degrees of pipe inclination.

4.3.2. Total pressure gradient profiles

The differential pressure between two pressure taps is given by the difference between two consecutive total pressure sensors. This pressure difference divided by the length of the section gives the pressure gradient. The figures in this section represent the pressure gradients of the datasets discussed in the previous section. In figures 4.8,4.9 and 4.10 the result of the modification is shown for the experiments with a flow velocities and pipe inclination angles of 5.5 m/s and 17.9^o, 5.7 and 28.9^o and 5.9 m/s and 44 ^{o}.

The peaks and dips that were visible in the figures of the total pressure profiles, caused by the local imperfections, are also visible in the total pressure gradient profiles. In the total pressure and total pressure gradient figures in the previous section, they can be identified as dips and peaks in comparison to the trends of the total pressure (gradient) profiles. The dips and peaks in the total pressure gradient profiles are identified at the same locations as in the total pressure profiles.

The ascending and descending sections are clearly distinguishable between 0 and 20 meters and 28 and 47 meters in figure 4.8. The ascending section is associated with the positive and the descending section with the negative values of the total pressure gradients. The bend is recognized as the three markers in the middle between the ascending and descending sections. Theoretically, the horizontal as well as the ascending and descending sections should have a constant pressure gradient. The dips and peaks probably reflect imperfections in the pressure taps or their alignment, stationary sand waves or bend effects. Especially in the starts of the ascending, descending and horizontal sections larger peaks are visible, but appear to dampen out over the course of the sections.

Similar to the total pressure profiles, the total pressure gradients follow the sequence of low to high concentrations. The higher concentration relate to higher total pressure gradients and the lower to the lower albeit hardly visible in some instances. In the bend and between descending and horizontal sections, the lines between the markers cross each other. This is a result of the total pressure gradients going from positive to negative values. The sequence in the negative total pressure gradient region (descending section) is still from low to high concentrations and low to high total differential pressure.

The total pressure gradient profiles are carefully examined to select the most constant sequences of data. The data from the corresponding pressure taps is then used as input for total pressure gradient analysis as a function of flow velocity (section 4.4. From figure 4.9 for instance, in the horizontal section, only the markers that have a reasonably constant course between them were used. In this case markers 18 to 25 were chosen for further calculations. The chosen sequence starts around 55 meters and ends around 77 meters. Table 4.2 displays which sensor numbers were selected for each section in each pipe inclination setting (numbers are found in figure 3.1.9).

	Sensor selection					
	Ascending		Descending		Horizontal	
	Start	End	Start	End	Start	End
17.9^o	4	7	12	17	24	34
28.9^o	2	5	14	18	24	32
44^o	1	3	16	18	26	34

Table 4.2: Sensor selection

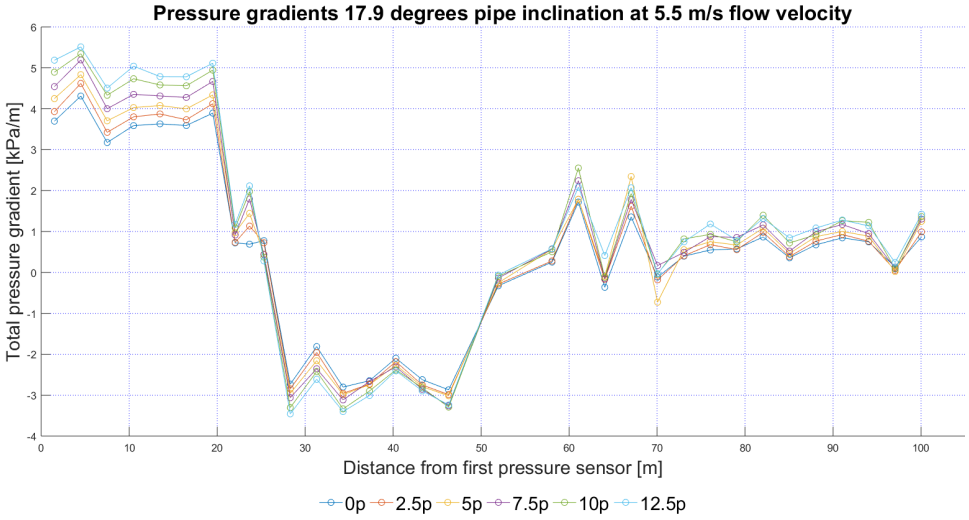

Figure 4.8: Total pressure gradinet profiles 17.9^o pipe inclination as a function of pipeline length at 5.5 m/s flow velocity

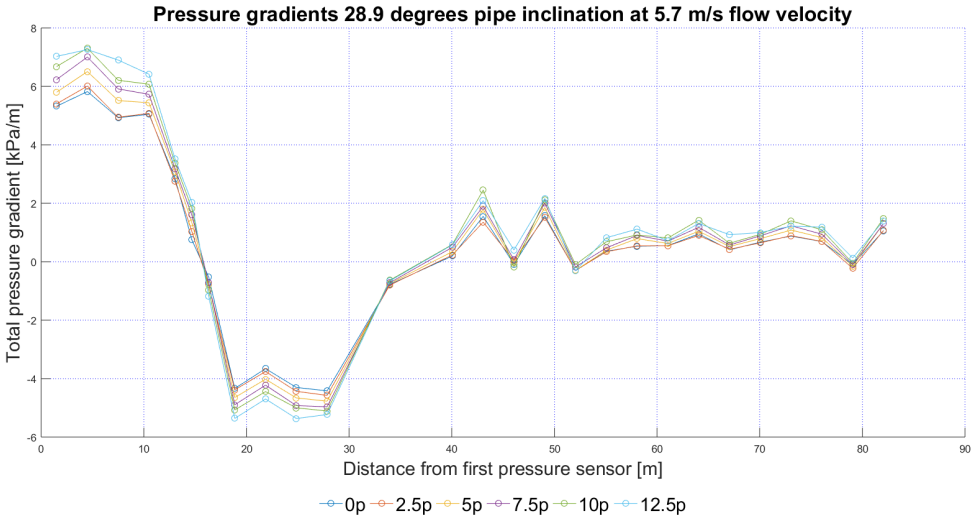

Figure 4.9: Total pressure gradinet profiles 28.9^o pipe inclination as a function of pipeline length at 5.7 m/s flow velocity

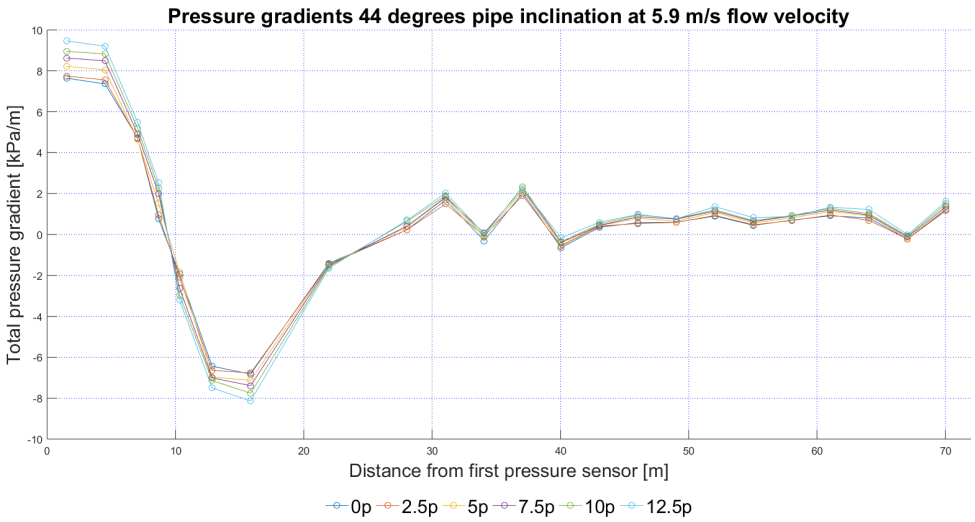

Figure 4.10: Total pressure gradinet profiles 44^o pipe inclination as a function of pipeline length at 5.9 m/s flow velocity

4.4. Pressure gradients and flow velocity

To gain insight in the data, it is plotted in similar diagrams as the i-v curves. In figure 4.11 to 4.22, the total pressure gradients are plotted as a function of flow velocity U in several $\frac{\Delta P}{L} - U$ diagrams. The recalculated delivered concentrations as a function of the flow velocity are found in the $C_{vd} - U$ diagrams. All flow directions have their own figures for every pipe inclination configuration, each inclination angle is discussed in a separate section. For reference purposes, the Darcy Weisbach curve for inclined or horizontal liquid flow is added to the $\frac{\Delta P}{L} - U$ diagrams. In the calculation of the Darcy Weisbach values, the pipe is assumed virtually hydraulically smooth. The concentrations in the total pressure gradient figures are expressed in desired delivered concentrations ('..p'). The actual delivered concentrations are mentioned in the introduction to every inclination angle and in the $C_{vd} - U$ diagrams.

4.4.1. Pressure gradients 17.9 degrees pipe inclination

This section contains the $\frac{\Delta P}{L} - U$ diagrams of the experiments with 17.9 degrees pipe inclination. Four figures are included, the first for the delivered concentration, the second, third and fourth for the (total) pressure gradients in horizontal, ascending and descending flow directions. The pressure gradient is displayed on the vertical axis and the flow velocity on the horizontal axis. The figures contain a line for calculated Darcy Weisbach water flow losses. If necessary it is compensated for the hydrostatic pressure gradient. The delivered concentrations were calculated using the correction factor that was determined in appendix C and mentioned in section 4.1. The averaged delivered concentrations are quantified as; 0p for water flow, 2.5p for 4%, 5p for 6%, 7.5p for 9%, 10p for 12.5%, 12.5p for 15%.

In figure 4.11, the delivered concentrations, calculated with the correction factor, are plotted as a function of the flow velocity. The figure is valid for the horizontal, ascending and descending sections of the flow loop. The data shows that the delivered concentrations, especially when they are over 7.5 %, decrease at flow velocities below 4.5 m/s.

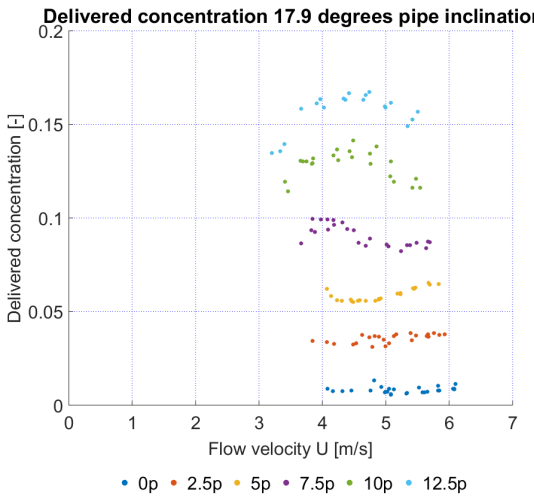

Figure 4.11: $C_{vd} - U$ diagram, delivered concentration 17.9 degrees pipe inclination

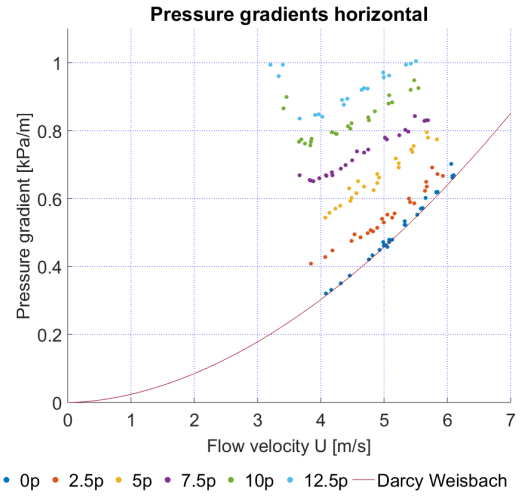

Figure 4.12: $\frac{\Delta P}{L} - U$ diagram horizontal section 17.9 degrese pipe inclination

Figure 4.12 displays the pressure gradients in the horizontal section as a function of the flow velocity in meters per second. The water flow gradients are well aligned with the Darcy Weisbach line. At higher flow velocities, the pressure gradients of the different concentrations are converging towards each other. The higher concentrations show an elevation in total pressure gradient at the lower flow velocities. A stationary bed was observed in the horizontal perspex section during those measurements. A percentage of the solids remains stationary in the pipe and is not measured by the ultrasonic density meter, therefore, the measured delivered concentration decreases with increasing bed height as visible in figure 4.11.

The results are quite neatly aligned in order of increasing delivered concentration. The lowest delivered concentration is closest to the Darcy Weisbach curve, the distance increases with increasing averaged delivered concentration.

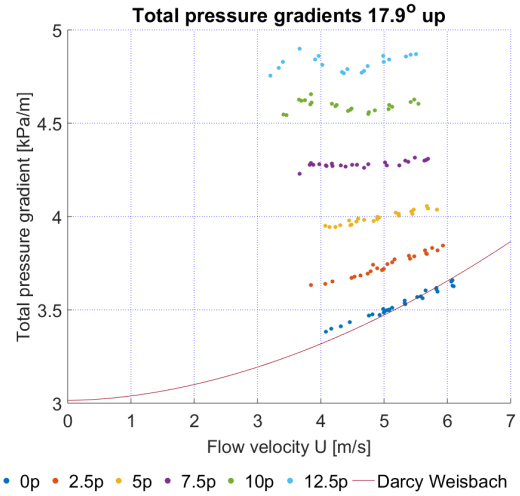

Figure 4.13: $\frac{\Delta P}{L} - U$ diagram ascending section 17.9 degrees pipe inclination

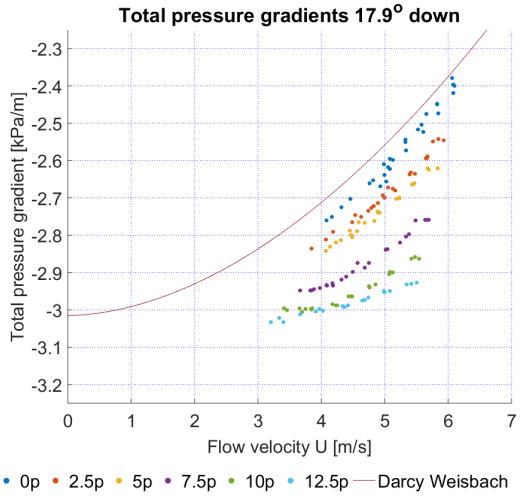

Figure 4.14: $\frac{\Delta P}{L} - U$ diagram descending section 17.9 degrees pipe inclination

Figure 4.13 displays the total pressure gradients in the ascending section during the same experiments as for the horizontal flow direction. Therefore, the delivered concentrations in figure 4.11 are applicable to these experiments as well. The Darcy Weisbach curve in the figure is compensated for the hydrostatic pressure gradient according to section 2.1.2. The calculated Darcy Weisbach values for horizontal water flow are increased with $\rho_l g sin(17.9)$ to account for the hydrostatic pressures that are included in the data from the total pressure sensors.

The sequence of total pressure gradient curves in the ascending flow direction is in order with increasing averaged delivered concentrations. The water curve has the lowest total pressure gradients and the highest concentrations correspond to the the highest total pressure gradients. In comparison to the horizontal total pressure gradients, the peak that is associated with the stationary bed shifts towards slightly higher flow velocities. This is an indication that deposits in ascending flow directions are become stationary at higher flow velocities than in horizontal flow directions. The decrease in delivered concentration towards lower flow velocities, visible in figure 4.11, appears to start at the same flow velocities as the start of the stationary bed in the ascending section. The trends of the total pressure gradient curves in the ascending section appear to stay mostly parallel relative to each other. In the higher delivered concentration ranges, the trends in total pressure gradient seem to diverge with increasing flow velocities.

In figure 4.14, the $\frac{\Delta P}{L} - U$ diagram of the descending section is plotted. Contrary to the other results, the highest average concentration corresponds with the lowest total pressure gradient and water flow with the highest. The hydrostatic pressure gradient $\rho_l g sin(-17.9)$ was added to the Darcy Weisbach curve, setting its values in the investigated flow velocity range below zero. The gradients in figure 4.14 diverge towards the higher flow velocities and converge towards the lower. Contrary to the pressure gradients in the ascending section, there is no indication of a stationary bed in the descending section.

4.4.2. Pressure gradients 28.9 degrees pipe inclination

The total pressure gradients of the experiments with 28.9 degrees pipe inclination, are divided over three $\frac{\Delta P}{L} - U$ diagrams, figures 4.16, 4.17 and 4.18. They contain the total pressure gradients for horizontal, ascend-

ing and descending hydraulic transport as a function of the flow velocity. The $C_v d - V$ diagram in figure 4.15 displays the recalculated delivered concentrations as a function of the flow velocity. The averaged delivered concentrations for the water tests correspond with 0p. The others with 1.5 % for 2.5p, 4 % for 5p, 7.5 % for 7.5p, 10 % for 10p and 15% for 12.5p. The calculated Darcy Weisbach curve for water flow ,with the hydrostatic pressure gradient added if necessary, is included in the figures for reference purposes.

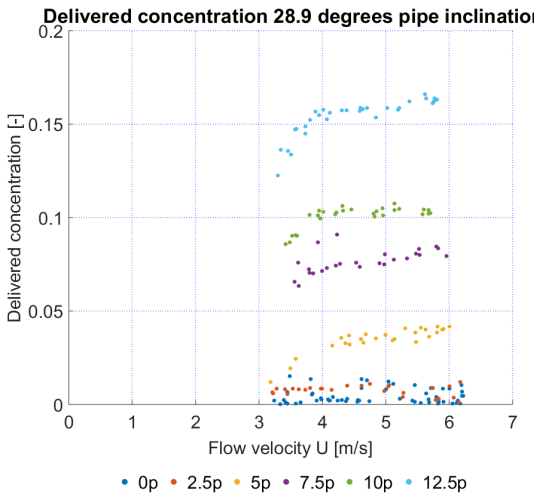

Figure 4.15: $C_{vd} - U$ diagram, delivered concentration 28.9 degrees pipe inclination

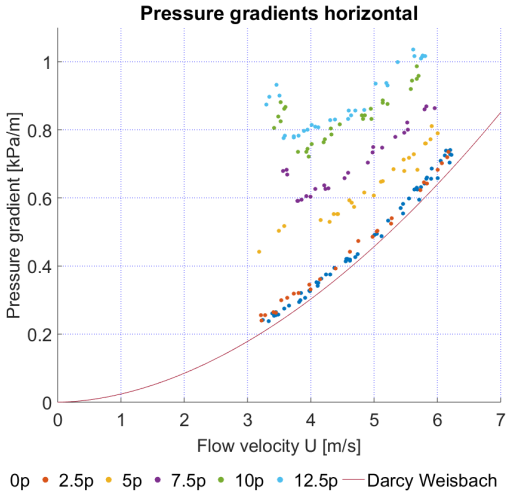

Figure 4.16: $\frac{\Delta P}{L} - U$ diagram horizontal section 28.9 degree pipe inclination

Similar to the $C_{vd} - V$ diagram in the previous section, the delivered concentration decreases with decreasing flow velocities. And similar to the results for 17.9 degrees pipe inclination, the decrease of delivered concentration is associated with the stationary bed in the horizontal and ascending sections.

Comparing figure 4.15 to figures 4.17 and 4.18, the concentrations appear proportional to the total pressure gradients in the ascending section. In the descending section the proportionality is inverse.

The horizontal pressure gradients in figure 4.16, show similar results as the horizontal pressure gradients for the experiments with 17.9 degrees pipe inclination. In the water flow gradients, some divergence from the calculated Darcy Weisbach values is visible. This indicates that some solids are present during the water flow (0p) experiments.

Figure 4.17 contains the $\frac{\Delta P}{L} - U$ diagram for the inclined ascending section of the experiments with 28.9 degrees pipe inclination. The results appear quite alike the 17.9 degree experiments with the bump for stationary bed shifting towards higher flow velocities. The bump that was clearly distinguishable in the 17.9 degree results, is smoothing out in the 28.9 degree results. To compensate for the hydrostatic pressure gradient, $\rho_l g sin(28.9)$ was added to the Darcy Weisbach values for horizontal water flow.

Similar to the results of the 17.9 degrees pipe inclination angle, the trends of the total pressure gradients in the ascending section, appear quite parallel to each other. The higher concentrations converge at the lower flow velocities. The higher pipe inclination angle causes higher total pressure gradients and bigger differences between the tested concentrations in the ascending flow direction.

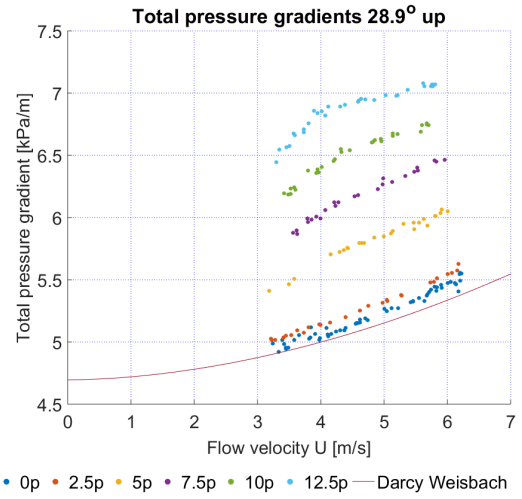

Figure 4.17: $\frac{\Delta P}{L} - U$ diagram ascending section 28.9 degrees pipe inclination

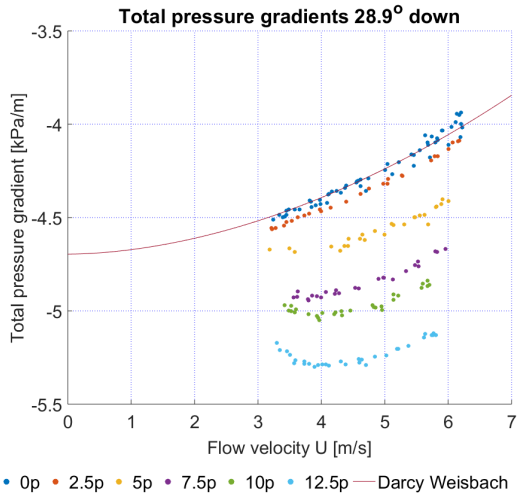

Figure 4.18: $\frac{\Delta P}{L} - U$ diagram descending section 28.9 degrees pipe inclination

The $\frac{\Delta P}{L} - U$ diagram of the descending 28.9 degree pipeline section is displayed in figure 4.18. The results are quite comparable to the results from the descending 17.9 degree pipeline section. The exceptions are that the total pressure gradients for the different delivered concentrations show more mutual distance. Morever, the total pressure gradients for decreasing flow velocities from 4 m/s display an increasing trend which is especially visible in the data of 12.5p concentration. This elevation is presumably caused by the stationary bed in the horizontal section since less solids particles are available, hence the increase in total pressure gradients. At increasing flow velocities, the total pressure gradients per concentration show a diverging trend and a converging trend towards lower flow velocities.

4.4.3. Pressure gradients 44 degrees pipe inclination

The $\frac{\Delta P}{L} - U$ diagrams for the horizontal, ascending and descending sections during the experiments with a pipe inclination of 44 degrees are displayed in figures 4.20, 4.21 and 4.22. The figures contain a Darcy Weisbach curve for water flow, if necessary compensated for the hydrostatic pressures. The 0p corresponds with water flow and the other five delivered concentrations are averaged at 2 % for 2.5p, 5 % for 5p, 7.5 % for 7.5p, 10 % for 10p and 13 % for 12.5p. Figure 4.19 displays the delivered concentration development at different flow velocities according to the calculations with the u-loop data. Similar trends as observed in the other inclination angles are visible in the delivered concentration development. The concentration decreases with decreasing flow velocity and appears proportional and inversely proportional with the total pressure gradients in ascending and descending flow directions.

Comparable to the other pipe inclination angles, the experiment results of the horizontal section show a peak in the total pressure gradient and a dip in delivered concentration when a stationary bed is observed in the horizontal perspex section. The trends of the results from the horizontal section converge towards each other during higher flow velocity regimes. This is clearly visible for the lowest concentrations (0p and 2.5p), where the trends of the pressure gradients at higher flow velocities converge, whereas for lower flow velocities they diverge. The order of concentrations is similar to the experiments with other inclination angles; the higher delivered concentrations correspond to higher total pressure gradients for all flow directions.

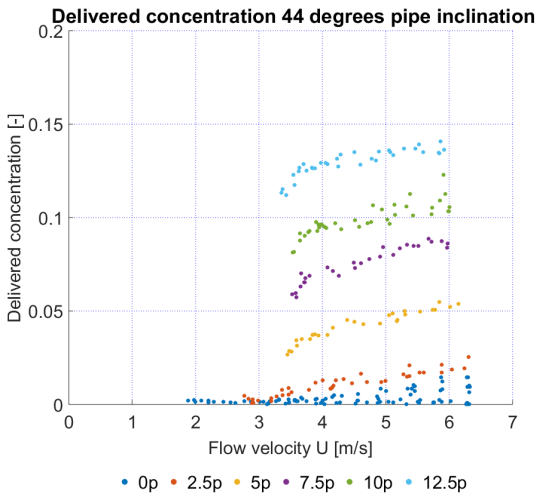

Figure 4.19: $C_{vd} - U$ diagram, delivered concentration 44 degrees pipe inclination

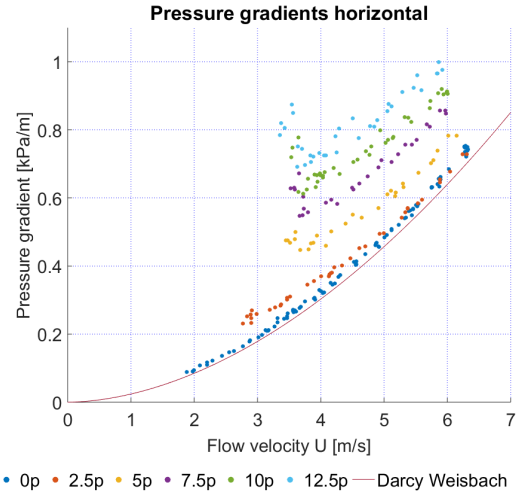

Figure 4.20: $\frac{\Delta P}{L} - U$ diagram horizontal section 44 degree experiments

The graph in figure 4.21 displays the total pressure gradients in the ascending section. The convergence of the water data and 2.5p for increasing flow velocities are also visible for these results. The elevation in total pressure gradient, associated with the stationary bed in the ascending section is almost fully smoothed out. The rest of the trends are quite comparable to the other pipe inclination angles, although the total pressure gradients are generally higher and so are the differences between the different averaged delivered concentrations. The calculated Darcy Weisbach values are increased with $\rho_l g sin(44)$ to account for the hydrostatic pressure gradient.

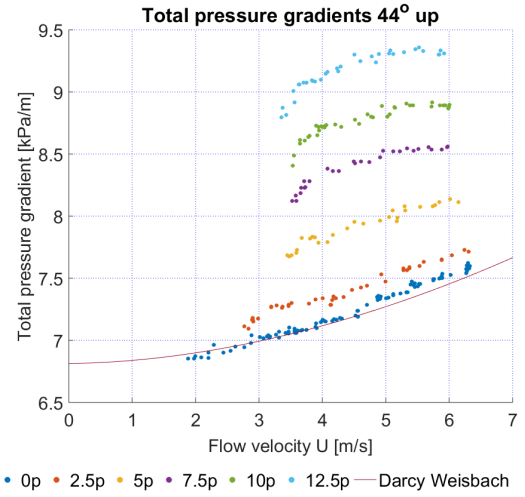

Figure 4.21: $\frac{\Delta P}{L} - U$ diagram ascending section 44 degree experiments

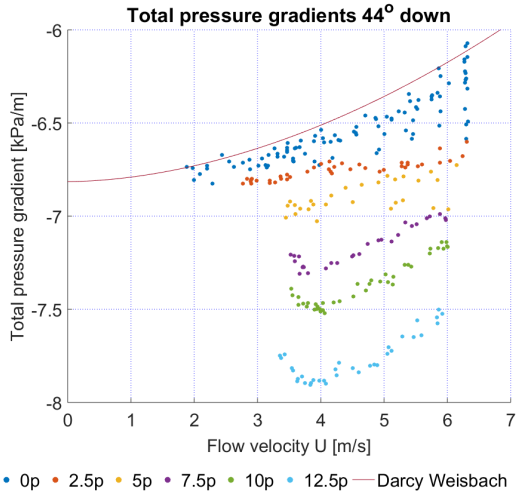

Figure 4.22: $\frac{\Delta P}{L} - U$ diagram descending section 44 degree experiments

Figure 4.22 contains the $\frac{\Delta P}{L} - U$ diagram for the descending section. In comparison to the other total pressure gradients for different inclination angles and different concentrations, a larger spread is observed in the values of the water flow experiment. The spread in the values is probably partly due to the smaller number of sensors in the inclined section and partly due to the spread in delivered concentrations (figure 4.19). In a shorter inclined pipeline section, less total pressure sensors are installed. This can make the results less reliable since a minor deviation in total pressure in one sensor has a larger effect on the averaged total pressure

gradient. When the delivered concentrations increase, the stability of the measurements seems to increase with less spread around the trends.

In comparison to the descending flow directions of other pipe inclination angles, a larger difference in total pressure gradient is observed between the different delivered concentrations. In general, lower total pressure gradients are witnessed in comparison to the results of the descending sections of other pipe inclination angles. As was observed in figure 4.18, the total pressure gradients of the higher concentrations and lower flow velocities, increase. This is an indication that the amount of the solids particles in the bed in the horizontal section is increasing with decreasing flow velocities.

4.5. Conclusion experiment results

This section contains the conclusions with regard to the results of the reference measurements, the accuracy of the measurements, the typical results and the total pressure gradients of the experiments for the horizontal, ascending and descending sections.

The reference measurements that are limited to the delivered concentrations, the total pressure (differentials) and total pressure gradients. The delivered concentration is corrected using the sample data, the u-loop and the ultrasonic density meter. The results from the ultrasonic density meter are divided by 1.9. The comparison of the pressure gradients from the differential and total pressure sensors proves that they function correctly. The correct functioning of the pressure sensors and flow meter is proven by the similar results of the calculated Darcy Weisbach water flow losses for virtually hydraulically smooth pipes and the total pressure gradients at different flow velocities for water flow in the horizontal, ascending and descending sections.

Higher inclination angles show a higher spread in total pressure gradients with different spreading in ascending, descending and horizontal sections. When slurries are tested, the results of the ascending section appear more constant improving with increasing delivered concentration. A small portion of the measurements can be viewed as less accurate than the other test results due to physical phenomena, availability or malfunctioning of sensors or the general set-up of the flow loop. Most of the results however, fall within a reasonable accuracy range when compared to the trends of the results.

All total pressure profiles have the same shape of over the length of the measurement section. In the ascending section the total pressure decreases and in the descending section it increases. In the horizontal section the total pressures decrease at a lower gradient than in the descending section. The total pressures for different concentrations converge towards the end of the flow loop. The higher concentrations correspond to higher total pressures and -pressure gradients. Some peaks and dips are observed due minor inconsistencies or imperfections in the components installed in the flow loop. The waves they cause dampen out the over the section downstream from the component. The total pressure gradient profiles are examined before calculating the averaged total pressure gradient over a section to select the sensors that display the most constant results and as little variations around the visible trends as possible.

The total pressure gradients for the horizontal section display an elevation for flow velocities at which a stationary bed is observed in the horizontal perspex section. Similar to the horizontal section, an elevation in total pressure gradients is observed in the ascending section. This elevation is presumably caused by a stationary bed and is observed at higher flow rates than the stationary bed in the horizontal section. At higher inclination angles this elevation in total pressure gradients smooths out. In the descending section, an elevation in total pressure gradient is observed at low flow velocities, high concentrations and increasingly high pipe inclination angles. It is presumably caused by the solids that remain stationary in the horizontal and ascending sections causing a decrease in delivered concentrations and a rise in total pressure gradient in the descending section. The delivered concentration appears to play an increasingly important role in the total pressure losses at increasing pipe inclinations. As trend of the delivered concentration is proportional to the trends of the total pressure losses in the ascending section and inversely proportional to the total pressure gradients in descending flow directions.

In some cases the water data of the total pressure gradient deviates from the calculated Darcy Weisbach line

due to the presence of solids in the system during the water tests. The values for the Darcy Weisbach water flow, in the inclined section, compensated for hydrostatic pressures, are closest to the lowest tested delivered concentrations.

The total pressure gradients in the ascending sections show mostly parallel trends with some instances of convergence between the different concentrations. In both the ascending and the descending sections, the mutual differences between different concentrations are observed to increase with increasing pipe inclination angles. The highest concentrations and highest pipe inclination correspond to the highest total pressure gradients in the ascending section. In the descending section the highest concentrations correspond with the lowest total pressure gradients.

5

Evaluation of results

In this chapter, an in depth analysis of the data, results and models is described over several sections. The data analysis section contains a comparison between different pipe inclination angles, delivered concentrations and flow rates. In the model section, the semi-empirical models from chapter 2 are compared with the data and the deviations or peculiarities are analysed. The primary aim of the settling slurries section is to illustrate the link between the experiment results and the observations and ideas from literature. Moreover, the ideas with regard to stratified flows, deposition limit velocities, the two- and three layer models and contact loads are discussed. The final section combines the conclusions with regard to the semi-empirical models and the observations from literature with the experiment results. A modification on the semi-empirical models is proposed with regard to the solids effect and suspension characteristics of the slurry flow.

The conclusion to this chapter answers four of the research questions with regard to the literature that is investigated for this thesis. The first question regards the three semi-empirical models: *"To what extent do the acquired results from the laboratory experiments agree with the estimated values from the semi-empirical models?"*.
The second question appears similar to the first but provides an answer with regard to the insights from past experiments: *"Do the acquired results from the laboratory experiments agree with the observations and insights from past experiments?"*.
The next question was formulated to account for the difference in length of the inclined pipeline section, it is shorter at larger pipe inclination angles. The question is: *"Are the semi-empirical models applicable on short inclined pipeline sections?"*.
The experiments conducted by other scientists were executed in flow loops with smaller pipe diameters. To test the applicability of those observations on larger diameter pipelines the final question reads: *"Are the results of experiments with small pipe diameters similar to the measurement results with larger pipe diameters?"*.
The combination of the aforementioned research questions should provide an answer to the main research question: *"Are the existing mathematical, physical and semi-empirical models for slurry transport in inclined pipelines applicable to large diameter inclined pipes?"*.

5.1. Data analysis

The first part of the evaluation focuses on a comparison with regard to pipe inclination angles, delivered concentrations, slurry flow rates and flow direction (ascending, descending and horizontal). In this section, the differences and similarities between different angles are discussed and the total pressure gradients in the different flow directions are compared, discussed and analysed.

Figure 5.1 contains all the pressure gradients of the experiments at different inclination angles. The figure is divided into six graphs, each displays a different desired concentration. The figures illustrate the comparison between different pipe inclinations and delivered concentrations. The green markers correspond with the pressure gradients in the horizontal section, the purple, yellow and red with the ascending sections at 17.9, 28.9 and 44 degrees. The three sub zero lines are the total pressure gradients in descending flow directions.

The continuous line in every graph is the calculated Darcy Weisbach curve for water flow losses in horizontal pipeline sections, it was included for reference purposes.

The graphs display a correlation between total pressure gradients and inclination angles. The highest total pressure gradients correspond with the highest inclination angles in the ascending flow direction. In the results of descending slurry flow, the lowest total pressure gradients correspond to the highest inclination angles.

The general observations by Diniz and Coiado, Graf et al. and Eltoukhy regarding horizontal and inclined up- and down flow directions appear to be valid for the measurements in this study. The d/D ratios of the experiments are almost equal with 0.0027 for Eltoukhy and Diniz's experiments and 0.00253 for the experiments conducted for this thesis. In line with the literature, the delivered concentration profile is found proportional to the total pressure gradients in the ascending section and inversely proportional to the descending. The ascending section is always associated with higher total pressure gradients than horizontal, the descending always with lower. In both experiment sets, higher mix flow velocities over 4 m/s correspond to higher total pressure gradients.

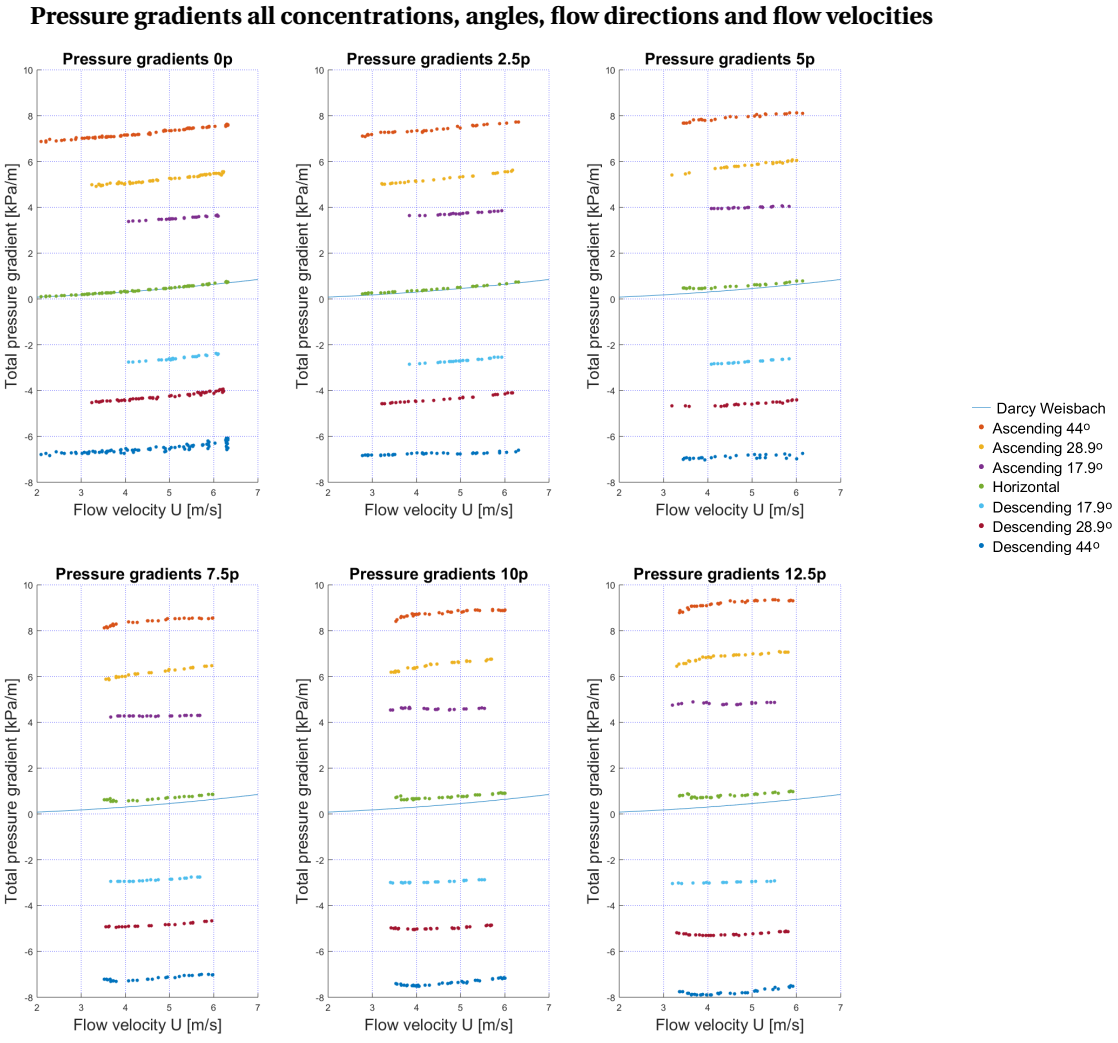

Figure 5.1: Total pressure gradients all inclination angles and concentrations

When two different desired concentrations are compared for horizontal flow, the presence of solids causes an increase in frictional losses. As a result, the horizontal pressure gradient increases with increasing concentra-

tion (figures 4.11,4.15, 4.19). In the ascending section, the suspended solids in the slurry influence the density of the mixture and therefore the weight of the slurry. The static pressure gradient caused by the suspension in the ascending section, increases with increasing inclination angles. Besides the gravitational mechanism, the pressure gradient increases due to the friction of the solids with the pipe wall. As the flow velocities increase, the total pressure gradients in the ascending flow directions increase.

Similar to the results in the ascending section, at increasing flow velocities from 4 m/s, the total pressure gradient in the descending section increases. At decreasing flow velocities below 4 m/s the total pressure gradient also increases. The minimum total pressure gradient lies around flow velocities of 4 m/s. At low flow velocities, the increase in total pressure gradient is probably caused by the decrease in solid particles present in the slurry flow due to the stationary bed in the horizontal section.

A comparison of the general shape of the ascending and descending sections of the same inclination angle show that the results are not mirrored in respect of their total pressure gradients. This indicates that the slurry in the ascending flow direction is subject to different mechanisms than in the descending flow direction.

In inclined slurry flow, the static pressure gradient plays major role in the value of the total pressure gradients. As the delivered concentration is increased, so does the total pressure gradient in the ascending section. In descending flow directions the inverse principle is observed (i.e. an increase in concentration causes a decrease in total perssure gradients).

5.2. Semi-empirical models

This section contains an analysis of the semi-empirical models for experiments with 17.9, 28.9 and 44 degrees pipe inclination. It is split into three sections in which the solids effect and the results ascending and descending flow directions are discussed. Each section contains a set of figures for different concentrations and inclination angles.

The basic structure of each semi-empirical model is similar, equation 5.1 displays the terms that are found in each model. Exponent X in the equation represents differences between the three semi-empirical models. For Worster and Denny it is 1, Gibert 1.5 and Wilson 1+M (see chapter 2).

$$i_{m,\omega}\rho_l g = i_l\rho_l g + (i_m - i_l)cos(\omega)^X\rho_l g + C_{vd}(S_s - 1)sin(\omega)\rho_l g + sin(\omega)\rho_l g = \frac{\Delta P}{L} \tag{5.1}$$

In equation 5.1, i_l corresponds to the calculated Darcy Weisbach friction losses and i_m is the mixture gradient that was measured in the horizontal section. This i_m iss chosen instead of a theoretical pressure gradient to allow for a focussed investigation on the effect of pipe inclination, without influences of inaccuracies in the prediction for horizontal flow.

The effects of the friction losses, the inclination angle, solids effect and the suspension term in the equation 5.1 are illustrated in figure 5.2. The graph contains a visual representation of the general structure of the-semi empirical models. The difference between two lines represents the term that is displayed between them. The full description of the semi-empirical model by Worster and Denny, with regard to total pressure gradients is plotted using the blue curve. The red curve represents the same semi-empirical model with the suspension term set at zero. The other two curves correspond with the calculated Darcy Weisbach values for water flow in horizontal and in ascending flow directions.

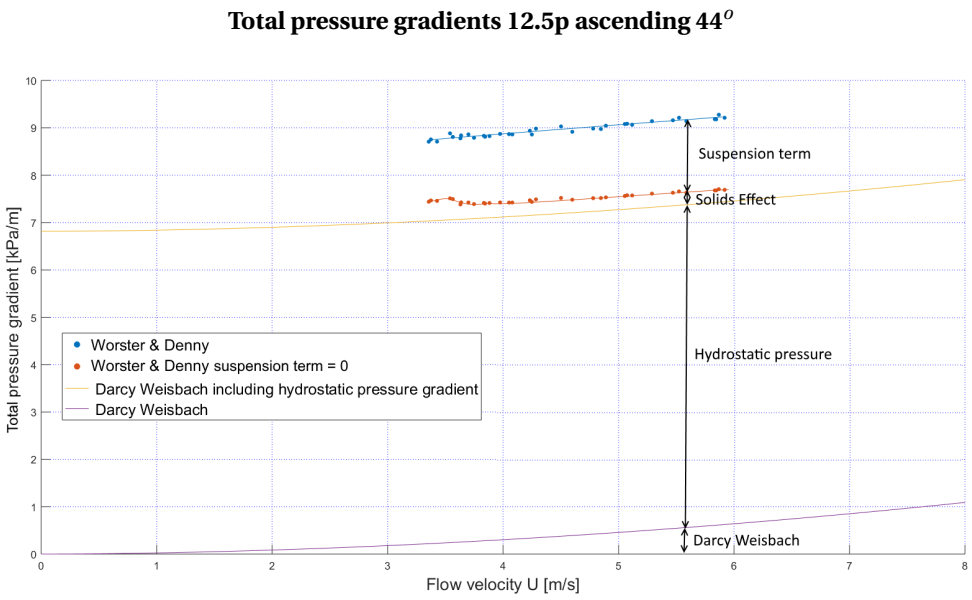

Figure 5.2: Visual representation of Worster and Denny model for heterogenous flow at 44 degrees pipe inclination and 12.5p.

The i_m that was used in the models is measured in the horizontal flow direction. The i_l is calculated using the Darcy Weisbach function for liquid flow losses. In horizontal flow directions, the pipe inclination angle (ω) is set at zero eliminating both the suspension term as well as the hydrostatic pressure gradient from the equation. Since the i_l for water flow losses and the i_l in the solids effect cancel out, $i_m = i_m$ remains. Therefore the results for horizontal flows are left out of the semi-empirical model analysis section.

5.2.1. Semi-empirical models solids effect

The solids effect is defined as hydraulic loss due to frictional resistance by the presence of solids (section 2.1.5). The graphs in figure 5.3 and figure 5.4 display the total pressure gradients of the different inclination angles for 12.5p. The sequence of the graphs is in the order of increasing pipe inclination angles. The data is split up into the different terms that describe the models (see page 54). In the figures, the yellow and purple lines represent the Darcy Weisbach curves for horizontal, ascending and descending flow directions. The calculated values for the Worster and Denny model are displayed with the suspension term set at zero (red triangular markers) and the full description(blue squares). The measured data is plotted using green markers.

As a result of the cosine, the solids effect determined with the semi-empirical models decreases with increasing inclination angles for both ascending as well as descending flow directions. The solids effect has a positive effect on the total pressure gradient, i.e. the total pressure losses increase due to the solids effect.

Due to the stationary bed in the horizontal sections, a step-change is visible in the pressure losses. At flow velocities below 3.5 m/s, the bed in the horizontal section is observed stationary. The stationary bed causes an increase in pressure losses in the horizontal section, and therefore an increase in the calculated solids effect for inclined flows. When the bed becomes stationary, the measured delivered concentration decreases since a part of the solids remains stationary and does not pass the density meter or the inclined section. This decrease of available solids for transport can cause a decrease in total pressure gradient in the ascending section or an increase in the descending section of the system where no stationary bed is present.

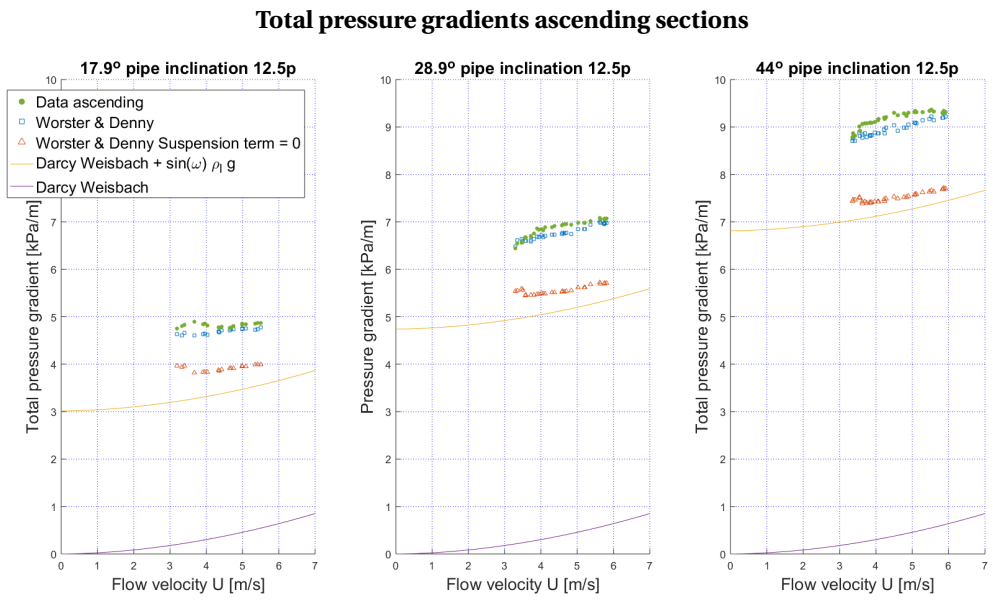

Figure 5.3: Total pressure gradients all ascending angles model structure, 12.5p

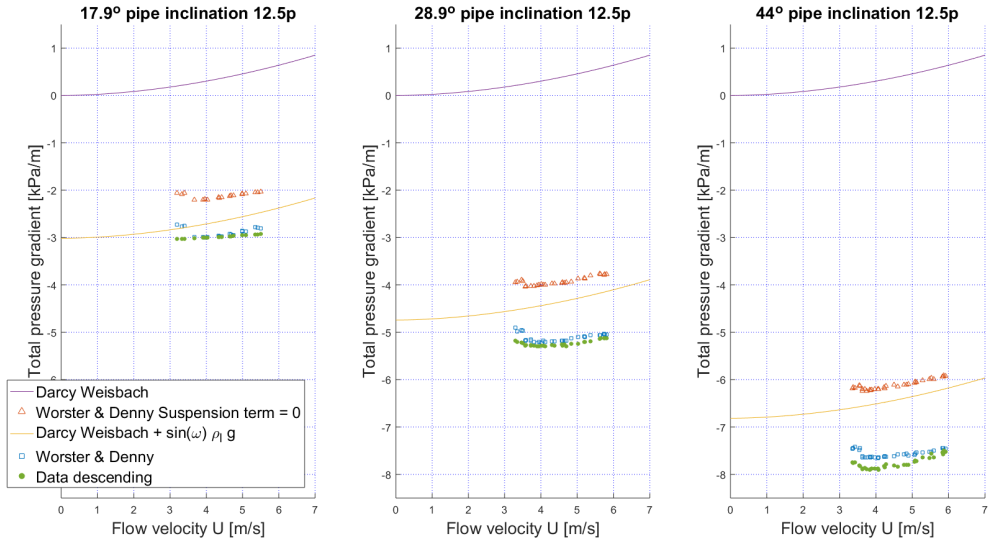

Figure 5.4: Total pressure gradients all descending angles model structure, 12.5p

5.2.2. Semi-empirical models ascending flow directions

This section contains the analysis of- and comparison between the semi-empirical models and the experiment results in ascending flow directions. Figures 5.5, 5.6 and 5.7 contain the graphs for the total pressure losses as a function of the flow velocities for all pipe inclination angles. Four figures are plotted for every pipe inclination angle to illustrate the effects for the 0p, 5p, 7.5p and 12.5p delivered concentrations. The blue curve represents the calculated Darcy Weisbach values for water flow losses including the hydrostatic pressure gradient, for reference purposes. The semi-empirical models are represented by the red pentagrams for Gibert, yellow diamonds for Wilson and purple squares for Worster and Denny. The measured data is included using the green markers.

The water flow measurements for all pipe inclination angles and semi-empirical calculations show great resemblance to each other in the 0p graphs. The calculated Darcy Weisbach curve for water flow losses has slightly lower values than both the data and the calculated results from the semi-empirical models. The reference measurements already revealed that some divergence due to the presence of solids in the water flow measurements is observed. During the water tests with 44 degrees pipe inclination, a larger spread in delivered concentration is observed compared to the other inclination angles. This spread causes an increased variation in the measured- and calculated total pressure gradients.

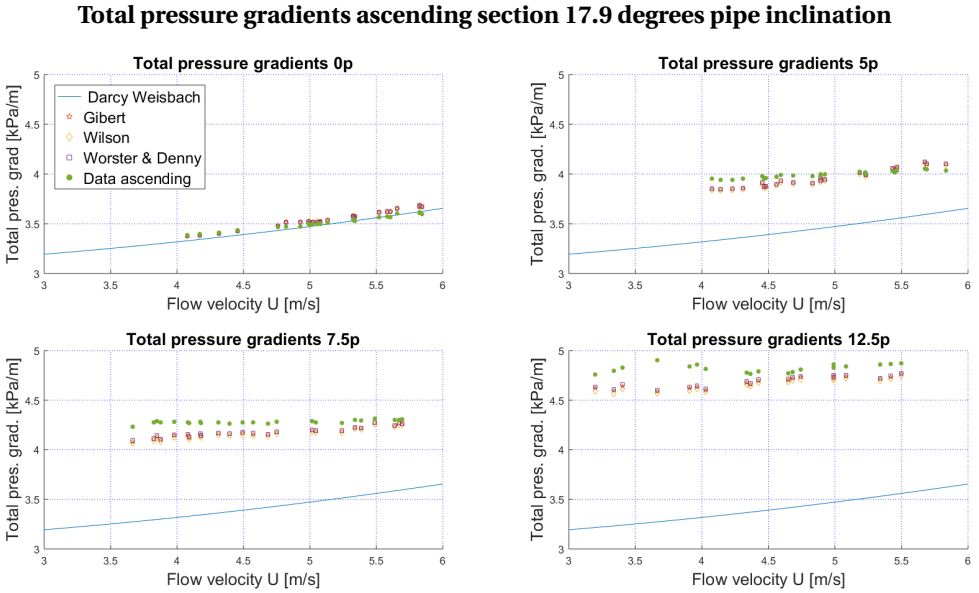

Figure 5.5: Total calculated and measured pressure gradients 17.9 degrees pipe inclination, ascending flow direction

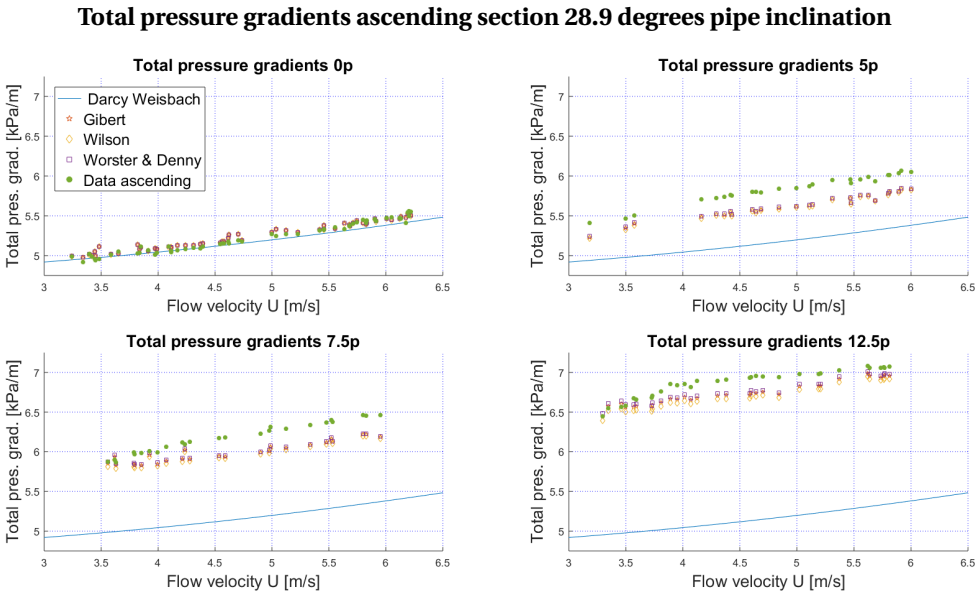

Figure 5.6: Total calculated and measured pressure gradients 28.9 degrees pipe inclination, ascending flow direction

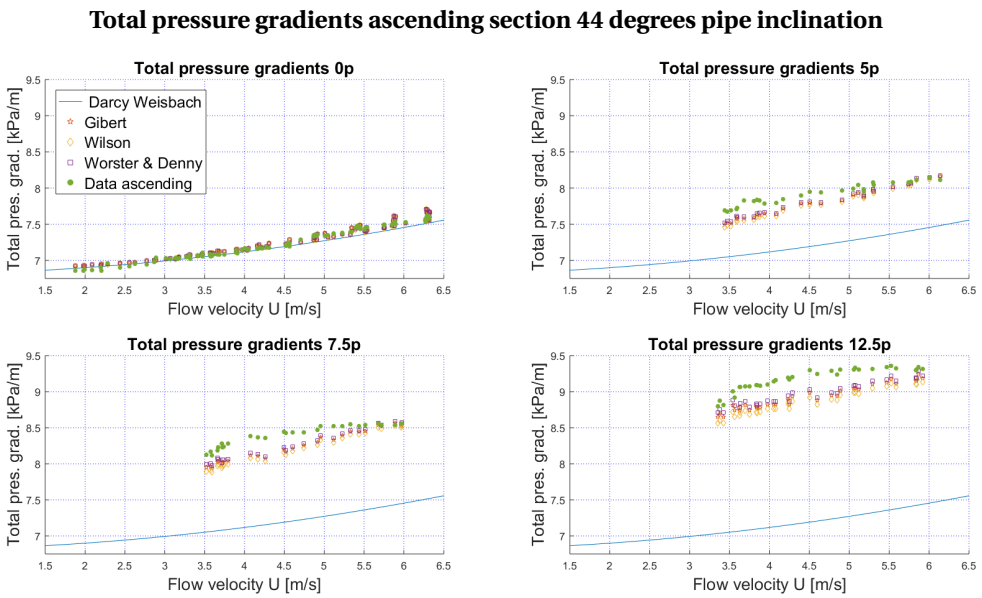

Figure 5.7: Total calculated and measured pressure gradients 44 degrees pipe inclination, ascending flow direction

The 0p and 2.5p calculated results and measured data are very close to the Darcy Weisbach curve, indicating that very low concentrations have little to no effect on the total pressure losses. An increase in in-situ concentration in the flow loop causes larger mutual differences between the different models among each other as well as between the models and the measurements due to the increasing solids effect. Higher inclination angles cause larger differences between the different semi-empirical models. The difference between the models is caused by the exponent that Gibert and Wilson added to the cosine of the solids effect term since the other input parameters are equal for the models. The increase in the exponent causes a lower value of the inclined solids effect term and the effect is amplified for higher inclination angles.

In the ascending section for all pipe inclination angles, the Worster and Denny model most accurately predicts the total pressure gradients, followed by Gibert and Wilson. In both the semi-empirical model calculations as well as the measured data, regardless of pipe inclination angle, increasing concentration causes an increase in total pressure losses. An increase in flow velocity also causes higher values in both the theoretical- as well as the measured total pressure gradients.

The total pressure losses in the ascending section are generally underestimated by the calculated values from the semi-empirical models. At lower concentrations this underestimation is usually less than at higher concentrations. At the lowest and the highest tested flow velocities, the underestimation is less than in the middle region of the flow velocity range. When the flow velocities are over 5.5 m/s. The semi-empirical model estimations and measured data are almost equal. At those higher flow velocities, the semi-empirical model and measured data similarities are most clearly visible in the 7.5 and 12.5 graphs of all inclination angles. At high flow velocities, it is presumed that the solids are suspended in the mixture flow, which will give an accurate estimation for both the suspension- as well as the solids effect terms in the semi-empirical models.

An input value of the semi-empirical model calculations is the delivered concentration that was determined during the experiments. The delivered concentration decreases when the flow velocity decreases (figures 4.11, 4.15, C.5) due to solids that remain stationary in the stationary beds. A stationary bed was observed in the horizontal perspex section at low flow velocities. In ascending flow directions, a decrease in delivered concentration is a cause for the measured total pressure gradients to decrease and thus converge towards the semi-empirical models at flow velocities below 3.75 m/s.

At increasing flow velocities over 3.75 m/s, the difference between calculated total pressure gradients and measured data increases and then decreases. As the models are calculated using the total pressure losses that

were measured in the horizontal section, they do not take the different stratification effects in the ascending sections in account. Assuming that the flow velocity at which stationary deposits are formed is higher in ascending flow directions than in horizontal, flow stratification can create a difference between the measured data and the values produced by the models. In the ascending 12.5p graphs, this divergence is observed for flow velocities between 3.75 and 4.5 m/s in the 17.9 degrees pipe inclination figure. The elevation in total pressure gradients associated with a stationary beds, appears to smooth out with increasing pipe inclinations. It is clearly distinguishable in the 12.5p graph of 17.9 degrees pipe inclination and completely smoothed out in the 12.5p graph of 44 degrees pipe inclination in figures 5.5 and 5.7. The semi-empirical model predictions of the total pressure gradients are not accurate when stratified beds are assumed.

5.2.3. Semi-empirical models descending flow directions

This section contains the analysis with regard to the semi-empirical models and experiment results in descending flow directions. The graphs with the total pressure gradient as a function of flow velocities are found in figures 5.8, 5.9 and 5.10. The different figures represent the different pipe inclination angles. Four figures are displayed for every pipe inclination angle to illustrate the effects of the 0p, 5p 7.5p and 12.5p concentrations. The calculated total pressure gradients using the semi-empirical models by Gibert, Wilson and Worster and Denny are represented with red pentagrams, yellow diamonds and purple squares. The calculated Darcy Weisbach values for inclined water flow losses are plotted using the blue curve and the measured data is included using the green markers.

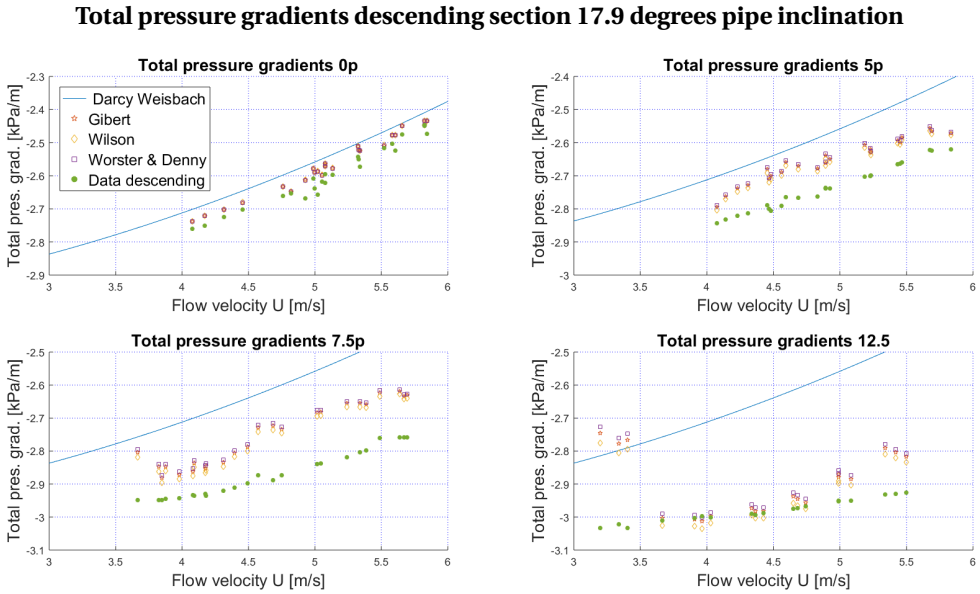

Figure 5.8: Total calculated and measured pressure gradients 17.9 degrees pipe inclination, descending flow direction

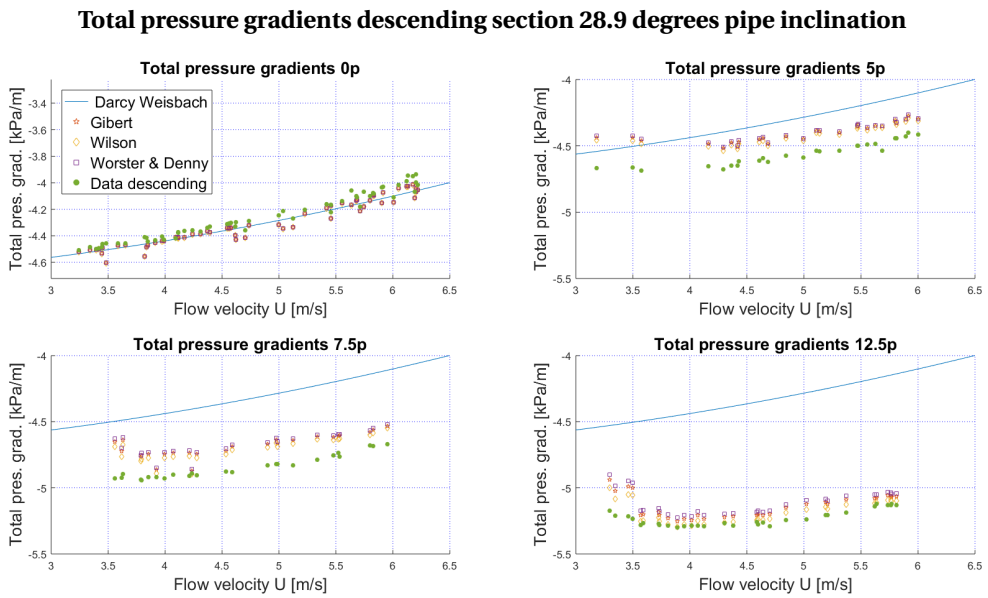

Figure 5.9: Total calculated and measured pressure gradients 28.9 degrees pipe inclination, descending flow direction

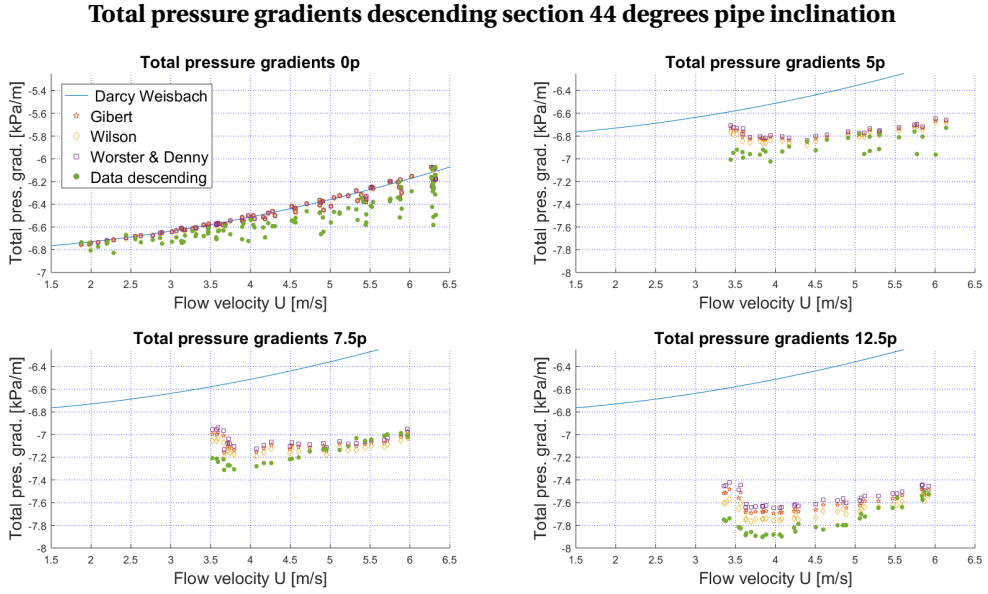

Figure 5.10: Total calculated and measured pressure gradients 44 degrees pipe inclination, descending flow direction

In the descending direction for all inclination angles, in the 0p graphs, the semi-empirical calculations show great resemblance to the measured data and the calculated values for Darcy Weisbach water flow. The 44 degrees pipe inclination results display the largest variations around the Darcy Weisbach curve. The pipeline section at 44 degrees pipe inclination is shorter than the 17.9 or 28.9 degrees sections. The shorter length can have an impact on the internal structure of the flow and cause larger deviations in total pressure gradients due to for instance, bends or flanges upstream. It can also be caused by the lower number of available pressure sensors in the inclined section at high pipe inclinations. Since the semi-empirical models were calculated using theoretical liquid flow losses and the horizontal pressure gradients, the models are closer to the Darcy Weisbach curve.

Comparable to the ascending flow directions, the 0p calculated total pressure gradients and measured data are very close to the Darcy Weisbach curve, indicating that very low concentrations have little to no effect on the total pressure losses. With increasing concentrations a decrease of pressure losses is observed regardless of pipe inclination or flow velocity. This phenomenon is visible in both the semi-empirical model calculations, as well as the measurement results. In the descending section, the calculated theoretical total pressure gradients generally overestimate the measured total pressure gradients.

Similar to the ascending flow directions, an increase in in-situ concentrations in the flow loop or pipe inclination causes larger mutual differences between the calculated values of the total pressure gradient. The difference between the models is caused by the exponent that Gibert and Wilson added to the cosine of the solids effect term. In otherwise equal equations, an increase in this exponent causes a decrease in the solids effect term which causes lower theoretical total pressure gradients. The increase in concentration causes an increase in solids effect which amplifies the effect of the exponent and the differences between the different theoretical total pressure gradients. The Wilson semi-empirical model uses the largest exponent, followed by Gibert and Worster and Denny. Therefore, the Wilson model most accurately predicts the total pressure gradients in descending sections, followed by Gibert and Worster and Denny.

The trends of the models and the measurements are generally parallel to each other. In the 12.5p figures at flow velocities below 3.5 m/s, the pressure losses estimated by the semi-empirical models have increased to over the Darcy Weisbach curve for water flow. It is assumable that this significant over-prediction is a result of an overestimation of the solids effect. Measured pressure gradients from the horizontal flow direction are used to calculate the solids effect in the inclined section. The pressure gradient in the horizontal flow increases due to the stationary bed, which causes an increase in the value of solids effect term in the semi-empirical models. The effect is dampened slightly due to the cosine and the exponent, however not enough to deliver an accurate prediction for low flow velocities.

A stationary bed is probably not present in descending flow directions, especially at higher pipe inclination angles. As a result, the total pressure losses at flow velocities below 3.5 m/s are subject to larger model overestimations than at higher flow velocities. The 7.5p and 12.5p graphs in the figures illustrate this idea. Besides the over prediction of the solids effect, the differences can be caused by an underestimation of the effect of the suspension term in the semi-empirical models. The combination is an indication that the effects of the suspension and stratification on the total calculated pressure gradient in the descending section are not correctly estimated by the semi-empirical models for stratified flow regimes. This indicates that the stratified bed is probably smaller than in ascending- and horizontal flow directions and more solids are transported suspended in the flow.

5.3. Settling slurries

In this section of the evaluation, the outcomes, observations and expectations of the experimental researches with smaller pipe diameters regarding stratified flows are evaluated. The observations with regard to the deposition limit velocity from chapter 2 are discussed and compared to the results of this research. The conclusions in the literature touching on suspended flows, moving or stationary beds and contact loads in inclined pipeline sections are compared to the observed phenomena during the experiments. In the final section, Matousek and Doron's two- and three layer model observations are evaluated.

5.3.1. Deposition limit velocity

As a result of experiments done by different researchers, the deposition limit velocity has several definitions. In this section, deposition limit velocity is defined the same as by De Hoog et al. [de Hoog et al., 2017]: the deposition limit velocity is the flow velocity at which a bed of stationary deposits is formed. In the experiments, the flow velocity was gradually decreased until a stationary bed was observed in the horizontal perspex section. In the literature it is agreed that the DLV in inclined sections is higher than in horizontal sections. According to Matousek and Vlasak the maximum DLV is found between 20 and 40 degrees of pipe inclination in ascending pipe sections. De Hoog observed the maximum at a pipe inclination angle of 30 degrees in ascending flow direction. In figure 2.9 the dimensionless maximum deposition limit velocities from researches

by Hashimoto et al., Wilson and Tse and de Hoog et al. are displayed as a function of pipe inclination angles.

The solids effect in the semi-empirical models for inclined pipelines, is based on horizontal flow. In horizontal flow directions, the stationary bed causes a higher pressure loss. When the ascending section is evaluated, the semi-empirical models do not take into account that the ascending flow has a higher DLV. The stationary and sliding beds appear at higher flow velocities in ascending flow directions. The semi-empirical models are based on an under estimation of the DLV in the ascending section. The maximum should be around 30 degrees of pipe inclination. According to the conclusions of De Hoog et al., Wilson and Tse, Hashimoto et al., Matousek and Vlasak, Doron, Spelay, Eltoukhy, Diniz and Coiado, the slurry flow in ascending flow directions becomes stratified at higher flow velocities higher than for horizontal flow. Comparing the results of the experiments, models and conclusions, the bed becomes stratified in the ascending pipeline section at 17.9 and 28.9 degrees pipe inclination at flow velocities between 3.5 and 4 m/s. Whether or not the bed indeed becomes stationary proved impossible to observe.

At increasing inclination angles, the stationary bed peak, smooths out, indicating that there is no longer a possibility for stationary bed formation. As the bed becomes stationary in the horizontal section, less solids are available in the rest of the system. Especially at 44 degrees pipe inclination, where a stationary bed is not possible, the declining amount of suspended material is a cause for decreasing total pressure gradients in the ascending flow direction and increasing total pressure gradients in descending flow.

5.3.2. Flow suspension and stratification

Solid particles in a slurry at high flow velocities are assumed suspended in all flow directions. At high flow velocities, turbulent eddies are large enough to suspend particles in the flow. As flow velocities decrease, the efficiency of turbulent suspension decreases. For relatively small solids particles, with d/D ratio below 0.1, turbulent suspension is more effective than for larger particles [Spelay et al., 2016]. Moreover, when higher flow velocities are tested, turbulent suspension is more effective due to the intensity of the velocity fluctuations.

De Hoog et al. and Vlasak used relatively large material, sometimes with d/D ratios over 0.1. As the inclination angles increase, the turbulent suspension mechanisms become less effective. With the result that the deposition limit velocity increases. The material that was used for the research conducted for this thesis, had a broad particle size distribution with d/D ratio of 0.00253. This similar to the experiments conducted by for instance Eltoukhy, Diniz and Coiado and Matousek. In line with the observations in their experiments, an increase in total pressure gradients was witnessed at low flow velocities in both the descending and ascending flow directions as a result of stratified flows.

When a flow becomes stratified, the submerged weight of the solid particles is transmitted to the pipe wall. This transfer of intergranular forces (i.e. mechanical friction) causes higher pressure losses and larger pressure gradients. In ascending flow directions, an increase in total pressure gradients was observed at flow velocities slightly higher than the DLV in horizontal sections. In accordance with the experiment results of de Hoog and Vlasak, this increase is associated with flow stratification. When the flow in the horizontal section was observed stratified, the total pressure gradients in the inclined ascending section decline. This effect is assigned to the decrease of the delivered concentration. In the descending section, the stratification of the horizontal bed caused an increase in total pressure gradient. As found by Eltoukhy, the delivered concentration in the ascending flow was found to be proportional with the total pressure gradients in ascending slurry flows and inversely proportional with descending flows.

In line with the literature, the total pressure gradients from the measurements in inclined ascending pipe flow were always higher than the horizontal hydraulic gradients and in inclined descending pipe flow always lower than horizontal, regardless of concentration or flow velocity. Furthermore, in line with literature, higher inclination angles cause higher total pressure gradients in ascending flow directions and lower total pressure gradients in descending flow directions. In general it was found that higher flow velocities cause higher hydraulic gradients.

5.3.3. Internal structure

Vlasak observed that the concentration in inclined slurry flow with large particles is linearly distributed with a value of 0 in the upper portion of the pipe and the maximum near the bottom. Pipe inclinations below ± 30 degrees, had little influence on the concentration distribution. At higher flow velocities, the concentration near the pipe bottom decreased with a greater effect for larger pipe inclination angles. The effect of the inclination angle on the pressure gradient of the mixture is mostly due to the static pressure gradients of the mixture.

Vlasak and Matousek concluded that the concentration in lower part of an inclined pipe cross section in the descending direction is higher than in horizontal or ascending flow directions. This is an indication of a larger or more compact moving bed at low flow velocities between 3 and 4 m/s in the descending flow direction. Assuming that it is present in the descending section of the set-up, since a stratified flow causes more friction pressure losses than suspended flows, the peak in total pressure gradients at low flow velocities in the descending section can be explained by a moving bed in descending flow directions.

In the literature, different observations were made for ascending and descending flow directions with regard to the internal structure of the flow. De Hoog et al. observed a lower bed height in the descending section than in the ascending section at equal flow velocities and concentrations. Unfortunately, the conclusions with regard to internal structure of the inclined slurry flow can not be validated.

5.3.4. Two and three layer models

The increase in DLV for higher inclination angles is not included in the semi-empirical models. As a result, the effects of stratified flows on the total pressure losses in ascending sections are under estimated and in descending flow directions they are over estimated. To account for flow stratification, Matousek and Shook and Roco came up with two layer models and Doron with a three layer mode. These physical models account for the differences in flow directions and flow regimes by accounting for the thickness of the stratified beds. The cosine and sine terms in the semi-empirical models do not cope with the different effects of flow stratification on the ascending and descending flow directions. Identifying different layers when modelling a flow can be a solution to the over- and underestimations of the models. However, these models need input values that are hard to observe or acquire (i.e. the friction on the interfaces, concentrations, bed heights and cross sectional areas of the different layers).

The semi-empirical models contain a term for the hydrostatics of the carrier liquid defined by the Darcy Weisbach pressure losses. The term for the solids effect accounts for effects caused by the stationary bed and the moving bed in the horizontal section. In ascending flow, the bed might be thicker, resulting in a higher solids effect. The over- and underestimations by the semi-empirical models are probably caused by the underestimation of the effects of the stratified beds on the total pressure gradients. The 2 or 3 layer models do take these effects into account. Unfortunately, they can not be verified due to lack of data on the layer thickness, velocity and visual observations of the layers in the inclined sections.

The results of the experiments were clearly influenced by a stratification effects during the tests. As stated by Matousek, a difference in pressure gradients was observed that was due to the different behaviour of the slurry in different flow directions and was especially caused by friction. As the flow velocity was decreased, the moving- or stationary beds had an impact on the total pressure gradients that is not included in the semi-empirical models for inclined slurry flows. Therefore, a different approach has to be taken with regard to the total pressure gradients prediction in the ascending and descending sections.

5.4. Semi-empirical model modification

Differences in stratified flow regimes for different flow directions apparently are the main cause for under- and overestimations of the total pressure gradients by the semi-empirical models. In this section, modifications on the the solids effect term are proposed which should have a positive effect on the accuracy of the predictions. Since different mechanisms are identified for different flow directions, the section is split into two parts regarding ascending- and descending flow directions.

According to the semi-empirical models, the influence of solids effect diminishes with higher pipe inclination angles. In ascending flow directions with stratified flow regimes, the solids effect appears to be underestimated. In descending the semi-empirical models increasingly overestimate the total pressure gradients with increasing pipe inclinations. The influence of the solids effect term and the suspension term are altered to find their impact on the total pressure gradients.

The shift in solids effect is accomplished by shifting the step change caused by the stationary bed peak of the solids effect. The step change is found by subtracting the value of the solids effect without a stationary bed from the the solids effect value with stationary bed. The value is then added to the solids effect values for flow velocities at which a stationary bed should be present in inclined pipe flows according to figure 2.9. As a stationary bed is observed in the horizontal perspex pipeline segment at flow velocities around 3.5 m/s, the deposition limit velocity for horizontal flow is assumed at 3.5 m/s. The deposition limit velocity shift for inclined pipeline sections, that was found by Wilson and Tse, Hashimoto and de Hoog et al. , is used as a reference. The deposition limit velocity for ascending flows with 17.9 and 44 degrees pipe inclination is assumed 20% higher than the DLV for horizontal flows according to figure 2.9. In 28.9 degrees pipe inclination, 30% increase in deposition limit velocity is expected. Using these values, the solids effect from the horizontal sections is shifted towards higher flow velocities for the ascending flow direction. In the descending flows, a decrease of the deposition limit velocity of 30% is assumed for all angles (according to figure 2.9). The shift of the solids effect to lower flow velocities for descending sections is achieved by assigning the values of the solids effect for higher flow velocities to lower measured flow velocities. The table in appendix D illustrates how the operation was conducted for 28.9 degrees pipe inclination. Figure 5.11 displays the values of the solids effect and its shifts for 28.9 degrees pipe inclination. The original solids effect for horizontal flow directions is plotted using blue line and dotted markers, the shifted effects for ascending and descending flows with red lines and circular markers and black lines and triangular markers. The figures for the other inclination angles are found in appendix D.

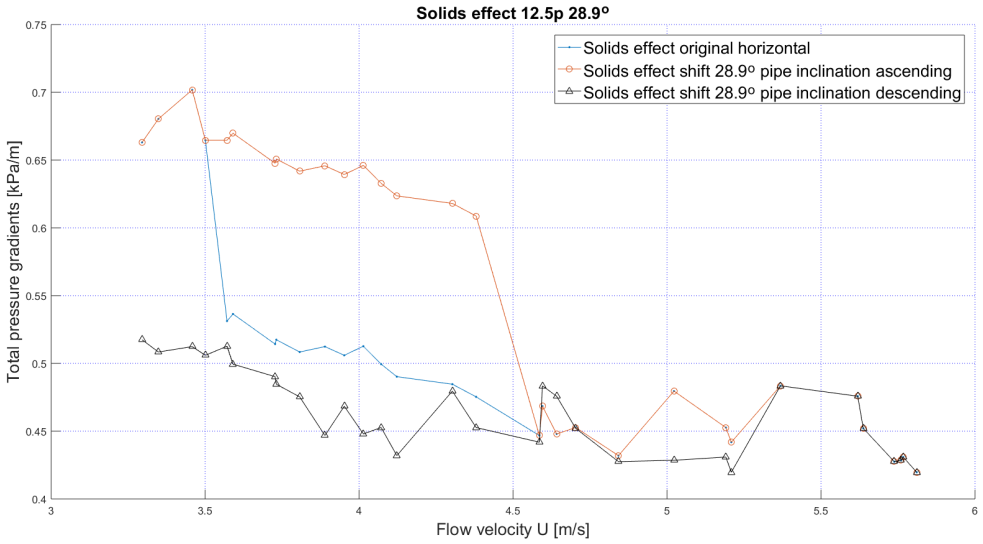

Figure 5.11: Solids effect shift due to higher and lower DLV in ascending, descending and horizontal flow direction for 28.9 degrees pipe inclination

5.4.1. Ascending flow directions

The shift is achieved in the semi-empirical models by eliminating the cosine from the equation to get rid of the general underestimation and the differences between the different semi-empirical models. The values of the solids effect for the deposition limit velocity in horizontal flow are shifted towards higher flow velocities. Figure 5.12 contains the calculated total pressure gradients according to the semi-empirical models (red pentagrams, yellow diamonds and purple squares). The measured total pressure gradients and the adapted semi-empirical model are included using yellow markers and blue circles.

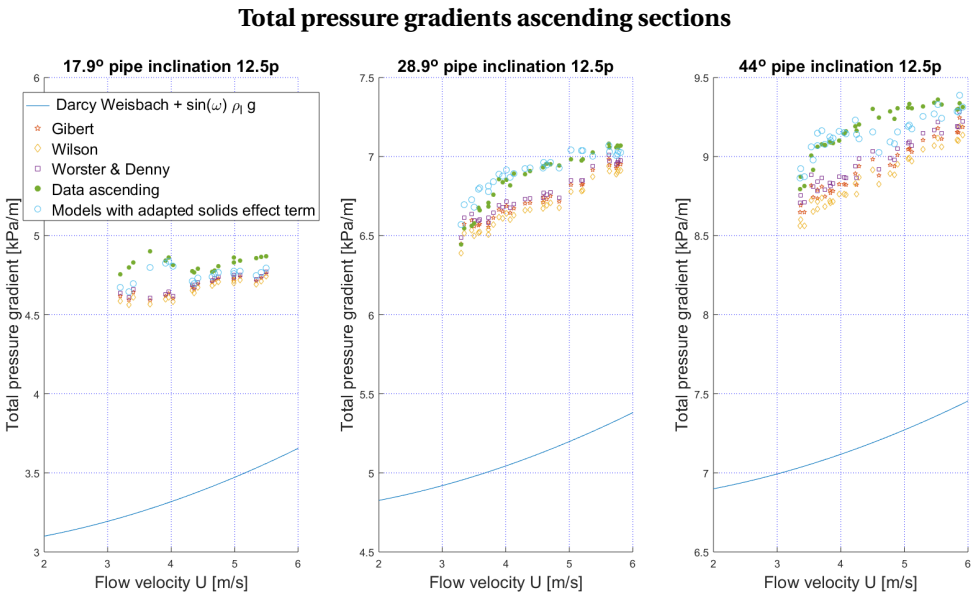

Figure 5.12: Total pressure gradients ascending sections: model modifications

As visible in figure 5.12, the change in the solids effect term has a positive effect on the accuracy of the prediction of the total pressure gradients. Moreover, the conclusion can be drawn that the semi-empirical models underestimate the solids effect in ascending sections during stratified flow regimes. This reveals that a stratified bed has an larger effect on the total pressure gradients in comparison to horizontal section. The increased effect indicates that the stratified bed in the ascending flow directions is thicker and forms at higher flow velocities than in horizontal flow directions. For the lowest and highest flow velocities in the figures, the semi-empirical models can remain unaltered with the condition that the cosine is eliminated from the equations.

5.4.2. Descending flow directions

In the evaluation of the semi-empirical models it became apparent that Wilson's variation on the Worster and Denny model most closely approaches the measured total pressure gradients in descending flow directions. In that model, the cosine and exponent of the solids effect term are lower than one and decrease with increasing inclination angles. This decreases the influence of the solids effect term on the theoretical total pressure gradient. The suspension term in the equations causes a lower total pressure gradient. Since the semi-empirical models overestimate the total pressure gradient, either the influence of the solids effect term is overestimated or the influence of the suspension term is underestimated.

Since a lower solids effect is associated with less solids in the stratified bed, more solids have to be suspended in the mixture flow. As more solids are suspended, the mixture density increases and so does the total pressure gradient in the inclined section ($P = \rho g H = \rho g L sin(\omega)$). The increase in pressure works in the flow direction decreasing the total pressure losses. An overestimation of the total pressure losses can be caused by an underestimation of the suspension term in the semi-empirical models for descending flow directions. For different pipe inclination angles, delivered concentrations and flow velocities, it is presumable that different suspension-stratification ratios are present. Full stratification is assumed at very low - and full suspension at very high flow velocities.

In figure 5.13, the Wilson model is plotted with the yellow diamonds. The Wilson model with the suspension term increased by 5 % is represented with red triangles. The influence of the solids effect shift on the total pressure gradients calculated with the Wilson semi-empirical model is represented by the purple circles. Darcy Weisbach frictional water flow losses and the hydrostatic gradient is represented with the blue line.

The figure represents the total pressure gradients as a function of flow velocity. The three inclination angles for 12.5p concentrations are included.

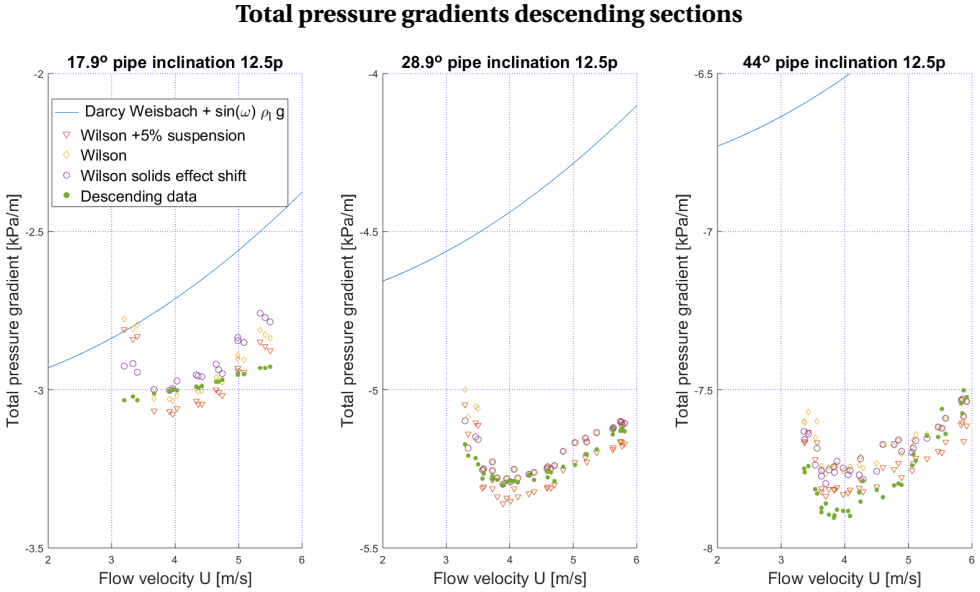

Figure 5.13: Total pressure gradients descending sections: model modification

Increasing the effect of the suspension term in the 44 degrees data appears to improve the results of the models for flow velocities between 3.5 and 5 m/s. This indicates that the effect of particle suspension on the total pressure gradients is indeed higher than anticipated. Over those flow velocities, the original model shows better results.

In the 28.9 degrees pipe inclination graph, an increase of 5 % of the suspension term seems to be too much for flow velocities between 3.5 and 4.5 m/s and too little below 3.5 m/s. At higher flow velocities (above 4.5 m/s) the 5% increase shows good similarities with the measured data. The results with a modified solids effect appear to show the most promising results for flow velocities below 5 m/s.

At 17.9 degrees pipe inclination, the total pressure gradients at flow velocities between 3.5 and 5 m/s are most accurately predicted by the original Wilson model. For higher flow velocities a lower total pressure gradient prediction is accomplished with the suspension term modification. At lower flow velocities, the solids effect shift becomes more dominant and the modification on the model with regard to the solids effect more accurately predicts the slurry behaviour.

As inclination angles are higher, the suspension becomes more dominant in the lower flow velocity ranges (below 3.75 m/s) with regard to the total pressure gradient. At lower inclination angles, the solids effect appears to play an increasingly important role in the total pressure gradient prediction. When higher flow velocities (over 4.5 m/s) are considered, the effects are inverse. A ratio between the suspended and stratified flow regime can be a cause for the faulty predictions, it is most probably a function of the deposition limit velocity, the flow velocity and the inclination angles.

5.5. Conclusion of result evaluation

Generally it was observed that higher pipe inclination angles or higher delivered concentration cause higher total pressure gradients in the ascending section and lower total pressure gradients in the descending sections. They are the result of a combination of (hydro)static and frictional gradients. In the ascending flow directions, the delivered concentration profiles are proportional with the total pressure gradient profiles. In

the descending section they are inversely proportional. The total pressure gradients in ascending flow direction are always higher than in horizontal flow direction and descending direction always lower.

The calculated solids effect in both ascending and descending sections decreases with increasing inclination angles as a result of the cosine in the solids effect term of the semi-empirical models. As indicated by the elevation in the total pressure gradient for ascending and descending flow directions at velocities around 3.5 m/s, the stratified bed in these sections might be thicker than predicted. However, since the models do not make a distinction between stationary and moving beds, this effect is hard to verify. In the semi-empirical models, the i_m from the horizontal measurements was used to determine the solids effect, as the concentration increases, so does the solids effect.

"To what extent do the acquired results from the laboratory experiments agree with the estimated values from the semi-empirical models?"

The calculated estimation of the total pressure gradients using the semi-empirical models is generally close to the measured total pressure gradients. However, the measured total pressure gradients are still marginally underestimated in the ascending and overestimated in the descending section by the calculated total pressure gradients especially in for stratified flow regimes. The semi-empirical model by Worster and Denny is closest to the measured results in the ascending flow direction and Wilson in the descending. The differences between the models are marginal (non existent for low concentrations) and are caused by the exponent attached to the cosine of the solids effect term. A result is that the increase of inclination angles decreases the differences between the different models since the impact of the solids effect on the total pressure gradient reduces. An increase in solids effect in the horizontal section increases the differences between the models.

"Do the acquired results from the laboratory experiments agree with the observations and insights from past experiments?"

In line with the conclusions from literature, the flow velocity at which stationary deposits are formed in ascending sections, increases with increasing pipe inclination until a maximum is reached around 30 degrees pipe inclination. In ascending flow, as the pipe inclination angle was increased, the peak associated with the stationary bed shifts towards higher flow velocities and gradually smooths out until it is no longer visible at 44 degrees pipe inclination.

As concluded in literature, regardless of concentration or flow velocity the total pressure gradients measured in ascending flow directions are always higher than the horizontal hydraulic gradients and descending always lower. Furthermore, in agreement with literature, higher inclination angles cause higher total pressure gradients in ascending flow directions and lower total pressure gradients in descending flow directions. Moreover, an increase in total pressure gradients was witnessed at low flow velocities in both the descending flow directions as a result of stratified flows. From literature it became apparent that this is caused by flow stratification as the mechanical friction of the solids with the pipe wall causes higher pressure losses. The internal structure properties that were observed in other researches can unfortunately not be validated. The delivered concentration was indeed found proportional with the total pressure gradients in ascending slurry flows and inverse proportional in descending flows.

Identifying different layers when calculating the pressure losses in a stratified flow, can be a solution to the over- and underestimations of the total pressure gradients by the semi-empirical models. However, the input values these models require such as the friction factors on the interfaces of the different layers or their cross sectional areas are difficult estimate.

"Are the results of experiments with small pipe diameters similar to the measurement results with larger pipe diameters?"

For this research 300 mm pipe diameter is used, which is twice the largest pipe diameter that was used in previous experimental researches. As mentioned before, the results are quite similar with regard to DLV and stratification. Different effectivenesses of turbulent suspension in relation to the pipe diameter play an important role in the frictional mechanisms inside the pipeline. More effective turbulent suspension due to

the d/D of 0.0025 causes different frictional pressure losses than the d/D of over 0.1 that is used in other researches.

"Are the semi-empirical models applicable on short inclined pipeline sections?"

The inclined pipeline section at 44 degrees pipe inclination is the shortest length that was tested. As it is still has a length 17.5 m, and a L/D of over 58, it can hardly be considered a short pipeline. However, it can be argued that the increased variations in the total pressure gradients of the descending section are caused by the (shorter) length of the pipeline section.

To increase the accuracy of the semi-empirical model predictions for stratified flows, a distinction is made between ascending and descending flow directions. The solids effect is shifted according to the Wilson and Tse graph to account for the different deposition limit velocities in inclined pipe flows. In ascending flow direction it is shifted towards higher flow velocities and in descending direction towards lower flow velocities. In the ascending flow direction this shift in solids effect, in combination with the elimination of the cosine, gives satisfying results with regard to the total pressure gradient prediction. This indicates that the stationary bed has equal effects on the total pressure gradients in ascending and horizontal flow directions but stationary deposits are formed at higher flow velocities than horizontal. In descending flow direction, a ratio between suspended particles and particles in the stratified bed becomes key in the accuracy of the prediction of the total pressure gradients for stratified flows. A modification on the semi-empirical models is required with regard to a ratio which is a function of the deposition limit velocity, flow velocity, pipe inclination angle and flow direction, to account for stratified and suspended flows in the ascending and descending flow directions.

6

Conclusions and recommendations

This chapter contains the conclusions and recommendations for further research. The main conclusions to this research are discussed over three sections with regard to the semi-empirical models, the link between the other studies in inclined pipeline transport and the answer to the main research question of this thesis. The conclusions are followed by recommendations for further research regarding the test setup, protocol and literature.

6.1. Conclusions

The objective of this thesis is to gather knowledge on the less documented and studied principles of inclined pipeline flows. This goal is reached by comparing the results and of experiments conducted with a flow loop with 300 mm pipe diameter to previously done researches and conceived ideas with regard to inclined slurry transport.

To gain insight in the characteristics of inclined slurry transport, a flow loop is used with a pipe diameter of 300 mm. The flow loop contains inclinable, horizontal and perspex measurement sections that cover a combined distance of over 110 meters. The inclinable section can reach pipe inclination angles of up to 45 degrees. The measurement section includes 34 total pressure sensors and 32 differential pressure meters, a flow meter, concentration meter, thermometers and a u-loop. The pump has capacity of 1600 m^3/h, its RPM, power and the pressures over it are recorded. The two slurry tanks have a capacity of 100 m^3 each and the setup can be cooled with a special cooling section. The used sand is considered broad graded and coarse and has a d_{50} of 0.77 mm.

Inclination angles of, 0, 17.9, 18.9 and 44 degrees are tested with six different delivered solids concentrations between 0 and 15%. Each test cycle is executed three times at several different flow rates. A water run is conducted to gain reference measurements. When the water cycle is done, the flow rate is increased to 1600 m^3/h, sediment is added and the flow rate is incrementally decreased in steps between 50 and 100 m^3/h.

6.1.1. Semi-empirical models

- The semi-empirical models do not account for differences in internal flow structure that occur in ascending and descending flow directions.
- The calculated estimation of the total pressure gradients using the semi-empirical models is generally quite accurate, especially for heterogeneous flow regimes.
- Although the semi-empirical models are quite close, the measured total pressure gradients are still marginally underestimated in the ascending and overestimated in the descending section especially in for stratified flow regimes.
- The semi-empirical model by Worster and Denny is closest to the measured results in the ascending flow direction and Wilson in the descending.

- The differences between the models are marginal (non existent for low concentrations) and are caused by the exponent attached to the cosine of the solids effect term.
- The increase of inclination angles decreases the differences between the different models since the impact of the solids effect on the total pressure gradient reduces. An increase in the measured solids effect in the horizontal section increases the differences between the models.
- Identifying different layers when calculating pressure losses in a stratified flow, can be a solution to the over- and underestimations of the total pressure gradients by the semi-empirical models. However, the input values these models require such as the friction factors on the interfaces of the different layers or their cross sectional areas are difficult estimate.

6.1.2. Observations in literature

In line with the observarions by de Hoog et al., Wilson and Tse, Hashimoto et al., Matousek and Vlasak, Doron, Spelay, Eltoukhy, Diniz and Coiado:

- The deposition limit velocity in ascending flows is higher than horizontal flow. In descending flow directions it is probably lower. The highest deposition limit velocity is found around 30 degrees pipe inclination in the ascending flow direction.
- At mixture flow velocities higher than the DLV, the bed moves, delivered concentration increases and the in-situ concentration decreases.
- Regardless of concentration or flow velocity, the total pressure gradients measured in ascending flow directions are always higher than the horizontal hydraulic gradients and descending always lower.
- The delivered concentration is proportional with the pressure gradients in ascending slurry flows and inverse proportional with descending flows.
- Higher inclination angles corresponded with higher total pressure gradients in the ascending flow and with lower total pressure gradients in the descending flow directions. Generally, higher flow velocities cause higher pressure gradients.

- The effect of the pipe inclination angles on the pressure gradient of the mixture is mostly due to the static pressure gradient of the mixture.
- An increase in total pressure gradients is witnessed for decreasing flow velocities in both the flow directions as a result of stratified flows.
- The mechanical friction of the solids with the pipe wall causes higher pressure losses. The internal structure properties that were observed in other researches can unfortunately not be validated.

6.1.3. Main research question

"Are the existing mathematical, physical and semi-empirical models and ideas with regard to slurry transport in inclined pipelines applicable to large diameter inclined pipes?"

For this research a pipe diameter of 300 mm is used, which is twice the largest pipe diameter of previous experimental researches. The results are quite similar with regard to DLV and stratification effects. Different effectivenesses of turbulent suspension in relation to the pipe diameter play an important role in the frictional mechanisms inside the pipeline. More effective turbulent suspension due to the d/D of 0.0025 causes different frictional pressure losses than the d/D of over 0.1 for other researches.

The semi-empirical models are quite accurate with regard to inclined pipe flows for heterogeneous flow regimes. The models do not take different flow regimes into account and have to be modified in order to account for flow stratification. A distinction is made between ascending and descending flow directions. The solids effect is shifted according to the Wilson and Tse graph to account for the different deposition limit velocities in inclined pipe flows. In the ascending flow direction this shift in solids effect, in combination with the elimination of the cosine, gives satisfying results with regard to the total pressure gradient prediction. In

descending flow direction, a ratio between suspended particles and particles in the stratified bed becomes key in the accuracy of the prediction of the total pressure gradients. A modification on the suspension and solids effect terms in the semi-empirical models is required. The ratio should be a function of the deposition limit velocity, flow velocity, pipe inclination angle and flow direction. In general, the conclusions from previous researches with regard to (smaller diameter) inclined slurry transport are applicable to the larger pipe diameters tested for this thesis research.

6.2. Recommendations for further research

The recommendations for further research with regard to inclined hydraulic transport are discussed in this section. Most of the recommendations are applicable to improving the test setup in order to investigate more flow characteristics. Further research is required with regard to some of the models and ideas that were found for this thesis.

- Add electro-resistive tomography instruments or radio metric density meters to the flow loop to gain insight in the internal structure of the slurry flows.
- Solve problems with regard to u-loop differential pressure sensors and density meter.
- Add perspex segments to the inclined sections of the flow loop to gain insight in the deposition limit velocities in inclined slurry transport.
- Increase pipe diameters of the flow loop since larger pipe diameters are used in the industry.
- Test more pipe inclination angles to create more complete picture of flow phenomena in inclined pipe flows.
- Increase pump capacity to test higher flow velocities and gain insight in turbulent suspension phenomena and its efficiency.
- Test larger particle sizes and sands with narrower particle size distributions.
- Increase delivered concentrations since concentrations of up to 15% were tested. In the industry, much larger delivered concentrations are the standard
- Validate the two and three layer models by Shook and Roco, Matousek and Doron.
- Combine experimental results with computational fluid dynamics to validate computer simulations with regard to slurry flows.
- Create modification on semi-empirical model in order to account for stratified inclined flows by adding factor which is a function of flow velocity, deposition limit velocity and inclination angles.

Bibliography

S.W. Churchill. Friction-factor equation spans all fluid-flow regimes. *Chemical Engineering*, 1977.

R. Clift and D.H.M. Clift. Continuous measurment of the density of flowing slurries. *International journal of multiphase flow*, 1981.

E. de Hoog, M. in 't Veld, J. van Wijk, and A. Talmon. An experimental study into flow assurance of coarse inclined slurries. In *18th int. conf. transport & sedimentation of solid particles, Prague, Czech republic.*, 2017.

V.E.M.G. Diniz and E.M. Coiado. Two-phase (solid-liquid) flow in inclined pipes. *Hydrotransport 14*, 1999.

P. Doron, M. Simkhis, and D. Barnea. A three layer model for solid flow in horizontal pipes. *Int. J. Multiphase flow, vol. 19*, 1993.

P. Doron, M. Simkhis, and D. Barnea. Flow of solid-liquid mixtures in inclined pipes. *Int. J. Multiphase flow, vol. 23*, 1997.

R. Durand. Basic relationships of the transportation of solids in pipes - experimental research. In *Proceedings Minnesota international hydraulics convention*, 1953.

R. Durand and E. Condolios. Transport hydraulique et decantation des materiaux solides. *Deuxiemmes Journees de l'Hydraulique*, 1952.

H.A. Einstein and W.H. Graf. Loop systems for measuring sand-water mixture. In *Proceedings American society civil engineers*, 1966.

M.A.R. Eltoukhy. Effect of pipe inclination on the sand-water mixture flow hydraulic gradient at different sand concentrations. *International journal of civil engineering and technology*, 2013.

R. Gibert. transport hydraulique et refoulement des mixtures en conduits. *Annales des ponts chaussees*, 1960.

W.H. Graf. *Hydraulics of sediment transport*. Water resources publications, 1984.

H. Hashimoto, K. Noda, T. Masayama, and T. Kawashima. Influence of pipe inclination on deposit velocity. In *Proceedings of the 7th international conference on hydraulic transport of solids in pipes.*, 1980.

V. Matousek. *Flow mechanism of sand-water mixtures in pipelines*. PhD thesis, Delft University of technology, 1997.

V. Matousek. Pressure drops and flow patterns in sand-mixture pipes. *Experimental thermal and fluid science, Elsevier*, 2002.

V. Matousek. Dredge pumps and slurry transport, 2004. Lecture notes for OE4625.

V. Matousek and P. Vlasak. Research advances in settling slurry flows. In *The 8th international conference for conveying and handling of particulate solids*, 2015.

C.A. Shook and M.C. Roco. *Slurry flow: principles and practice*. Butterworth and Heinemann, 1991.

R.B. Spelay, R.G. Gillies, S.A. Hashemi, and R.S. Sanders. Effect of pipe inclination on the deposition velocity of settling slurries. *The Canadian journal of chemical engineering*, 2016.

P. Vlasak, Z. Chara, and J. Konfirst. Conveying of coarse particles in inclined pipes. *Journal of Hydrology and Hydromechanics*, 2014.

K.C. Wilson and J.K.P. Tse. Deposition limit for coarse-particle transport in inclined pipes. In *9th international conference on hydraulic transport of solids in pipes.*, 1984.

K.C. Wilson, G.R. Addie, A. Sellgren, and R. Clift. *Slurry transport using centrifugal pumps*. Springer science and business media, New York, New York, USA, third edition edition, 2006. ISBN 9780387232621.

R.C. Worster and D.F. Denny. Hydraulic transport of solid material in pipes. In *Proceedings of the insitution of mechanical engineers*, 1955.

A

Test matrix

Test matrix		
Day	Inclination angle [degrees]	Concentration [percentage]
1	0	0
2	0	2.5
3	0	5
4	0	7.5
5	0	10
6	0	12.5
7	changing inclination angle	
8	changing inclination angle	
9	17.9	0
10	17.9	2.5
11	17.9	5
12	17.9	7.5
13	17.9	10
14	17.9	12.5
15	changing inclination angle	
16	changing inclination angle	
17	28.9	0
18	28.9	2.5
19	28.9	5
20	28.9	7.5
21	28.9	10
22	28.9	12.5
23	changing inclination angle	
24	changing inclination angle	
25	44	0
26	44	2.5
27	44	5
28	44	7.5
29	44	10
30	44	12.5

Table A.1: Experiment planning

B

Test setup design

This appendix includes the autocad drawings of the test setup. The overviews. The top and side views and the side views of the inclinables section including scaffolding.

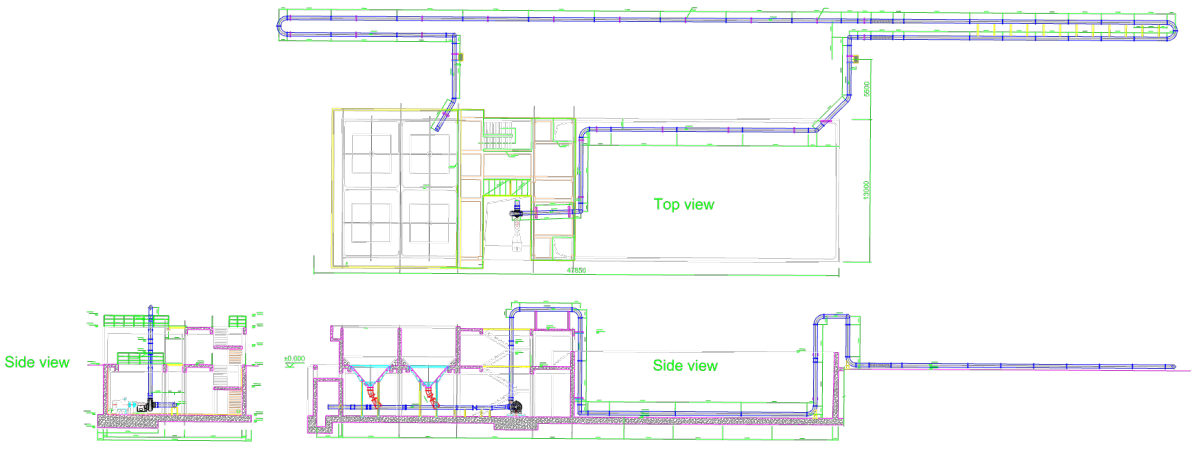

Figure B.1: Overview of the setup

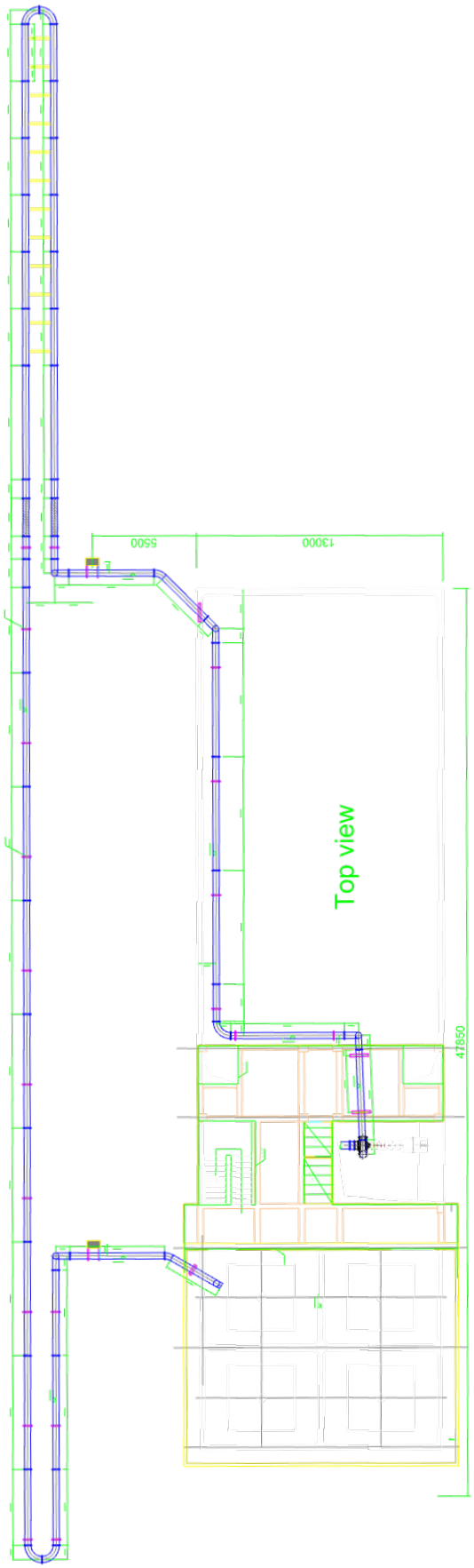

Figure B.2: Top view of setup

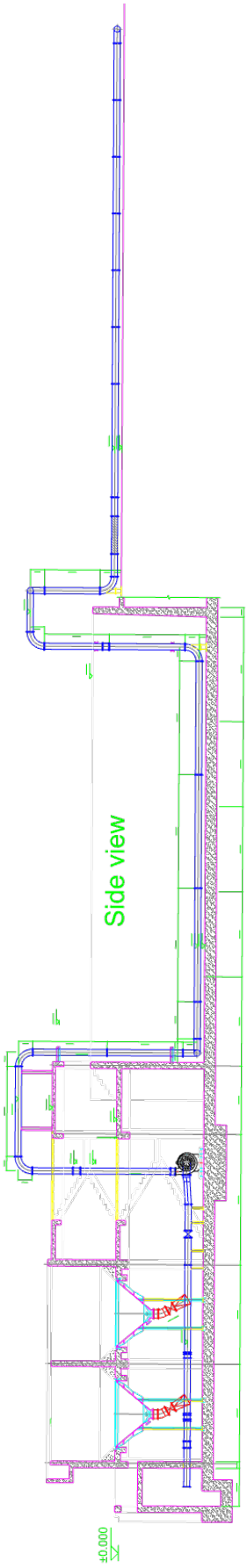

Figure B.3: Side view of setup

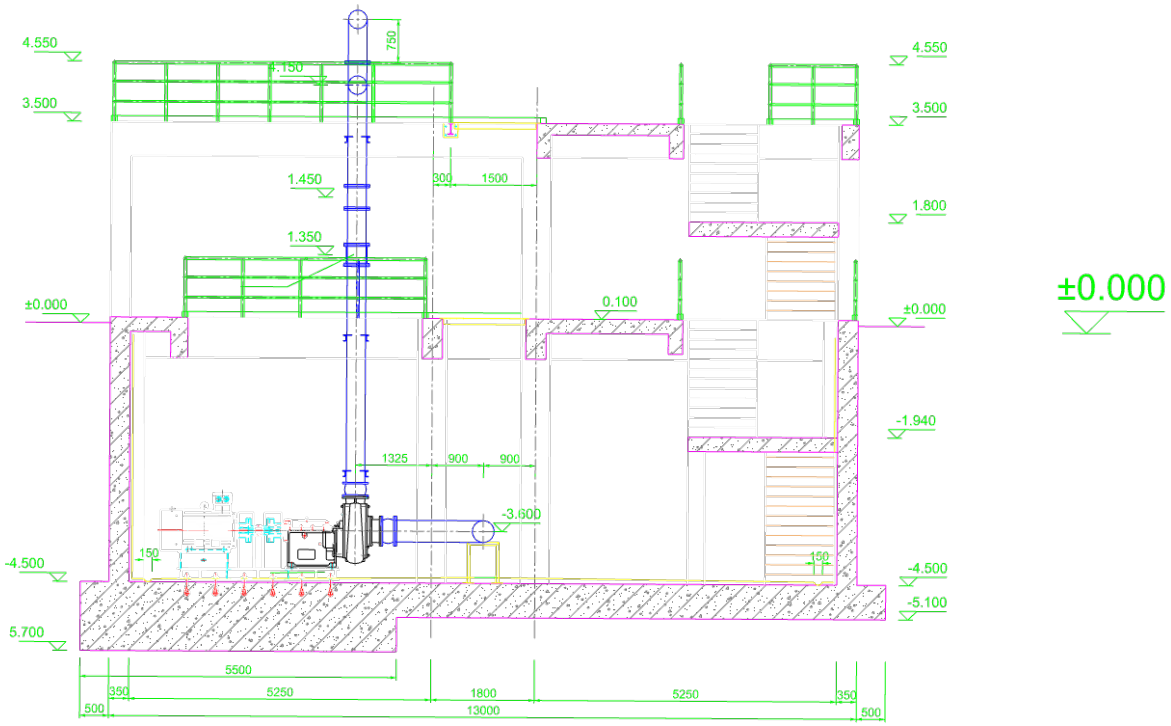

Figure B.4: Side view of setup

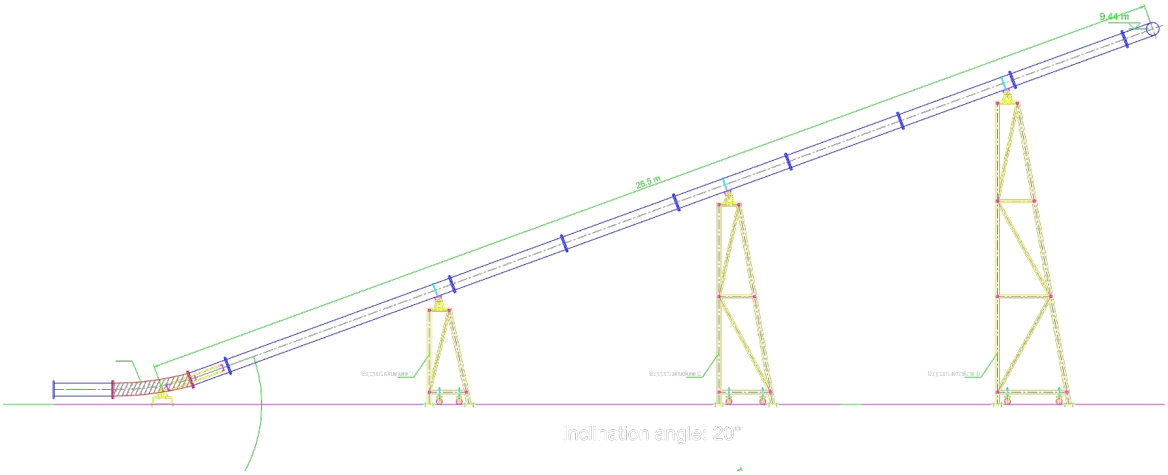

Figure B.5: Side view of inclinable section at 20 degrees inclination

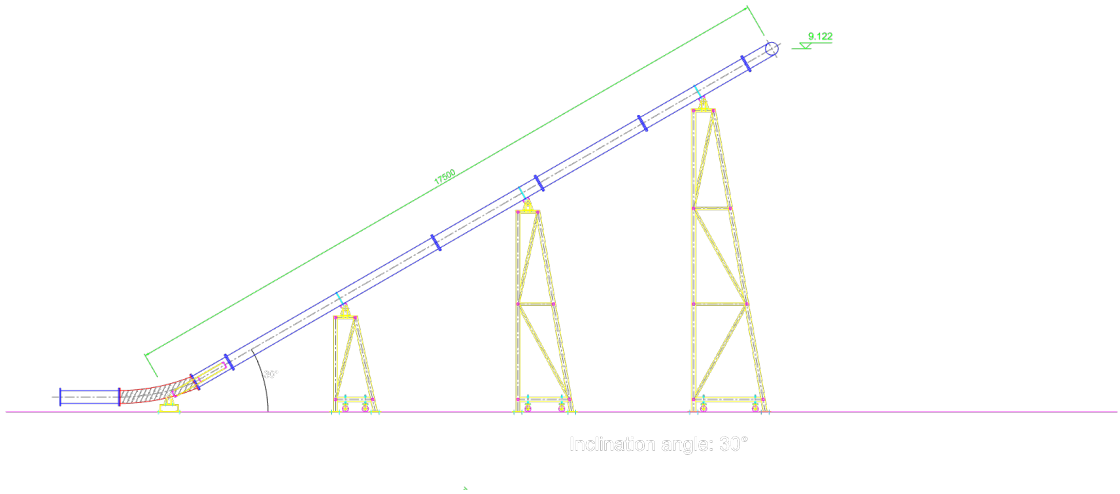

Figure B.6: Side view of inclinable section at 30 degrees inclination

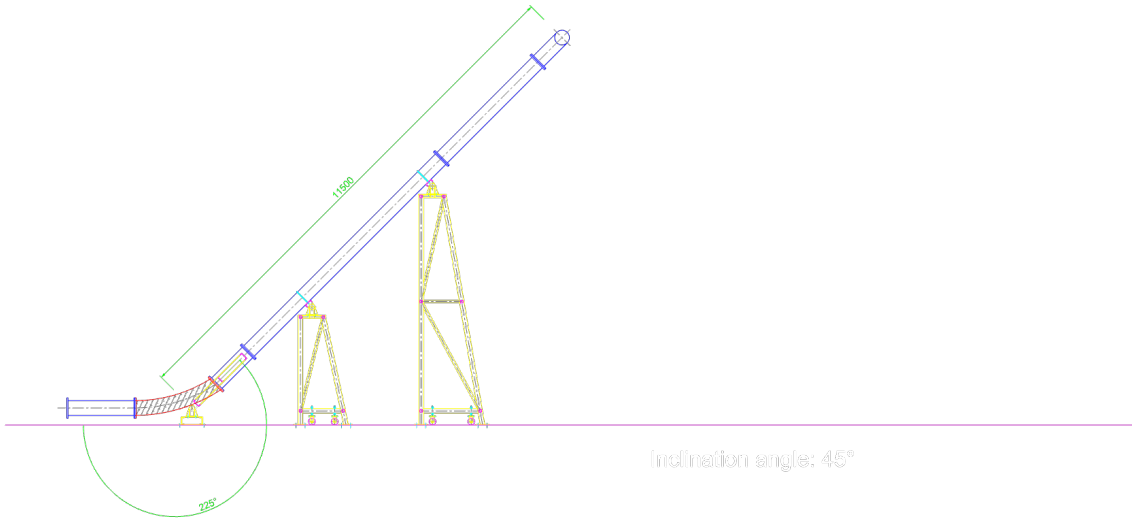

Figure B.7: Side view of inclinable section at 45 degrees inclination

C

U-loop concentration determination

This appendix focuses on the recalculation of the u-loop data that was gathered during the experiments. The differential pressure sensor calibration provided faulty data and therefore it has to be recalculated. This recalculation within the dataset in combination with finding the correct mixture density, can be done using the method described in this appendix. The examples used to describe the method and find the concentrations were taken from the 45 degree inclination angle experiments, they are presumed to be valid for the other angles, concentrations and differential pressures as well.

Basis for concentration determination

The basic idea of this concentration determination method is based on the assumption that the u-loop has the same type of error in all the water flow experiments, as well as the slurry flow experiments. It is presumed that this error is based on a misalignment of the pressure taps that leads to a cross over of dynamic pressure during the experiments. The goal of the method is to find the correct concentration and density of the mixture in the system. Instead of recalibrating the data to fit the theoretical curves, this method focuses on adjusting the theoretical curves to fit the raw data of the liquid flow experiments. Using these adjusted theoretical curves, the density of the other experiments is found.

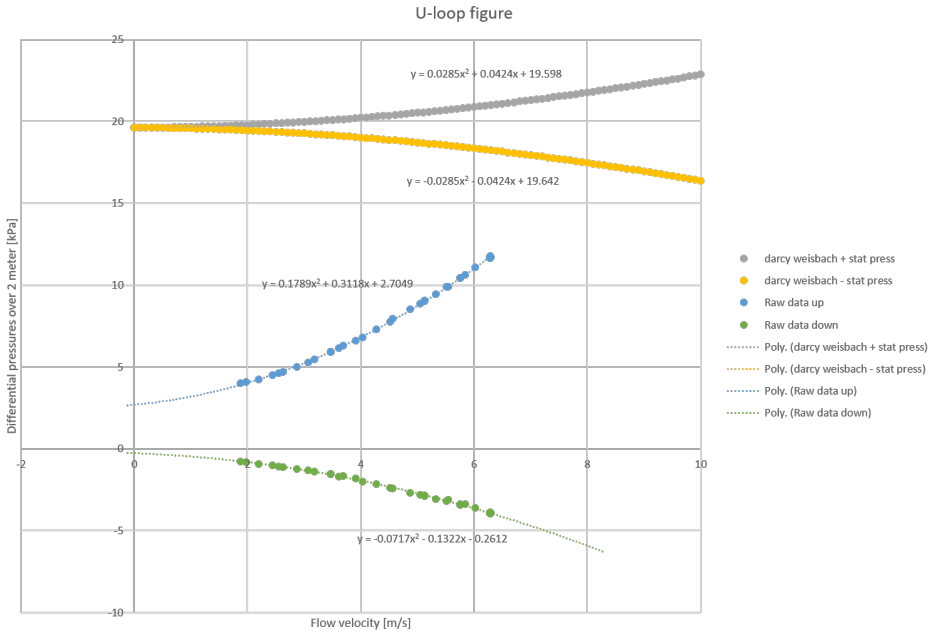

Figure C.1: U-loop, raw data and calculated data for a water flow experiment

The u-loop figure on page 82 contains 4 pressure differential functions. They are all based on a height difference of 2 meters between the pressure taps. Two of them contain the raw data for the up- and down going legs of the u-loop during two of the liquid flow experiments. The other two lines contain the corresponding values using Darcy Weisbach. On the horizontal axis, the flow velocity in m/s is plotted. The vertical axis contain the pressure in kPa. The misalignment is clearly visible in the figure since the raw data should fit the Darcy Weisbach curves. This means that the raw data is subject to a certain offset and gradient compared to the Darcy Weisbach function.

Physics

The method is mainly based on this pressure balance equation:

$$\Delta P_{raw} = offset_{up} + \frac{\rho_m \Delta h g}{1000} + c_U \left(\frac{\rho_m}{\rho_w}\right)\left(\frac{U}{U_{max}}\right)^2 \tag{C.1}$$

From equation C.1 it is visible that the measured differential pressure of the mixture ($\Delta P_{stat,m,up}$)is built up of three components. The first term is the offset of the Darcy Weisbach calculations for the up going leg. It can be viewed as a compensation for the difference between the calculated static pressure and the measured static pressure of the liquid flow experiments. The offset is calculated by subtracting the static pressure differential (Darcy Weisbach ΔP at $U = 0$) from the measured static pressure differential in the U-loop. In the ascending leg of the U-loop, the offset is set at $\Delta P_{raw,up}|_{U=0} - \rho_w g \Delta h = 3.1 - 19.62 = -16.52 kPa$. The Descending leg of the U-loop has an offset of $-0.39 - 19.62 = -20.11 kPa$

The second term is the static pressure of the mixture. ρ_w is the water density, g is the gravitational acceleration constant and Δh is the height difference between the differential pressure taps. Since the gathered data from the experiments come in kPa and the theoretical calculations in Pa, the second term in the equation C.1 has to be divided by 1000.

Term three contains the compensation for the gradient. It accounts for the effect of the velocity (U) on the slurry. c_U is a constant multiplication factor in the velocity term, it is found iteratively by modifying it until the line fits over the measured raw data for the liquid flow. In the ascending leg of the u-loop 8.732 was found and in the descending leg -3.52 was found for the c_U.

Ascending leg

Starting with the ascending leg of the u-loop, the equation that was found using the previously described method is:

$$\Delta P_{up,raw} = offset_{up} + \frac{\rho_m \Delta h g}{1000} + c_{U,up}\left(\frac{\rho_m}{\rho_w}\right)\left(\frac{U}{U_{max}}\right)^2 = \\ -16.52 + \frac{\rho_m * 2 * 9.81}{1000} + 8.732\left(\frac{\rho_m}{1000}\right)\left(\frac{U}{6.3}\right)^2 \tag{C.2}$$

In figure C.2, the raw data is plotted together with the theoretically determined data. The lines correspond with the theoretical data and the markers with the measured differential pressure data. The marker names in the legend contain the desired concentration percentages and the lines the actual concentrations.

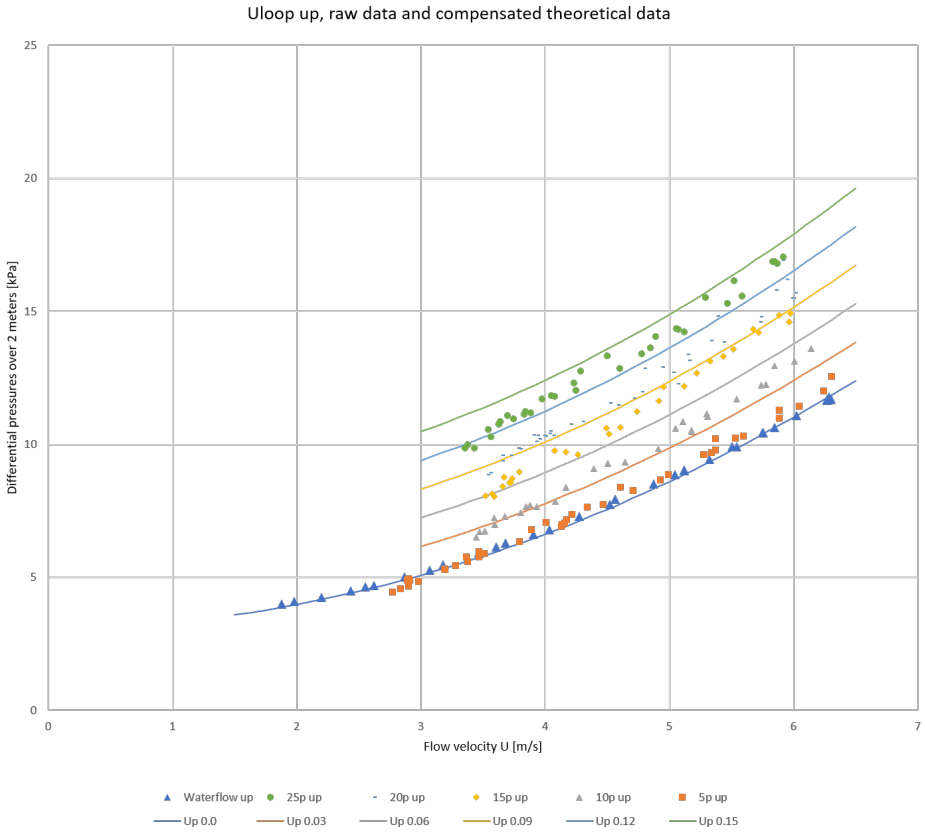

Figure C.2: U-loop: ascending leg, raw data and theoretically calculated data for different concentrations and flow rates

Descending leg

For the descending leg of the u-loop, the equation that was found using the previously described method is:

$$\Delta P_{down,raw} = offset_{down} + \frac{\rho_m \Delta h g}{1000} + c_{U,down}\left(\frac{\rho_m}{\rho_w}\right)\left(\frac{U}{U_{max}}\right)^2 = \\ -20.11 + \frac{\rho_m * 2 * 9.81}{1000} - 3.52\left(\frac{\rho_m}{1000}\right)\left(\frac{U}{6.3}\right)^2 \tag{C.3}$$

In figure C.3, the raw data is plotted together with the theoretically determined data. The lines correspond with the theoretical data and the markers with the measured differential pressure data. The marker names in the legend contain the desired concentration percentages and the lines the actual concentrations.

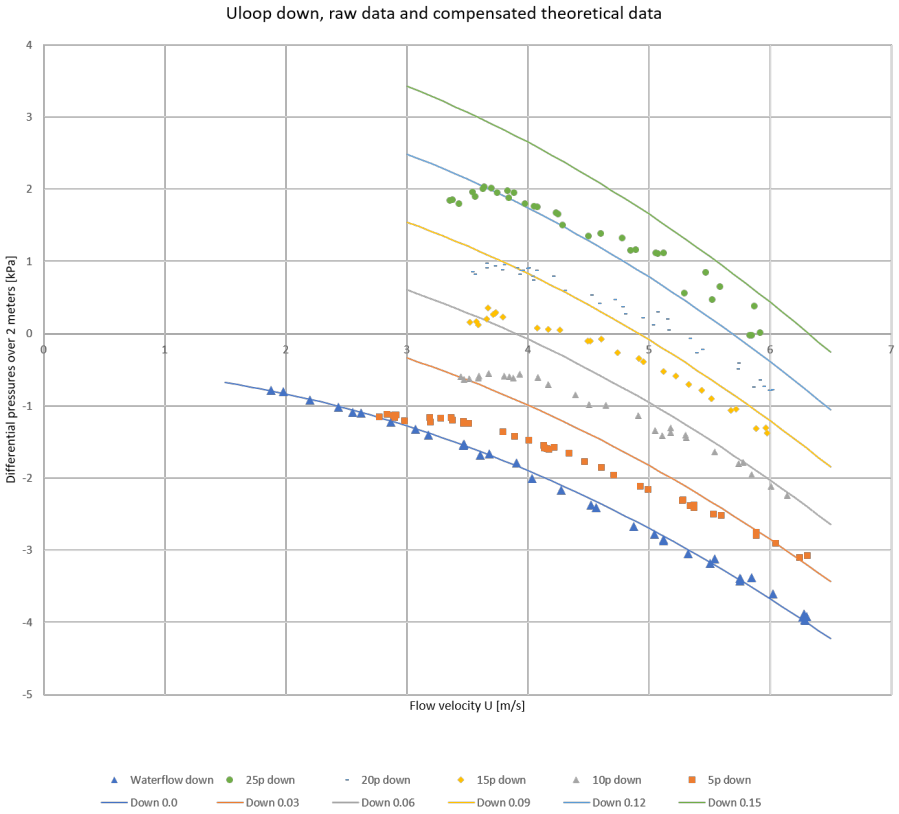

Figure C.3: U-loop: descending leg, raw data and theoretically calculated data for different concentrations and flow rates

Concentrations

Figure C.4 contains the results of both the up and down going legs of the u-loop as determined in the previous subsections. The liquid flow profiles align nicely with the theoretical curves for liquid flow in both the up- and downcomer of the u-loop. In the higher concentration regions, the raw data displays cross-over behaviour between two different concentrations. It is presumably caused by a few phenomena. One of them is only visible in the lowest flow regimes where the bed is regarded stationary. A stationary bed in the system causes less sediment to flow through the u-loop, therefore it will show a lower concentration than present in the flow loop. Another phenomenon causing the cross over is the settling of the suspension profile in the u-loop as well as the slurry tanks. The heavier particles will not be completely suspended any more and settle in the slurry tank or move through the system more slowly. Causing a lower pressure differential in the u-loop which causes cross over behaviour from higher to lower concentrations when the flow rate is decreased.

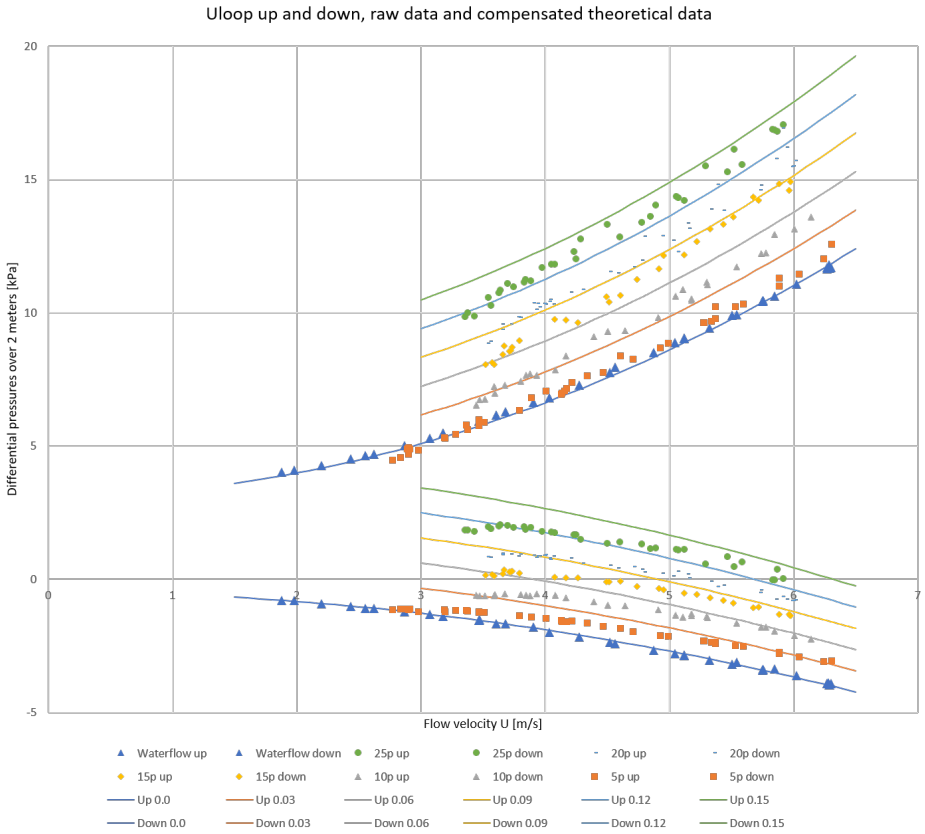

Figure C.4: U-loop: combined, raw data and theoretically calculated data for different concentrations and flow rates

Figure C.5 contains the measured concentrations from the density meter divided by the concentrations as they were determined with the u-loop. The results from ultrasonic density meter appear to be roughly twice the actual concentration as determined with the the u-loop. It is assumed that this factor 1.8 is valid for all the concentration measurements. On page 45 the results from the previously stated method are put into figures, the same conclusion is drawn: the ultrasonic density meter is a factor 1.8 off. It is noticeable that the difference in between the u-loop and the ultrasonic density meter is higher at lower concentrations and lower velocities. This effect is caused by the sinking of the particles, making them slower than the slurry. The values of the concentrations are lower, making the effect on the quotient larger which creates a resonance effect. The research was based on the concentration as it was calculated using the u-loop.

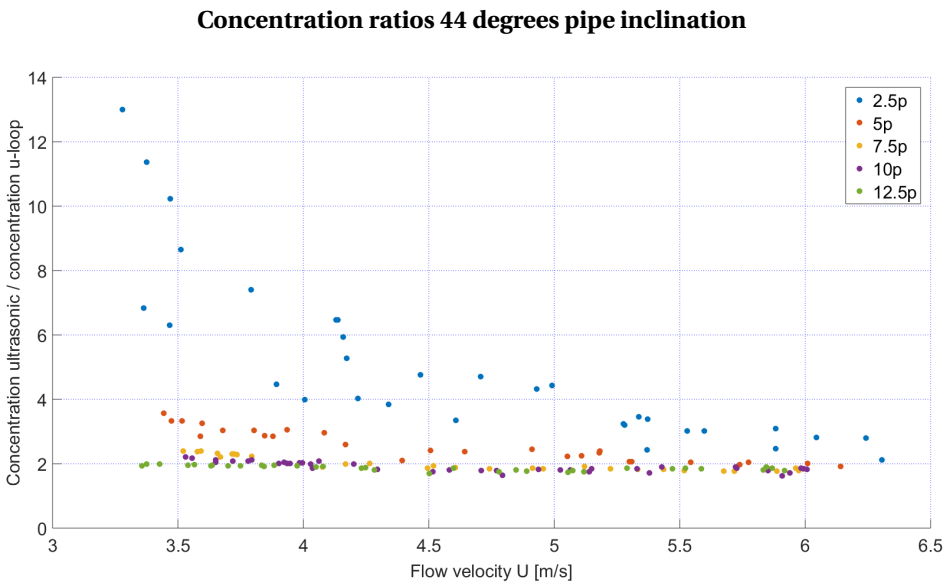

Figure C.5: Ratio ultrasonic concentration measurement and concentration according to u-loop as a function of flow velocity at 44 degrees inclination

30 degree inclination results

It was found that the offset and gradient of the results of the differential pressure meters on the u-loop changes over the course of the 30 degree inclination experiments. Especially the offset shows an increasing trend. The different water runs, show different outcomes with regard to the differential pressure meters. This was visible when the theoretical curve was fitted to the curve containing the results of the water runs that were conducted before every experiment. These changes were counteracted by determining the offset and gradient of the water flow for every experiment using the method previously described for the 45 degrees experiments. The modification gave the correct results with regard to the concentration. The same method as described in the previous section was used, with the exception that it was done for every water run.

20 degree inclination results

During the 20 degree inclination experiments, there were no consistent results available with regard to the u-loop. Therefore, it is presumed that the concentration meter has the same deviation as was determined in the previous sections of this appendix.

Table C.1 contains the delivered concentrations as they were calculated using the u-loop and the method described above. Throughout this thesis, the notation, "12.5p" for instance, is used instead of 15% to keep the terminology uniform for different inclination angles. The original desired concentrations are displayed in the first column of the table, the modified desired concentrations are seen in the last.

Desired and realised delivered concentrations

Desired concentration [-]	Realised Delivered concentrations [-]			Modified desired concentration [-]
Pipe incliation angles [^{o}]	17.9	28.9	44	
0p	0	0	0	0p
5p	4	1.5	2	2.5p
10p	6	4	5	5p
15p	9	7.5	7.5	7.5p
20p	12.5	10	10	10p
25p	15	15	13	12.5p

Table C.1: Desired and delivered concentrations

D

Solids effect shifts

Solids effect shift 28.9 degrees pipe inclination descending section

Solids effect shift descending		
Flow velocity U	Solids effect original	Solids effect descending
3.29514	0.06759	0.05275
3.34823	0.06936	0.05183
3.45784	0.07154	0.05223
3.50064	0.06775	0.05158
3.57098	0.05415	0.05226
3.59033	0.05468	0.05091
3.72711	0.05242	0.04997
3.73098	0.05275	0.04940
3.80684	0.05183	0.04845
3.88888	0.05223	0.04555
3.95167	0.05158	0.04775
4.01372	0.05226	0.04566
4.07158	0.05091	0.04615
4.12239	0.04997	0.04403
4.30272	0.04940	0.04889
4.38002	0.04845	0.04614
4.58529	0.04555	0.04504
4.59543	0.04775	0.04928
4.64132	0.04566	0.04850
4.70317	0.04615	0.04608
4.84208	0.04403	0.04358
5.02249	0.04889	0.04368
5.19092	0.04614	0.04393
5.20863	0.04504	0.04278
5.36813	0.04928	0.04928
5.61913	0.04850	0.04850
5.63719	0.04608	0.04608
5.73778	0.04358	0.04358
5.76008	0.04368	0.04368
5.76666	0.04393	0.04393
5.81081	0.04278	0.04278

Figure D.1: Solids effect shift in descending and horizontal flow direction for 28.9 degrees pipe inclination

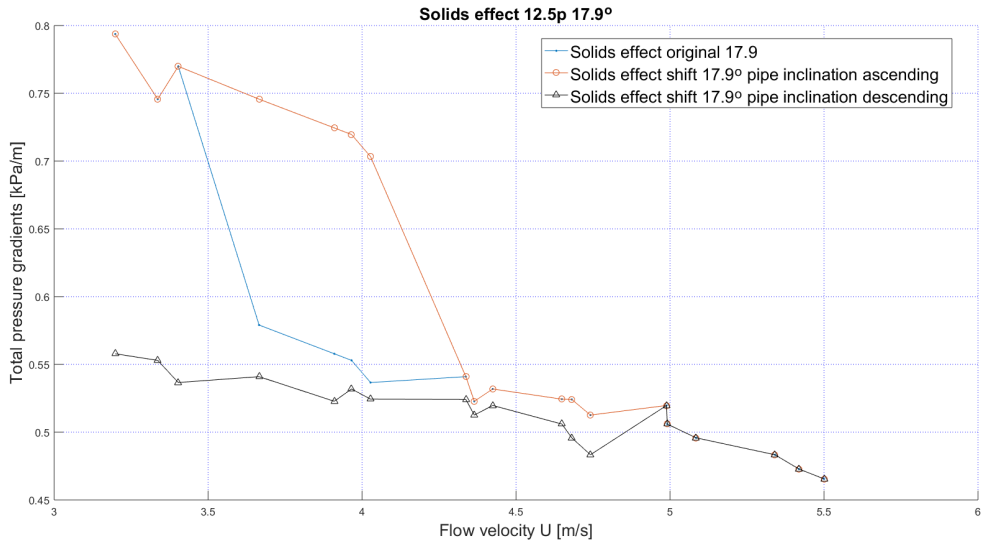

Figure D.2: Solids effect shift due to higher and lower DLV in ascending, descending and horizontal flow direction for 17.9 degrees pipe inclination

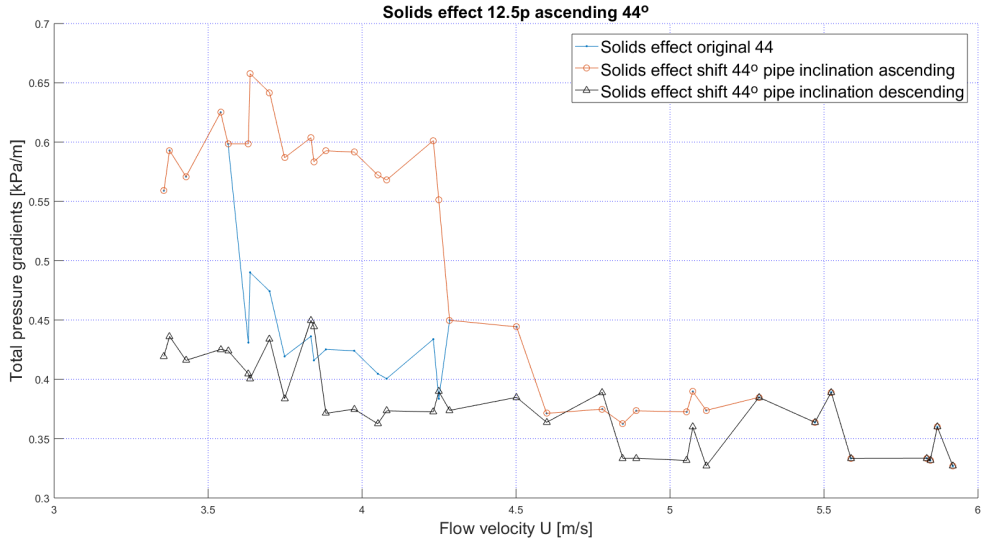

Figure D.3: Solids effect shift due to higher and lower DLV in ascending, descending and horizontal flow direction for 44 degrees pipe inclination